Functional analysis of molars in “symmetrodontan” mammals

Dissertation

zur

Erlangung des Doktorgrades (Dr. rer. nat.)

der

Mathematisch-Naturwissenschaftlichen Fakultät

der

Rheinischen Friedrich-Wilhelms-Universität Bonn

vorgelegt von

Thorsten Plogschties

aus Bonn

Bonn, 2019

Anfertigung mit Genehmigung der Mathematisch-Naturwissenschaftlichen Fakultät der Rheinischen Friedrich-Wilhelms-Universität Bonn

1. Gutachter: Prof. Dr. Thomas Martin
2. Gutachter: Prof. Dr. Martin Sander

Tag der Promotion: 14.02.2020
Erscheinungsjahr: 2020

Table of Contents

List of Figures

List of Tables

List of Abbreviations

Institutional Abbreviations	
AMNH	American Museum of National History (New York, USA)
DORCM	Dorset County Museum (Dorchester, UK)
FMNH	Field Museum of Natural History (Chicago, USA)
IP FUB	Freie Universität Berlin, Institute of Paleontology (Berlin, Germany)
MNA	Museum of Northern Arizona (Flagstaff, USA)
NHM	Natural History Museum (London, UK)
OMNH	Sam Noble Museum (Norman, USA)
RAS	Institut royal des Sciences naturelles de Belgique (Brussels, Belgium)
SNP	Muséum national d'Histoire naturelle (Paris, France)
UM	University of Montana (Missoula, USA)
UMNH	National History Museum of Utah (Salt Lake City, USA)
UMZC	Cambridge University Museum of Zoology (Cambridge, UK)
USNM	(Smithsonian) National Museum of Natural History (Washington D.C., USA)
YPG	Yizhou Fossil & Geology Park (Yizhou, China)
YPM	Peabody Museum of Natural History (Yale, USA)
ZMFK	Zoological Research Museum Alexander Koenig (Bonn, Germany)

Modular tooth structure nomenclature (modified from Schultz et al., 2017b)	
cusps	
upper cusp XY	CPXY
lower cusp xy	cpxy
hypoflexid	hfd
metacone	ME
metaconid	me
metastyle	MTS
paracone	PA
paraconid	pa
parastyle	PAS
protocone	PR
protoconid	pr
stylocone	ST
cingulum/cingulid/crests	
cingulid	[cgd]
cingulum	[CG]
crista	[C]
cristid	[c]
links	
*	between cusps surfaces
~	between crests
_	between cingula/ cingulids
positions	
l	lingual
b	buccal
d	distal
m	mesial
a	apical

Other Abbreviations	
wr-cycle	Chewing cycle with a roll of the lower dentition
wor-cycle	Chewing cycle without a roll of the lower dentition
OFA	Occlusal Fingerprint Analyser. A software to reconstruct the chewing cycle
t-s	time step

Abstract

The “symmetrodontan” molar pattern is characterized by triangulation of the main cusps in combination with a reversed-triangle occlusion. In the fossil record, the “symmetrodontan” molar pattern occurred in various taxa of Mesozoic mammals with an insectivorous diet. These taxa were traditionally summarized in the paraphyletic group “Symmetrodonta”.

In molar evolution, the “symmetrodontan” molar pattern is nested in-between the cusp-in-line type of “triconodontans” and the pretribosphenic molars of Cladotheria. Within the evolution of the „symmetrodontans“, their molar morphology evolved towards a more acute triangulation of the three main cusps and sharp shearing crests. On the base of this triangulation, the "symmetrodontans" can be differentiated into three groups. The early diverging Woutersiidae, Tinodontidae, and Kuehneotheriidae encompass the obtuse-angled “symmetrodontans”. Spalacotheriidae comprises the acute-angled “symmetrodontans”, and Zhangheotheriidae, formerly included into the acute-angled “symmetrodontans”, are herein classified as an intermediate-angled taxon.

The functional molar occlusion analysis of representatives of each class revealed that all “symmetrodontans” performed a one-phased transverse upward movement of the lower jaw, with a slight mesial or distal shift. Another feature that all “symmetrodontans” had in common, was the embrasure shearing. All studied “symmetrodontans”, except for Kuehneotheriidae, performed an embrasure shearing, in which two upper molars embraced one lower molar. The embrasure shearing of kuehneotheriids, in contrast, was proceeded within the cusp level.

Despite the similarity of the mandible movement, the respective groups have a unique mode of functional occlusion. Generally, *Woutersia butleri* (Woutersiidae) comminuted food by puncture-crushing, *Kuehneotherium praecursoris* (Kuehneotheriidae) by puncture-shearing, *Maotherium sinense* (Zhangheotheriidae) by blunt-shearing, and *Spalacolestes cretulablatta* (Spalacotheriidae) by shear-cutting. Additionally, as a result of their higher width/length-ratio, the acute-angled “symmetrodontans” inflicted more damage to the prey, than the obtuse-angled ones.

Similar to the majority of extant insectivorous mammals, “symmetrodontans” probably were opportunistic and generalistic feeders, due to their endothermic metabolic system, but with some limitations. The first limitation was the size of the prey, and the second was its composition ([in-]tractability), whereby the intractability increases with the size of the prey. Apart from the prey size Woutersiidae and Zhangheotheriidae could handle, their molars were better suited for comminuting more intractable prey (e.g. coleopterids), by virtue of the lower sharpness of the molar cusps, cusp tips, and crests. The kuehneotheriid molars, with a higher cusp and cusp tip sharpness, were more efficient in comminuting tractable

invertebrates (e.g. annelids), within the prey size they could handle. Similar to shrews, the range of the prey preference of the Spalacotheriidae was mainly limited by the size of their molars, and therefore by the size of the respective spalacotheriid species. Small spalacotheriid species preyed on smaller invertebrates, larger species consumed larger prey, whereby the composition of the prey was of minor importance.

The morphology of spalacotheriid molars resembles the theoretical model of an ideal insectivore molar, which is called protoconoid. The main features of the protoconoid can also be seen in the extinct Dryolestida (Cladotheria), as well as in certain extant insectivorous mammals, that have reduced the tribosphenic molar pattern to a zalambdodont or dilambdodont pattern (e.g. Solenodontidae, Soricidae). Dryolestida, zalambdodont and dilambdodont mammals, and Spalacotheriidae first punctured and trapped their prey with their molar cusps, and then shear-cut the food items like a cigar cutter. The secondary simplification of the tribosphenic molars towards the protoconoid suggests that this molar pattern is the most successful adaptation and specialization for a highly insectivorous diet (“hyperinsectivory”).

1 Introduction

1.1 The evolutionary development of the molars

The masticatory system of mammals plays an important role in achieving their immense diversity. Due to evolutionary changes in modern mammals, the masticatory system is highly adapted to their preferred diet. Essential for an efficient diet comminution is the morphology and the interaction between the dentition, which leads to an increase in the digestive efficiency to gain maximum assimilation of nutrients (Prinz and Lucas, 1997; Prinz et al., 2003). Mammals depend on consuming high amounts of calories, due to their endothermic way of life (Clarke and Pörtner, 2010). During evolution, mammalian dentition adapted to different kinds of food and it is thus possible to distinguish the preferred diet of mammalian species by the morphology of their teeth (Ungar, 2010). While herbivore dentitions need to rip-off, grind, and crush plant components, carnivores use their teeth to catch prey and to tear the prey's flesh apart. It is important to note, that the variety of modern mammal molar morphologies only has one evolutionary predecessor, the tribosphenic molar (Cope, 1883; Osborn, 1888; Hiiemäe, 1976; Thenius, 1989; Flynn et al., 1999; Luo et al., 2002; Woodburne et al., 2003; Luo, 2007; Davis, 2011; Conith et al., 2016).

Simpson (1936) first used the term "tribosphenic molar", and described the innovative features of this molar type in detail. The innovation of the tribosphenic molar, in contrast to the pretribosphenic molar, is a neomorphic lingual cusp (protocone) on the upper molar, which occluded in the distal basin (talonid) of the lower molar (Fig. 1). The talonid was formed by rearranging existing cusps, in combination with the development of neomorphic cusps (Simpson, 1936). The advantage for mammals, that have tribosphenic molars, is to puncture-crush, and shear their prey, like their ancestors, but also to squeeze, and grind food items. The squeezing and grinding function happened due to the interaction of the protocone and the talonid, comparable to a pistil and mortar action (Simpson, 1936). The capability to squeeze and grind food was an important premise for the rise of the herbivores (Kielan-Jaworowska et al., 2004; Ungar, 2010; Evans and Pineda-Munoz, 2018). Based on the fossil *Juramaia sinensis* Luo, Yuan, Meng & Ji, 2011 the divergence

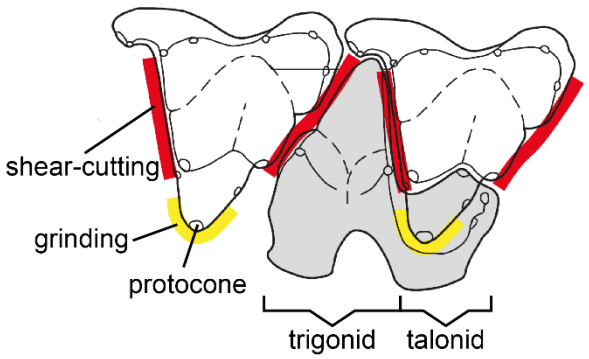

Fig. 1: The upper (white) and lower (grey) tribosphenic molars in occlusion. Only the important structure are labeled and the molars are simplified. The shear-cutting crests are marked in red, and the grinding areas in yellow. (Modified from Kielan-Jaworowska et al., 2004)

of Eutheria and Metatheria lineages could be dated back to the Middle Jurassic (160 Ma), and also the minimum age of the tribosphenic molar origin.

The development towards the tribosphenic molar is often referred to as the Cope-Osborn theory (Cope, 1883; Osborn, 1897; Gregory, 1934). In their studies, Cope and Osborn described the basic, principle evolutionary steps from a unicuspid (haplodont) tooth towards the tribosphenic molar in detail (Fig. 2). In the course of evolution, small cusps evolved mesially and distally to the primal cusp of the unicuspid tooth. This configuration of three main cusps in line is typical for the paraphyletic "Triconodonta". Prominent representatives of this molar configuration are *Morganucodon* Kuehne, 1949 (Upper Triassic - Lower Jurassic) or *Triconodon* Owen, 1949 (Upper Jurassic). Further evolutionary steps involved a buccal shifting of the two accessory cusps next to the main cusps of the upper molars, and a lingual shifting of the two side cusps next to the lower main cusp (Crompton and Jenkins, 1968, 1973). The resulting reversed-triangle pattern is typical for the paraphyletic "Symmetrodonta". While early-diverging "symmetrodontans" like *Woutersia* Sigogneau-Russell, 1983 (Upper Triassic) are characterized by three blunt main cusps, the pointed molar cusps of Late Cretaceous taxa like *Spalacolestes* Cifelli & Madsen, 1999 are connected via sharp crests.

During the following evolutionary steps, the reversed-triangle pattern was modified successively into the tribosphenic molar. For that matter, some cusps underwent further shifting, and new cusps were developed. An early representative of the Tribosphenida is *Pappotherium pattersoni* Slaughter, 1965 (Lower Cretaceous).

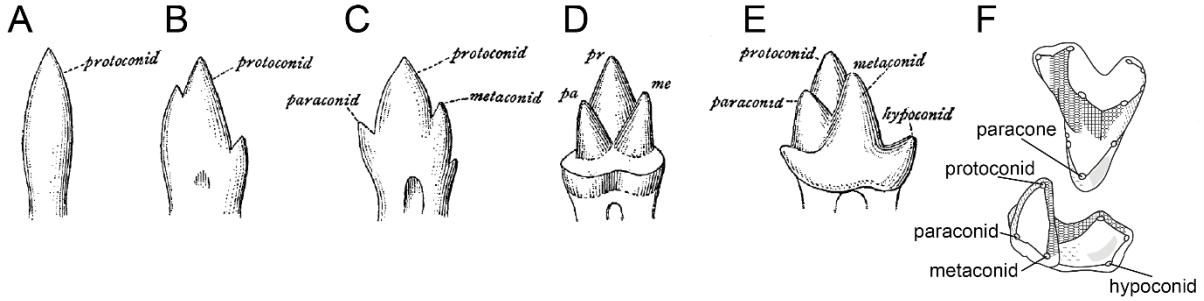

Fig. 2: Important steps in the evolution of the tribosphenic molar. A: A unicuspid lower tooth of a non-mammalian amniote. B: A pre-triconodont tooth of *Dromatherium* (therapsid). C: A triconodont lower tooth of *Microconodon* (therapsid). D: A symmetrodont lower molar of *Spalacotherium*. E: A pretribosphenic lower molar of *Amphitherium.* F: Tribosphenic upper and lower molars of *Pappotherium*. (A-E: Modified from Osborn, 1897; F: Modified from Kielan-Jaworowska et al., 2004)

It is important to mention that one principle of the Cope-Osborn theory has been revised by Patterson (1956). Cope (1883) and Osborn (1897) assumed that each primal unicuspid cusp of the mammalian ancestor is homologous to the upper and lower molar main cusp of the tribosphenic molar (protocone, protoconid). Patterson (1956) discovered that this inverse homology of the Cope-Osborn theory was an erroneous assumption and that the upper molar main cusp (protocone) of the tribosphenic molar evolved secondarily.

Nevertheless, the principles of Cope and Osborn's tritubercular theory are still valid today. Another discovery, that needs to be addressed, is that the structural morphology of the tribosphenic molar evolved independently on Gondwana and Laurasia (Luo et al., 2001; Davis, 2011). Nevertheless, the Tribosphenida, as defined by McKenna (1976), are most likely monophyletic (Davis, 2011).

1.2 "Symmetrodonta"

"Symmetrodontans" are a poorly known, paraphyletic group of small Mesozoic mammals (*sensu lato*). They are characterized by a triangular arrangement of the molar main cusps, and lacking both, talonid cusps and a protocone. The upper and lower molars are arranged in a reversed-triangle pattern with one upper molar occluding between two lowers (two-to-one occlusion) (Fig. 3). The simple reversed-triangular molar morphology represents a fundamental step in the mammalian evolution (Crompton and Sita-Lumsden, 1970; Kielan-Jaworowska et al., 2004). Functionally and structurally, this morphology is intermediate between the "triconodont" cusp-in-line molar pattern and the more derived molars of the Tribosphenida (Patterson, 1956; Crompton and Jenkins, 1967). The "symmetrodontan" molar pattern evolved more than once among the mammalian evolution and cannot be seen as an apomorphy which is unique to "Symmetrodonta" (Rougier et al., 1996; Pascual et al., 2002; Kielan-Jaworowska et al., 2004). Therefore, the term "symmetrodontan" should only be used in a descriptive sense, and not taxonomically.

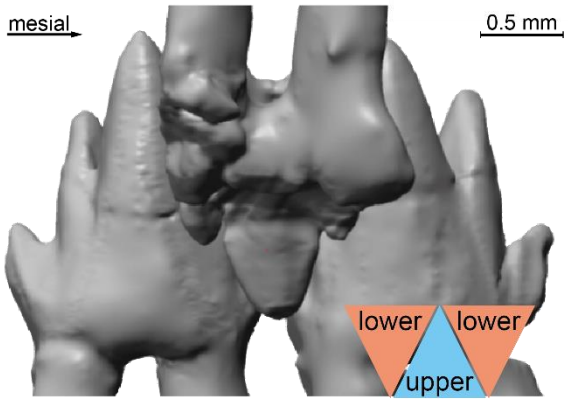

Fig. 3: The reversed-triangle and two-to-one occlusion pattern on the example of *Maotherium sinense* (YFGP 1724, right molars).

Within the "symmetrodontans" traditionally two groups are distinguished. The obtuse-angled Kuehneotheriidae and Tinodontidae, in which the three main cusps are arranged at an angle greater than 90°, and the acute-angled Spalacotheriidae, in which the angle between the main cusps is less than 90° (Li and Luo, 2006; Ji et al., 2009; but according to Averianov et al. (2013) the transition between obtuse-angled and acute-angled is at 80°). Another group of "symmetrodontans" is the intermediary Zhangheotheriidae. The zhangheotheriids comprise acute-angled as well as obtuse-angled taxa.

The fossil record shows that "symmetrodontans" were almost worldwide distributed and they appeared in the Upper Triassic (Norian) and went extinct in the Upper Cretaceous (Maastrichtian) (c.f. Tab. 1 - Tab. 3). The fossil record of the "symmetrodontans" is sparse. Most of the "symmetrodontan" fossil findings are isolated teeth and teeth bearing jaw

fragments. An extraordinary exception are the “symmetrodontan” fossils of the lower part of the Jehol Group, Yixian Formation (Barremian) in Northeastern China (Pan et al., 2013). Almost complete specimens and articulated skulls, including their dentition, were found in this Lagerstätte (Hu et al., 1997; Rougier et al., 2003; Luo and Ji, 2005; Li and Luo, 2006; Ji et al., 2009; Bi et al., 2016; Plogschties and Martin, 2019). These fossils are representatives of the zhangheotheriids and spalacotheriids.

1.2.1 The diet of “symmetrodontans”

Due to the small body size and the tooth morphology, it can be assumed that “symmetrodontans” preferred insectivorous (terrestrial invertebrates) diet (Kielan-Jaworowska et al., 2004). The body size can be estimated on the basis of the well-preserved Jehol Group fossils and on calculations based on the dentition (Kay, 1975). This results in a body size for “symmetrodontans” ranging between that of the shrew *Sorex trowbridgii* and the marsupial *Monodelphis domestica* (Kielan-Jaworowska et al., 2004).

The tooth morphology shows that the primary functions of “symmetrodont” molars were puncture-crushing and shearing. These two functions are also mainly used by extant insectivores (Crompton et al., 1998; Evans, 2005). Gill et al. (2014) demonstrated, based on finite element analysis of lower jaws and a microwear study, that it is possible to differentiate the preferred insectivorous diet between species, in this case, *Morganucodon* (“Triconodonta”), and *Kuehneotherium* Kermack, Kermack ,and Mussett, 1968 (“Symmetrodonta”). They concluded that *Kuehneotherium* more likely preferred a “soft” insectivore diet, whereas *Morganucodon* preferred “hard” prey. This conclusion is supported by an experimental study of Conith et al. (2016), in which simplified models of the *Kuehneotherium* and *Morganucodon* dentition “chewed” different “food” items. Another approach to determine the preferred prey is to study the molar shape and morphology in detail (Lucas and Luke, 1984; Strait, 1993; Evans and Sanson, 1998; Evans, 2005; Evans and Sanson, 2006; Anderson and La Barbera, 2008)

1.2.2 A systematic overview of “symmetrodontans”

Due to the fact that most of the “symmetrodontan” fossils are only isolated teeth, the phylogenetic relationships between them,as well as the phylogenetic position of the “symmetrodontan” taxa, is still unsolved. Recent phylogenetic analysis support at least the monophyly of zhangheotheriids and spalacotheriids, and their affiliation to the Mammalia (Averianov et al., 2013; Bi et al., 2014; Krause et al., 2014; Luo et al., 2015; Huttenlocker et al., 2018). To avoid confusion, in this study the term Mammalia will be used *sensu lato* and includes the Mammaliaformes Rowe, 1988 and the mammalian crown group (Luo et al., 2002; Kielan-Jaworowska et al., 2004). In terms of the evolutionary development of the “symmetrodontan” molars, the zhangheotheriids have an intermediate molar morphology,

and the spalacotheriids the most derived ones. The Zhangheotheriidae and Spalacotheriidae are summarized in Table 1.

The earliest diverging “symmetrodontans” are Woutersiidae and Kuehneotheriidae (Tab. 2). They have the most primitive “symmetrodontan” molar morphology and are classified as obtuse-angled “Symmetrodonta”.

For completeness, Table 3 contains the remaining “Symmetrodonta” including Tinodontidae and *Gobiotheriodon*. These taxa are classified as obtuse-angled “symmetrodontans”.

In this work, the following taxa are excluded from the “Symmetrodonta”:

- The Thereuodontidae Sigogneau-Russell and Ensom, 1998, because Martin (2002) and Averianov (2002) argued that the Thereuodontidae teeth are milk teeth of stem zatherians. The same applies to *Atlasodon monbaroni* Sigogneau-Russell, 1991.
- *Bondesius ferox* Bonaparte, 1990, because Averianov (2002) placed *Bondesius* within the Dryolestida.
- “Amphidontidae” Simpson, 1925, are excluded based on results of recent studies, which included the type genus *Amphidon superstes* Simpson, 1925 into the “Amphilestidae” (Rougier et al., 2001; Rougier et al., 2007a; Gao et al., 2010). Furthermore, according to Kielan-Jaworowska et al. (2004) the other “amphidontid” taxa, e.g. *Manchurodon simplicidens* Yabe and Shikama, 1938, and *Nakunodon paikasiensis* Yadagiri, 1984 are not unequivocally diagnosable based on the available data.

Tab. 1: Summary of Zhangheotheriidae and Spalacotheriidae, and their temporal and geographic occurrence according to the fossil record.

Taxon	Temporal Occurrence	Geographic Occurrence
Zhangheotheriidae		
Anebodon luoi Bi, Zheng, Meng, Wang, Robinson, and Davis, 2016	Barremian	China
Kiyatherium cardiodens Maschenko, Lopatin, and Voronkevich, 2002	Barremian	Russia
Maotherium asiaticum Ji, Zhang, Yuan, Xu, 2009	Barremian	China
Maotherium sinense Rougier, Ji, and Novacek, 2003	Barremian	China
Zhangheotherium quinquecuspidens Hu, Luo Li, Wang, 1997	Barremian	China
Spalacotheriidae		
Akidolestes cifellii Li and Luo, 2006	Barremian	China
Aliaga molinensis Cuenca-Bescos, Canudo, Gasca, Morena- Azanza, and Cifelli, 2014	Barremian	Spain
Heishanlestes changi Hu, Fox, Wang, and Li, 2005	Aptian	China
Infernolestes rougieri Cifelli, Davis and Sames, 2014	Berriasian	USA
Lactodens sheni Han and Meng, 2016	Barremian	China
Shalbaatar bakht Nassov, 1997	Turonian	Uzbekistan
Spalacolestes cretulablatta Cifelli and Madsen, 1999	Albian	USA
Spalacolestes inconcinnus Cifelli and Madsen, 1999	Albian	USA
Spalacotheridium mckennai Cifelli, 1990	Turonian	USA
Spalacotheridium noblei Cifelli and Madsen, 1999	Albian	USA
Spalacotherium evansae Ensom and Sigogneau-Russell, 2000	Berriasian	Great Britain
Spalacotherium henkeli Krebs, 2000	Barremian	Spain
Spalacotherium hookeri Gill, 2004a	Berriasian	Great Britian
Spalacotherium taylori Clemens and Lees, 1971	Valanginian	Great Britain
Spalacotherium tricuspidens Owen, 1854	Valanginian	Great Britain
Spalacotheroides bridwelli Patterson, 1955	Albian	USA
Symmetrodontoides canadensis Fox, 1976	Maastrichtian	USA
Symmetrodontoides foxi Cifelli and Madsen, 1986	Campanian	USA
Symmetrodontoides oligodontos Cifelli, 1990	Turonian	USA
Symmetrolestes parvus Tsubamoto, Rougier, Isaji, Manabe, and Forasiepi, 2004	Hauterivian	Japan
Yaverlestes gassoni Sweetman, 2008	Barremian	Great Britain

Tab. 2: Summary of Kuehneotheriidae and Woutersiidae, and their temporal and geographic occurrence according to the fossil record.

Taxon	Temporal Occurrence	Geographic Occurrence
Kuehneotheriidae		
Kuehneotherium praecursoris Kermack, Kermack, and Mussett, 1968	Norian Rhaetian	Great Britain, Greenland France, Luxemburg
Kuehneotherium stanislavi Debuysschere, 2017	Rhaetian	France
Fluctuodon necmergor, Debuysschere, 2017	Rhaetian	France
Kotatherium haldanei Datta, 1981	Lower Jurassic	India
Kuehneon duchyense Kretzoi, 1960 *nomen dubium*	Lower Jurassic	Great Britain
Woutersiidae		
Woutersia butleri Sigogneau-Russell and Hahn, 1995	Rhaetian	France
Woutersia mirabilis Sigogneau-Russell,1983	Rhaetian	France

Tab. 3: Summary of “Symmetrodonta” incertae sedis and Tinodontidae, and their temporal and geographic occurrence according to the fossil record.

Taxon	Temporal Occurrence	Geographic Occurrence
incertae sedis		
Gobiotheriodon infinitus Trofimav, 1980	Aptian or Albian	Mongolia
Tinodontidae		
Tinodon bellus Marsh, 1879 Synonyms= ***Menacodon*** Marsh, 1887 ***Eurylambda*** Simpson, 1929 ***Amphidon aequicrurius*** Simpson, 1925 ***Tinodon lepidus*** Marsh, 1879	Kimmeridgian Berriasian Berriasian	USA Great Britain Portugal
Tinodon micron Ensom and Sigogneau-Russell, 2000	Berriasian	Great Britain

1.3 Dryolestida, the closest relative to the acute-angled "symmetrodontans"

Dryolestida are pretribosphenic Cladotherians, which are nested in-between the spalacotheriids (acute-angled "symmetrodontans") and prototribosphenidans (e.g., *Vincelestes*), and therefore are on the stem lineage of the tribosphenidans (Martin, 1999; Luo, 2007; Chimento et al., 2012; Schultz and Martin, 2014). In the fossil record, this taxon appears in the Middle Jurassic and disappears in the early Paleocene. Fossil remains of Dryolestida were found in North America, South America, Europe, and Asia (Lillegraven and McKenna, 1986; Ensom and Sigogneau-Russell, 1998; Martin, 1999; Gelfo and Pascual, 2001; Martin and Averianov, 2010; Schultz and Martin, 2011; Chimento et al., 2012). Like in "symmetrodontans", the molars of the Dryolestida are arranged in a (acute) reversed-triangle pattern. Dryolestidans show an additional groove (hypoflexid) at the distal side of the lower molars, in which the paracone occluded and was guided along the mastication path. The hypoflexid separates the trigonid from the unicuspid talonid (Schultz and Martin, 2014). In the course of evolution, the hypoflexid got extended and became an important structure for shearing food. During the progressing evolution of the mammalian molars towards the tribosphenic type, the talonid basin, in which the neomorphic protocone occluded, became more important for food mastication. As a consequence, the hypoflexid was reduced, and the talonid basin became more prominent. However, a minor occlusion between the paracone and the hypoflexid occurs in the tribosphenic molars.

1.4 Tooth-wear

During the chewing process, teeth are exposed to mechanical stresses and strains. Due to these mechanical stresses and strains, teeth get worn down. This results in loss of tooth material (enamel and dentin) and leveling of the tooth surface, and sometimes whole chunks of the teeth can be chipped off. The cause of mechanical wear can be subdivided into two categories: attrition and abrasion (Grippo et al., 2004; Barbour and Rees, 2006).

Abrasion, in terms of tooth wear, is the physical irreversible removal of enamel and dentine due to the contact of tooth-exogenous agent-tooth contact. In this process, the abrasive nature of the diet plays a major role in the form and intensity of the wear. While enamel undergoes a slow removal because of its hardness, the softer dentine will be removed more quickly. The difference in hardness is the result of the varying organic and chemical compositions of these two materials. Enamel consists of crystalline calcium phosphate (95%-97%; ($Ca_5OH[PO_4]_3$), mucopolysaccharides (up to 4%) and water.

Dentine, on the contrary, contains phosphoric apatite crystallites (up to 70% $Ca[Ca_3(PO_4)2]_3(OH)_2$), collagen (20%) and water (10%) (Chun et al., 2014).

For this reason, enamel ranks 5 on Mohs scale (Knoop hardness of 200-500) and dentine falls between 2 and 3 on Mohs scale (Knoop hardness of 40-70) (Meredith et al., 1996). In progressing abrasion the varying hardnesses cause discontinuities or steps between dentine and enamel (Greaves, 1973; Rensberger, 1973; Costa and Greaves, 1981). In the case of “symmetrodontans”, these steps are mainly visible on areas of apical wear. Apical wear in these taxa originated mainly by puncture-crushing the prey with almost no tooth-tooth contact. Crompton and Hiiemäe (1970) observed that during puncture-crushing, the prey was pre-comminuted and prepared for the actual mastication. The puncture-crushing is one type of the power stroke (see chapter 1.5).

Attrition, in terms of tooth wear, describes the physical process, in which enamel or dentine is removed by direct tooth-tooth contact, during chewing (Eccles, 1982; Grippo et al., 2004; Barbour and Rees, 2006). The results of attritional wear are polished, light-reflecting, flattened areas called wear facets. Wear facets are developed at areas, where upper and lower teeth get in contact and slide past each other (Butler, 1972). This way, wear facets on the lower teeth have matching antagonistic facets on the opposing upper teeth. Microscopic particles, which are sitting between these counterparts, cause faint scratches on the polished wear facets. These faint scratches are called striations (Butler, 1972). Sources of the microscopic particles are for example dust, fine sediments, and hard constituents of the food. The constituents of the latter are for instance phytoliths of plants or mineral inclusions of insect exoskeletons. (Walker et al., 1978; Evans and Sanson, 2005; Sanson et al., 2007; Hummel et al., 2011). The orientation of the striations and facets are usable indicators to reconstruct the relative movement of the lower jaw during the chewing cycle (Butler, 1972; Kay and Hiiemäe, 1974; Schultz and Martin, 2014). In addition, the extent of attrition facets and their characteristics can be used to categorize specimens into dental age stages (Litonjua et al., 2003; Anders et al., 2011).

A further cause of loss of tooth material is corrosion. Corrosion means the weakening, and destruction of the tooth surface by chemical or electrolytic processes (Grippo et al., 2004).

Attrition, abrasion, and corrosion, may occur simultaneously, sequentially or alternately during the dynamics of inter-occlusal activity (Grippo et al., 2004).

1.5 Mastication

Chewing food is important for sufficient assimilation of nutrients. The smaller the food particles, the larger the attacking area for the digestive enzymes. It is important to note, that just puncturing the prey also assists in digestion (Prinz et al., 2003). The basic principle of chewing starts with an orthal movement of the lower jaw towards the upper jaw. Subsequently, food is trapped in-between the teeth and gets under pressure. The size and shape of the contact areas determine the type of deformation and division of food items, and the subsequent direction of movement of the lower jaw (Schultz, 2012). The different types of deformation and division are classified as shearing, (opposing) crushing, and grinding (Simpson, 1933; Kay and Hiiemäe, 1974; Ungar, 2015).

Crompton and Hiiemäe (1969, 1970) subdivided the chewing cycle into three phases: The preparatory stroke, the power stroke, and the recovery stroke. The preparatory stroke is the phase, in which the lower jaw moves upwards and medially, ending with the first tooth-exogenous agent-tooth or tooth-tooth contact (Crompton and Hiiemäe, 1969, 1970; Kay and Hiiemäe, 1974). The power stroke is subdivided into a crushing-puncture stroke and a shearing stroke. During the crushing-puncture stroke, food is divided and prepared in adequate pieces to get chewed (Crompton and Hiiemäe, 1970). While the food is being punctured-crushed, teeth normally are not getting in contact. The shearing stroke starts with the first tooth-tooth contact. Mills (1955) and Kay and Hiiemäe (1974) subdivided the shearing stroke further into two phases. The first phase is the buccal phase (Mills, 1955) or phase I (Kay and Hiiemäe, 1974), which involves an upward movement until maximum intercuspation (centric occlusion; see chapter 2.6) of the dentition is reached. The subsequent phase is the lingual phase (Mills, 1955) or phase II (Kay and Hiiemäe, 1974), which comprises the movements after the maximum intercuspation until the recovery stroke starts. It has always been assumed that phase II only occurs during mastication, in which tribosphenic molars and their evolutional successors are involved. However, Schultz et al. (2017a) re-examined *Docodon victor* and found evidence, that *Docodon victor* and presumably, therefore, other pretribosphenic taxa also had a phase II. After the shearing stroke, when the facets lose contact and the downward movement of the lower jaw begins, the recovery stroke starts. The recovery stroke ends at the point where the maximum gap between the jaw apparatuses is reached during mastication, and the cycle starts again. It should be noted, that some researchers use the terms power stroke and shearing stroke synonymously.

Most of the extant mammals perform a unilateral, and transverse chewing motion during one cycle, in which only one side of the jaw, the active side, is processing food, whereas the non-active side, the balancing side, is only in motion without any food processing involvement (Crompton and Hiiemäe, 1970; Kay and Hiiemäe, 1974). This can also be

presumed for the “symmetrodontans”. Due to the fact that most jaw findings of Mesozoic mammals are isolated hemimandibles (Cifelli and Madsen, 1999), it can be assumed that the symphysis was unfused in most taxa (Crompton and Hylander, 1986). This leads to the hypothesis, that the mastication in “symmetrodontans” and other Mesozoic mammals involved rotation of the active hemimandible around the longitudinal axis (Patterson, 1956; Oron and Crompton, 1985; Crompton and Hylander, 1986; Crompton, 1995; Lieberman and Crompton, 2000; Bhullar et al., 2019).

2 Terminology and conventions

A variety of terminologies and conventions has been established regarding tooth morphology. The following chapter is a summary of the cusp terminology and facet nomenclature, which is used in the present study. In addition, guidelines concerning the use of anatomical terms of location, mandible movements, and anatomical abbreviations are defined.

2.1 Anatomical terms of location/directions

To describe the location and orientation of tooth structures the anatomical directions are adapted from Lucas (2004) and Hillson (2005) (Fig. 4). In addition, “apical” is used to describe the direction towards the tip of a tooth cusp (apex), and “basal” as the direction towards the root (Smith and Dodson, 2003). Upper teeth are abbreviated with uppercase letters, lower teeth with lowercase letters. The number behind a letter refers to the tooth position (e.g., M3 = third upper molar).

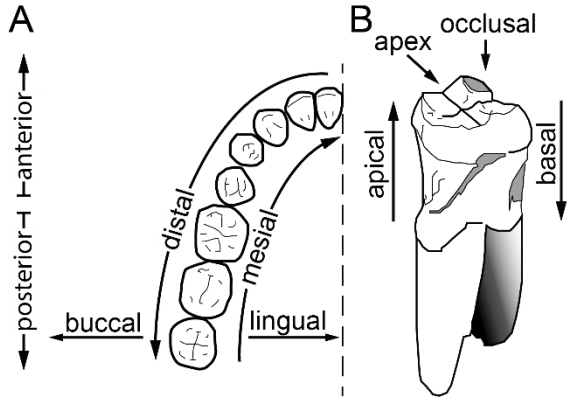

Fig. 4: The anatomical directions in occlusal view (A), and in lateral view (B). (A: Modified from Lucas, 2004; B: Modified from Smith and Dodson, 2003)

2.2 Terminology of the mandible movements during mastication

The terminology of Grossnickle (2017) was adopted to determine the mandible movements during mastication:

- **Pitch** means rotation around a medio-laterally oriented axis through both condylar processes. This rotation results in an up-/downward movement of the mandible.
- **Yaw** describes a lateral movement of the mandible, in which the active site moves lingually. This is done by rotating the mandible around a dorsoventrally oriented axis.
- **Roll** is the rotation around a longitudinal axis that connects the jaw joint and the mandibular symphysis of one hemimandible. This movement rotates the tooth row of the active hemimandible towards lingual. If the symphysis is unfused, like in Mesozoic mammals, the hemimandibles rotate independently.

2.3 Cusp terminology and tooth structure conventions

Osborn (1888) realized that the cusps of teeth of early mammals can be homologized with those of the tribosphenic molar. He developed a standardized designation for the molar cusps. Throughout history, this terminology was modified and adjusted to newly gained knowledge. For instance, Patterson (1956) later recognized that the main cusp of the upper pretribosphenic molar, which Osborn (1888) called protocone, is not homologous with the protocone of the tribosphenic molar. Consequently, Patterson proposed to call the pretribosphenic cusp paracone (eocone). Basically, The cusp terminology of Crompton (1971) is used in this study (with some exceptions), which is a combination of the terminologies established by van Valen (1966) and Szalay (1969). Terms that were defined by other authors and are not from Crompton's terminology are herein summarized:

The disto-labial cusp of the upper molars is called "C" according to Kielan-Jaworowska et al. (2004) instead of "c" as in Crompton (1971).

Hu et al. (1997) argued that the upper molar mesio-labial cusp of the zhangheotheriid *Zhangheotherium tricuspidens* is too large and positioned too far lingually to be homologous to cusp B (stylocone). They termed this cusp B' and regarded it either as homologous to a much smaller cusp in a comparable position in other "symmetrodontans" or a neomorphic cusp. Therefore, in the present study, the designation B' for the mesio-labial cusp of the upper molars was adopted for *Maotherium sinense*, as well as the cusp terminology of *Maotherium sinense* from Rougier et al. (2003).

The cusp situated distally to the metaconid is termed cusp d according to Davis (2011). Cusp d is either homologous to the hypoconulid (Butler, 1939; Rougier et al., 2007b) or to the hypoconid (Mills, 1964; Lopatin and Averianov, 2006).

The accessory molar cusps of woutersiids are difficult to homologize, therefore the cusp terminology of Butler (1997) was adopted (see also Luo and Martin, 2007). Due to their position and orientation, the molar main cusps were homologized with those of the other “symmetrodontans” (see Tab. 4).

Tab. 4: Cusp homology of the upper and lower main cusps of *Woutersia* sp.

upper molars	
cusp A	paracone
cusp B	stylocone
cusp C	metacone
lower molars	
cusp a	protoconid
cusp b	paraconid
cusp c	metaconid

The term cingulum refers to an enamel ridge along the base of an upper molar crown and cingulid to an enamel ridge along the base of a lower molar crown (Butler, 1978).

Gregory (1922) distinguished between primary trigon in “Pre-Tribosphenida” and secondary trigon in Tribosphenida; the primary trigon is spanned between paracone, stylocone, and metacone, whereas the protocone, paracone, and metacone form the secondary trigon. In this study, the term trigon refers to the primary trigon. The basin surrounded by the protoconid, paraconid, and metaconid is called trigonid (Gregory, 1922).

With a few exceptions, the cusp acronyms were taken from Schultz et al. (2017b), see list of abbreviations (page XI).

2.4 Contact area, crest, and cingulum/cingulid nomenclature

To describe virtual abrasion or attrition contact areas (collision areas) the modular wear facet nomenclature of Schultz et al. (2017b) was applied and modified. The modular contact area labeling system basically consists of two modules, the first module is the acronym for the cusp, and the second module is the acronym for the position (see abbreviation list, page XI). For example, PA-mb stands for a mesio-buccally positioned collision area on the paracone. The dominant direction of the collision area position is labeled first. This way, PA-mb means the collision area on the paracone is mainly lying mesially but has a (slight) buccal shift. In some cases a third module was needed to define a position more precisely, e.g. PA-mb-a means the contact area is mesio-buccally positioned at the paracone tip (apex). If a collision area extends over two or more cusps, the acronyms are composed like this: PA*ME*MTS-dl. This abbreviation stands for a disto-lingually oriented collision area below the paracone, metacone, and metastyle.

Two overlapping collision areas, which are formed sequentially by different antagonists, are numbered consecutively, for instance, pr-db (1), pr-db (2).

Two occluding antagonistic collision areas are combined as pairs: pr-d/PA-m, which means that the distal area of the protoconid occludes with the mesial side of the paracone.

The Modular Contact Area Labelling System was further extended to determine contact areas on crests, cingula, and cingulids. The acronym [C]PA-m stands for a mesial crest of a paracone. In order to name connected crests, the abbreviations of the crests were combined like [C]PA~MTS. This abbreviation depicts a crest, which is connecting the paracone and metastyle. If another cusp sits on the crest between the two cusps, like the metacone in *Dryolestes leiriensis*, the nomenclature can be extended: [C]PA~ME~MTS. An uppercase [C] refers to a crista, whereas a lowercase [c] refers to a cristid. Cingula [CG] and cingulids [cgd] are described likewise. For example, the complete upper lingual cingulum of *Maotherium sinense* is labeled as [CG]CPB'_PA_ME. To refer to only the lingo-mesial part of the cingulum, then the acronym [CG]CPB'_PA is used. If the contact area is restricted to a small cingulum/cingulid area below a cusp, the abbrevation looks like [CG]PA-d, which in this case depicts the cingulum area below the distal area of the paracone.

2.5 Definition of the food comminution types (masticatory operations), with remarks to fracture and loading geometry

The purpose of mastication is to fracture food into small bits, till it can be swallowed and sufficiently digested. Two principles are often addressed as important factors for comminuting food, first the loading geometry, which includes strains and stresses, and second the fracture geometry (Lucas, 1979, 2004; Berthaume, 2016; Thiery et al., 2017). These principles are the basics of materials science.

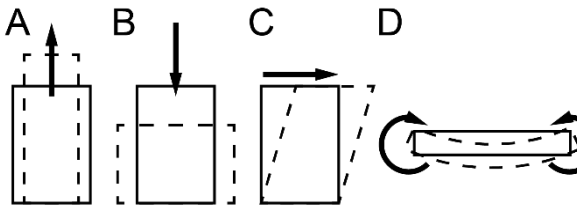

Fig. 5: The basic types of loads, tension (A), compression (B), and shear (C). De facto, this loads occurs in combination, like bending (D), which is a combination of tension and compression. The arrows indicate the way in which the loads are applied. The solid lines represent the undeformed shape of an object and the hashed lines represent the object shape after deformation. (Modified from Berthaume, 2016)

Three basic types of loading geometry exist: tension, compression, and shear (Fig. 5). These "pure" loadings could potentially lead to fracture or fragmentation of solids. Tensile loading acts directly away from an object in a perpendicular direction to the surface. Compressive loading is the opposite of tensile loading and acts towards the object's surface. Shear loading involves a force, which is directed parallel to the object's surface. All loading regimes can occur solitary or in combination like in bending, in which tension and compression are involved. However,

in mastication, only compression is readily available for comminuting food. But during compression, all these loadings can lead to a combination of compressive, tensile, and shear strains because of internal stresses (Lucas, 2004).

Fracture geometry is divided into three basic modes of stress (Wang, 1996) (Fig. 6). Each mode describes a possible direction in which a crack could grow through an inherent micro-crack, which compromises the strength of an object (Berthaume, 2016).

- **Mode I** is the “crack opening” mode, in which tensile stresses are involved. The tensile stresses cause that the crack surfaces are pulled apart in front of the crack tip. An example of mode I fracture is cleaving wood.
- **Mode II** (sliding mode) involves an in-plane shearing. Shear stresses force a crack to propagate in a plane like at a punch press or a shear metal shearing machine.
- **Mode III** (tearing mode) entails out of plain stresses, in which a crack is propagating through an out of plane shear force like along scissor blades.

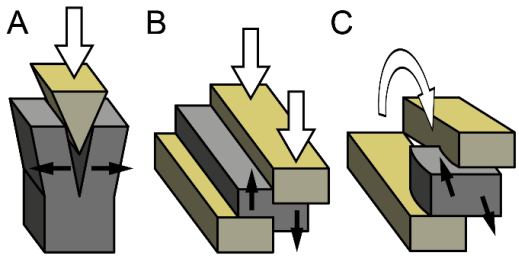

Fig. 6: Modes of fracture. A: Mode I, the crack opening mode. The crack propagates mainly through tensile forces. B: Mode II, the crack mainly propagating through an in plane shear force. C: Mode III, the crack mainly propagate through an out of plane shear force. The white arrows indicate the direction of the applied load. The black arrows indicate the direction of the resulting force. (Modified from Berthaume, 2016)

According to Berthaume (2016) and Thiery et al. (2017), these three modes of fractures basically explain how teeth work. Lucas (2004) on the contrary argued, that none of these fracture modes explain how teeth comminute, for example, elastic food, under the influence of tensile (or compressional) stresses. In his opinion only the study of mechanisms of fracture prevention in foods matters for understanding tooth form and how the form influences the fracturing of food. Furthermore, he argues that terms like shearing, grinding, crushing, puncturing, squeezing, cutting, etc. are only simplifications of complex actions and that these terms have no analytic value. Nevertheless, these “break-down” synonyms help to describe specific patterns of tooth/food interactions, and in this study, the following terms of actions are used to describe how “symmetrodontan” dentitions break down food:

- **Crushing** is executed by an orthal compressive load until the food surface structure gives in under the pressure and the crack(s) freely propagate(s) in any direction (Nutcracker).
- **Puncturing** is executed by an orthal compressive load, and the crack(s) propagate(s) in front, or along the displacement, of the cusp(s) (Jackhammer)**.**
- **Shear-cutting** divides food via two sharp crests (scissors, cigar cutter).
- **Plane-shearing** is food comminution between two plane surfaces, which moves past each other.

- **Blunt-shearing** involves two blunt crests, which move past each other. The process is similar to shear-cutting, but blunt-shearing tears food items apart along the blunt crests rather than cutting it.
- **Compressional-shearing** is an action in which food gets compressed between two tooth structures.

All actions are performed by specialized tooth structures, comparable to tools and target specific, mechanical food properties (Thiery et al., 2017).

2.6 Remarks on the terms “centric occlusion” and “maximum intercuspation”

In chapter 1.5 “centric occlusion” and “maximum intercuspation” were addressed without further explanation, but clarification is needed for these terms.

A dentition’s “centric occlusion” is defined as the position in which the lower jaw is more or less symmetrically placed in the sagittal midline. “Maximum intercuspation” is a state of a dentition, in which for example the protocones (or all cusps in general) are fully occluded into their associated talonid basins (or interdental spaces). In primates (including humans) “centric occlusion” coincides with the “maximum intercuspation” due to the immobile symphysis. Therefore in dentistry, the terms “centric occlusion” and “maximum intercuspation” are used synonymously (Davies and Gray, 2001). Crompton and Hiiemäe (1970) realized that this is not the case in taxa with a mobile symphysis, which perform a unilateral chewing movement. In mammals with a unilateral movement the state of “maximum intercuspation” is only given for the active side. They proposed to extend the term “centric occlusion” with the preposition “unilateral” for taxa with a mobile symphysis. In addition, they suggest to indicate the active side (“left”/”right”) if it is necessary. Kay and Hiiemäe (1974) argued that, due to the preposition, the synonymy of “centric occlusion” and “maximum intercuspation” is given again, as it refers only to one side of the dentition. For taxa with a tribosphenic dentition, the “maximum intercuspation” is the point, in which phase I ended and phase II started. For most pretribosphenic taxa the term “maximum intercuspation” is problematic due to the absence of phase II. Even if “maximum intercuspation” refers only to the maximum collision area of the upper and lower pretribosphenic dentition this term cannot be used in the sense of the end of the shearing stroke. The reason for that is that in mammals with pretribosphenic molars the dentition´s maximum collision area can occur before the end of the shearing stroke (e.g. *Dryolestes leiriensis*).

Herein, the end of the shearing stroke for pretribosphenic taxa is defined as the “maximum mandibular closure”, and the point of “maximum intercuspation” is equivalent to the highest

value of the upper and lower molars total collision area, which can be determined by the OFA software (Kullmer et al., 2009).

3 Material and methods

3.1 Examined material

“Symmetrodontan” fossils are quite rare, and it is often difficult to loan them for study from collections. Due to this fact, the material had to be examined on site in several natural history museums. The following museums were visited: Museum of Northern Arizona (Flagstaff, USA), National History Museum of Utah (Salt Lake City, USA), and Sam Noble Museum (Norman, Oklahoma, USA). During the visits, molds of the most informative tooth-bearing jaw fragments and isolated teeth were taken. Several specimens were loaned from UMNH, OMNH, and YFGP. In addition, some “symmetrodontan” teeth and casts of teeth were available in the Institute of Geosciences, University of Bonn. Furthermore, Prof. Richard Cifelli of the OMNH provided µCT-data of some teeth. For more details see Table S1, Appendix. The teeth, which deemed informative for this study were selected according to three main criteria:

- The first criterion is the extent of tooth wear and whether the wear provides information to reconstruct a chewing movement of the masticatory apparatus.
- The second one is the completeness of the teeth. Damaged teeth are almost useless to evaluate the contact areas of the teeth during chewing.
- The third criterion is the dental position of the teeth within a taxon. To reconstruct a proper chewing cycle with the OFA, one upper molar, which matches at least the position of one lower molar, is needed.

All in all, it was possible to examine and collect material of five “symmetrodontan” families (Kuehneotheriidae, Spalacotheriidae, Zhangheotheriidae, Woutersiidae, Tinodontidae), and some “Symmetrodonta” indet. The provenance of these fossils is Belgium, Spain, France, Great Britain, China, and the USA. All studied specimens are listed in Table 5.

Tab. 5: List of the studied “symmetrodontans”.

Taxon	Inventory number	Locality	Description
Kuehneotheriidae	HLV 1R	Belgium, Habay la Vieille	Mx
Kuehneotheriidae	RAS 786	France, Rosieres aux Salines	mx
Kuehneotheriidae	RAS 796	France, Rosieres aux Salines	Mx
Kuehneotheriidae	RAS 813	France, Rosieres aux Salines	px
Kuehneotheriidae	RAS 847	France, Rosieres aux Salines	Px or px
Kuehneotheriidae	RAS 850	France, Rosieres aux Salines	px
Kuehneotherium praecursoris	NHM PV M 19143	Great Britain, Pontalun Quarry 1	m3
Kuehneotherium praecursoris	NHM PV M 19168 ? / C 857	Great Britain, Pontalun Quarry 1	M
Kuehneotherium praecursoris	NHM PV M 19771	Great Britain, Pontalun Quarry	M4
Kuehneotherium stanislavi,	SNP 75 L	France, Saint Nicolas de Port	Mx
Maotherium sinense	YFGP 1724	China, Yixian Formation, Lujatun Member (Jehol Group)	maxilla fragment with M2-M3; mandible fragment with 3p, m1-m5
Peralestes longirostris (*Spalacotherium tricuspidens*)	NHM PV OR 47740	Great Britain, Durdlestone [Durlston] Bay	maxilla fragment with 1P and M1-M6
Spalacolestes cretulablatta	OMNH VP 026688	Utah, Cedar Mountain Fm.	M4
Spalacolestes cretulablatta	OMNH VP 026693	Utah, Cedar Mountain Fm.	M4
Spalacolestes cretulablatta	OMNH VP 027421	Utah, Cedar Mountain Fm.	mandible fragment with m4-m5
Spalacolestes cretulablatta	OMNH VP 029600	Utah, Cedar Mountain Fm.	mandible fragment with m4-m7
Spalacolestes cretulablatta	OMNH VP 029611	Utah, Cedar Mountain Fm.	M2
Spalacolestes cretulablatta	OMNH VP 030611	Utah, Cedar Mountain Fm.	M4
Spalacolestes cretulablatta	OMNH VP 030627	Utah, Cedar Mountain Fm.	m4
Spalacolestes cretulablatta	OMNH VP 033043	Utah, Cedar Mountain Fm.	m5
Spalacolestes cretulablatta	OMNH VP 033060	Utah, Cedar Mountain Fm.	M3
Spalacolestes cretulablatta	OMNH VP 033231	Utah, Cedar Mountain Fm.	M4

Tab.5: List of the studied “symmetrodontans”, continued.

Taxon	Inventory number	Locality	Description
Spalacolestes inconcinnus	MNA V 6247, OMNH VP 69062	Utah, Cedar Mountain Fm.	Px?
Spalacolestes inconcinnus	OMNH VP 033027	Utah, Cedar Mountain Fm.	dp3?
Spalacolestes inconcinnus	OMNH VP 033034	Utah, Cedar Mountain Fm.	M2
Spalacolestes inconcinnus	OMNH VP 033897	Utah, Cedar Mountain Fm.	m3
Spalacolestes inconcinnus	OMNH VP 033911	Utah, Cedar Mountain Fm.	maxilla fragment with M4
Spalacotheridium mckennai?	MNA V 6046, OMNH VP 025524	Utah, Straight Cliffs Fm.	m3?
Spalacotheridium noblei	OMNH VP 025828	Utah, Cedar Mountain Fm.	m4
Spalacotheridium noblei	OMNH VP 026692	Utah, Cedar Mountain Fm.	M4
Spalacotheridium noblei	OMNH VP 027261	Utah, Cedar Mountain Fm.	m3
Spalacotheridium noblei	OMNH VP 027461	Utah, Cedar Mountain Fm.	M6
Spalacotheridium noblei	OMNH VP 030623	Utah, Cedar Mountain Fm.	m2
Spalacotheridium noblei	OMNH VP 033041	Utah, Cedar Mountain Fm.	m3
Spalacotheridium noblei	OMNH VP 033053	Utah, Cedar Mountain Fm.	m5
Spalacotheridium noblei	OMNH VP 033061	Utah, Cedar Mountain Fm.	M2
Spalacotheridium noblei	OMNH VP 033895	Utah, Cedar Mountain Fm.	M3
Spalacotheridium noblei	OMNH VP 033900	Utah, Cedar Mountain Fm.	m3
Spalacotheriidae	MNA V 6305, OMNH VP 025531	Utah, Straight Cliffs Fm.	maxilla fragment with Px
Spalacotheriidae	OMNH VP 030610	Utah, Cedar Mountain Fm.	Mx
Spalacotheriidae	OMNH VP 032953	Utah, Cedar Mountain Fm.	Mx
Spalacotheriidae	OMNH VP 071070	Wyoming, Morrison Fm.	mx
Spalacotheriidae	OMNH VP 071071	Wyoming, Morrison Fm.	mx
Spalacotheriidae	OMNH VP 071072	Wyoming, Morrison Fm.	Mx
Spalacotheriidae	OMNH VP 071073	Wyoming, Morrison Fm.	Mx

Tab.5: List of the studied “symmetrodontans”, continued.

Taxon	Inventory number	Locality	Description
Spalacotherium evansae	DORCM GS 0380	Great Britain, Isle of Purbeck	mx
Spalacotherium evansae	DORCM GS 0684	Great Britain, Isle of Purbeck	Mx
Spalacotherium evansae	DORCM GS 1075	Great Britain, Isle of Purbeck	mx
Spalacotherium evansae?	DROCM GS 0689	Great Britain, Isle of Purbeck	Mx
Spalacotherium henkeli	IP FUB TH 11	Spain, Galve	m1
Spalacotherium henkeli	IP FUB TH 12	Spain, Galve	m1
Spalacotherium henkeli	IP FUB TH 13	Spain, Galve	M5
Spalacotherium henkeli	IP FUB TH 14	Spain, Galve	M5
Spalacotherium henkeli	IP FUB TH 15	Spain, Galve	Px
Spalacotherium henkeli	IP FUB TH 17	Spain, Galve	Px
Spalacotherium tricuspidens	NHM PV M 5633	Great Britain, Isle of Purbeck	mandible fragment with c and 2p
Spalacotherium tricuspidens	NHM PV OR 46019	Great Britain, Isle of Purbeck	mandible fragment with 4m
Spalacotherium tricuspidens	NHM PV OR 47750	Great Britain, Isle of Purbeck	mandible fragment with 5m
Spalacotheroides bridwelli	FMNH PM 0933	Texas, Greenwood Canyon	mandible fragment with mx
Spalacotheroides bridwelli	FMNH PM 1133	Texas, Greenwood Canyon	mx
“Symmetrodonta” indet.	MNA V 4630, OMNH VP 023811	Utah, Wahweap Fm.	Mx
“Symmetrodonta” indet.	MNA V 6224, OMNH VP 69059	Utah, Dakota Fm.	Mx
“Symmetrodonta” indet.	MNA V 6342, OMNH VP 69067	Utah, Dakota Fm.	mx
“Symmetrodonta” indet.	MNA V 6364	Utah, Straight Cliffs Fm.	px
“Symmetrodonta” indet.	MNA V 6433, OMNH VP 69060	Utah, Dakota Fm.	mx
“Symmetrodonta” indet.	MNA V 6796, OMNH VP 69058	Utah, Dakota Fm.	px
“Symmetrodonta” indet.	SNP 16	France, Saint Nicolas de Port	m
“Symmetrodonta” indet.	UMNH VP 12810	Utah, Loc. 99	mx

Tab.5: List of the studied “symmetrodontans”, continued.

Taxon	Inventory number	Locality	Description
“Symmetrodonta” indet.	UMNH VP 12860	Utah, Loc. 420	mx
“Symmetrodonta” indet.	UMNH VP 12861	Utah, Loc.420/MNA 1187	mx
“Symmetrodonta” indet.	UMNH VP 14147	Utah, Loc. 424	Mx
“Symmetrodonta” indet.	UMNH VP 14151	Utah, Loc. 424	mx
“Symmetrodonta” indet.	UMNH VP 17294	Utah, Loc. 424	mx
Symmetrodontoides canadensis	OMNH VP 066370	Montana, Eagle Fm.	m1
Symmetrodontoides canadensis	OMNH VP 066371	Montana, Eagle Fm.	m4
Symmetrodontoides canadensis	OMNH VP 066372	Montana, Eagle Fm.	m6 or m7
Symmetrodontoides canadensis	OMNH VP 066373	Montana, Eagle Fm.	posterior px
Symmetrodontoides canadensis	OMNH VP 066374	Montana, Eagle Fm.	px
Symmetrodontoides foxi	MNA V 4522; OMNH VP 023800	Utah, Wahweap Fm.	m7
Symmetrodontoides foxi	MNA V 4653, OMNH VP 023814	Utah, Wahweap Fm.	Mx
Symmetrodontoides foxi	MNA V 6461	Utah, Wahweap Fm.	m7
Symmetrodontoides foxi	OMNH VP 020135	Utah, Wahweap Fm.	m4
Symmetrodontoides oligodontos	MNA V 6047; OMNH VP 025525	Utah, Straight Cliffs Fm.	mx?
Symmetrodontoides oligodontos	MNA V 6048; OMNH VP 025526	Utah, Straight Cliffs Fm.	M1 or M2
Symmetrodontoides oligodontos	MNA V 6755; OMNH VP 025538	Utah, Straight Cliffs Fm.	mx
Symmetrodontoides oligodontos	OMNH VP 029040	Utah, Straight Cliffs Fm.	M2
Thereuodon taraktes	DORCM GS 419	Great Britain, Isle of Purbeck	deciduous teeth
Thereuodon taraktes	DORCM GS 665	Great Britain, Isle of Purbeck	deciduous teeth
Thereuodon taraktes	DORCM GS 679	Great Britain, Isle of Purbeck	deciduous teeth

Tab.5: List of the studied “symmetrodontans”, continued.

Taxon	Inventory number	Locality	Description
Tinodon bellus	YPM VP 011843	Wyoming, Albany County	mandible fragment with m1-4
Tinodon bellus	YPM VP 013644.A, OMNH VP 056826	Wyoming, Morrison Fm.	mandible fragment with 3p, m1-m4
Tinodon lepidus	AMNH 101145	Wyoming, Morrison Fm.	mandible with 1p
Tinodon lepidus	USNM 2131; OMNH VP 056835	Wyoming, Morrison Fm.	mandible fragment with c, 3p, m1-3
Tinodon lepidus	YPM VP 011845	Wyoming, Albany County	mandible fragment with m1, m3
Tinodon lepidus?	YPM VP 013645	Wyoming, Albany County	mandible with fragment mx
Tinodon micron?	DORCM GS 1110 (GS 550)	Great Britain, Isle of Purbeck	px or Px
Woutersia butleri	SNP 082 W	France, Saint Nicolas de Port	Px
Woutersia butleri	SNP 088 W	France, Saint Nicolas de Port	Mx
Woutersia butleri	SNP 517 W	France, Saint Nicolas de Port	mx
Woutersia butleri	SNP 720	France, Saint Nicolas de Port	Mx
Woutersia mirabilis	SNP 052 W	France, Saint Nicolas de Port	Mx
Woutersia mirabilis	SNP 426 W	France, Saint Nicolas de Port	px?
Woutersia mirabilis	SNP RAS 706	France, Saint Nicolas de Port	mx
Woutersia mirabilis	SNP RAS 884	France, Saint Nicolas de Port	Mx
Woutersia mirabilis	SNP RAS 975	France, Saint Nicolas de Port	mx
Woutersia mirabilis?	SNP 719	France, Saint Nicolas de Port	Mx
Woutersia mirabilis?	SNP 9FW	France, Saint Nicolas de Port	mx

3.2 Molding and casting procedure

The molds of the examined fossils were made by using the two-component silicone Provil novo light™ (Heraeus Kulzer). Provil novo light is a product used by dentists and dental laboratories. With its high impression molding accuracy (≤ 0.1 mm), it is especially suitable for small tooth wear features such as striations. Provil novo light is coated onto the teeth with a dispensing gun and hardens within a few minutes into a flexible material. Afterward, each mold was encapsulated with Provil novo Putty Regular. This is another two-component silicone, which is firmer than Provil novo light, and serves as a supporting jacket. The two components of Provil novo Putty Regular were kneaded by hand.

To manufacture casts of the molds a two-component epoxy resin was used. The resin (RenLam™ M-1; Huntsman Advanced Materials) and the curing agent (Ren HY 956; Huntsman Advanced Materials) were mixed, and the grey pigment Araldite DW 0137 (Huntsman Advanced Material) was added. At first, the interior walls of the molds were wetted with the resin, and the molds were placed in a vacuum chamber to remove air inclusions. After the inclusions were removed, the complete molds were then poured out with the epoxy resin, and again exposed to a vacuum. The resin hardens within 24 hours.

3.3 Scanning electron microscope study

To study tooth wear, a scanning electron microscope (SEM) (CAMSCAN MV 2300, Electron Optic Services) was used. The advantage of an SEM over a reflected light microscope is the higher resolution and greater depth of field. For this reason, SEM is an appropriate choice to study really small objects. A disadvantage is that an object of interest has to be sputtered with a very thin layer of gold to improve conductivity. Due to the fact that the gold layer cannot be easily removed, it was not possible to study original fossil material. Thus, only casts were examined with the SEM.

3.4 Reflected light microscopy

The loaned fossils were studied with a reflected light microscope (Axio Zoom.V16; AxioCam HRc, Zeiss), as there was no permission to sputter coat them or to make casts. For imaging, z stack photos were taken and merged into one picture to achieve a better depth of field. The imaging was performed with the software ZEN Pro (Zeiss).

3.5 Virtual 3D-model generation procedure

To create 3D-models of the molars, either the original material or molds were scanned with a high-resolution computed tomography (µCT) scanner (v|tome|x s 240; phoenix|x-ray General Electrics). Molds, instead of casts, were used to perform the µCT-scan because the silicone molding material has a higher density than the epoxy resin cast material. This results in better contrast and therefore in a higher quality of the µCT-data. With the µCT data, virtual 3D-models were created using the software datos|x (GE Electronics phoenix|x-ray), VGSTUDIO MAX (Volume Graphics) and AVIZO (Visualization Sciences Group, VSG). For post-processing, measurements, and analyses, the software Polyworks (InnovMetric Software Inc.) was used. During the post-processing of the polygonal 3D-models, some teeth were mirrored, displaced tooth fragments were repositioned as accurately as possible, and gaps were carefully closed (Fig. S1, Appendix). The file types STL and PLY were used for further processing of the 3D models.

3.6 Orientation of virtual “symmetrodontan” molars in a virtual space

To define a reference plane for measurements and analyses, all polygonal models had to be oriented in the same way in virtual space. One method to get this reference plane is to place a *best-fit* plane through the cervical line (Ulhaas, 2006; Engels, 2011; Anders, 2011). But this method is not feasible for “symmetrodontans”. They do not possess a distinct cervical line. Subsequently, Schultz (2012), and Schwermann (2015) developed other methods to define a reference plane, but these methods cannot be used for “symmetrodontans” either. In Schultz’s (2012) method, an important structure for producing the reference plane is a central root below the trigonid, and the method of Schwermann (2015) is based on the presence of the paraconid and the visibility of the crown root transition. These structures are absent in "symmetrodontans". Hence, a new orientation method for “Symmetrodonta” was developed in the current study. The aim was to develop a routine, which can be applied to almost all “symmetrodontan” molariforms regardless of their condition of conservation or morphology. The only requirement for producing a reference plane for “symmetrodontan” molars is the presence of an intact protoconid. This method was performed with Polyworks and was successfully tested with molars of spalacotheriids, zhangheotheriids, kuehneotheriids, and woutersiids. The 3D-models were oriented as follows:

Step one:

Two cross sections were created, which have to be as parallel as possible to the occlusal view. The position of the first cross section is immediately below the protoconid apex at an unworn level. The second cross section is at the base of the protoconid directly above the higher indentation between protoconid and metaconid, or protoconid and paraconid (Fig. 7, A).

Step two:

Between 30 to 50 points were set in a regular distance onto the upper cross section outline. Then the points were hidden. This point setting procedure was performed three times, and an average point (**POINT 1**) of the three sets of points was created. This procedure was executed with the second cross section, too, which results in a second point (**POINT 2**). Next, a vector was created (vector **um**) connecting **POINT 1** and **POINT 2**. The Vector **um** points apically (Fig. 7, A).

Step three:

A point was set onto the most mesial position of the lower cross section and hidden. Next, a point onto the most distal position of the lower cross section was set and hidden, too. This was repeated nine times, and an average point (**POINT 3**) of these 20 points was created. **POINT 3** was duplicated (**POINT 3.1**) and projected onto vector **um**. A vector connecting **POINT 3** and **POINT 3.1** (vector **vm**) was created. The Vector **vm** points buccally for left teeth, and lingually for right teeth (Fig. 7, B).

Step four:

Using vector **um** and **vm**, a plane (**E1)** was created. Then, a vector (**wm**) was set perpendicular to plane **E1,** with its origin in **POINT 3.1**. The vector **wm** points mesially.

Step five:

Plane **E2** was generated by using vector **um** and vector **wm**.

Step six:

Plane **E3** was generated by using vector **vm** and vector **wm** (Fig. 7, C).

Step seven:

This procedure was done for each lower molar of one set (see chapter 3.7 for the definition of a set) and an average of the vectors and planes was created. The average of each type of vector (**average_um**, **average_vm**, **average_wm**), or their corresponding planes (**average_E1**, **average_E2**, **average_E3**) can be used to produce the new coordinate system.

The **x-axis (+)** points mesially, the **y-axis (+)** points buccally (left teeth), respectively lingually (right teeth), and the **z-axis (+)** points apically.

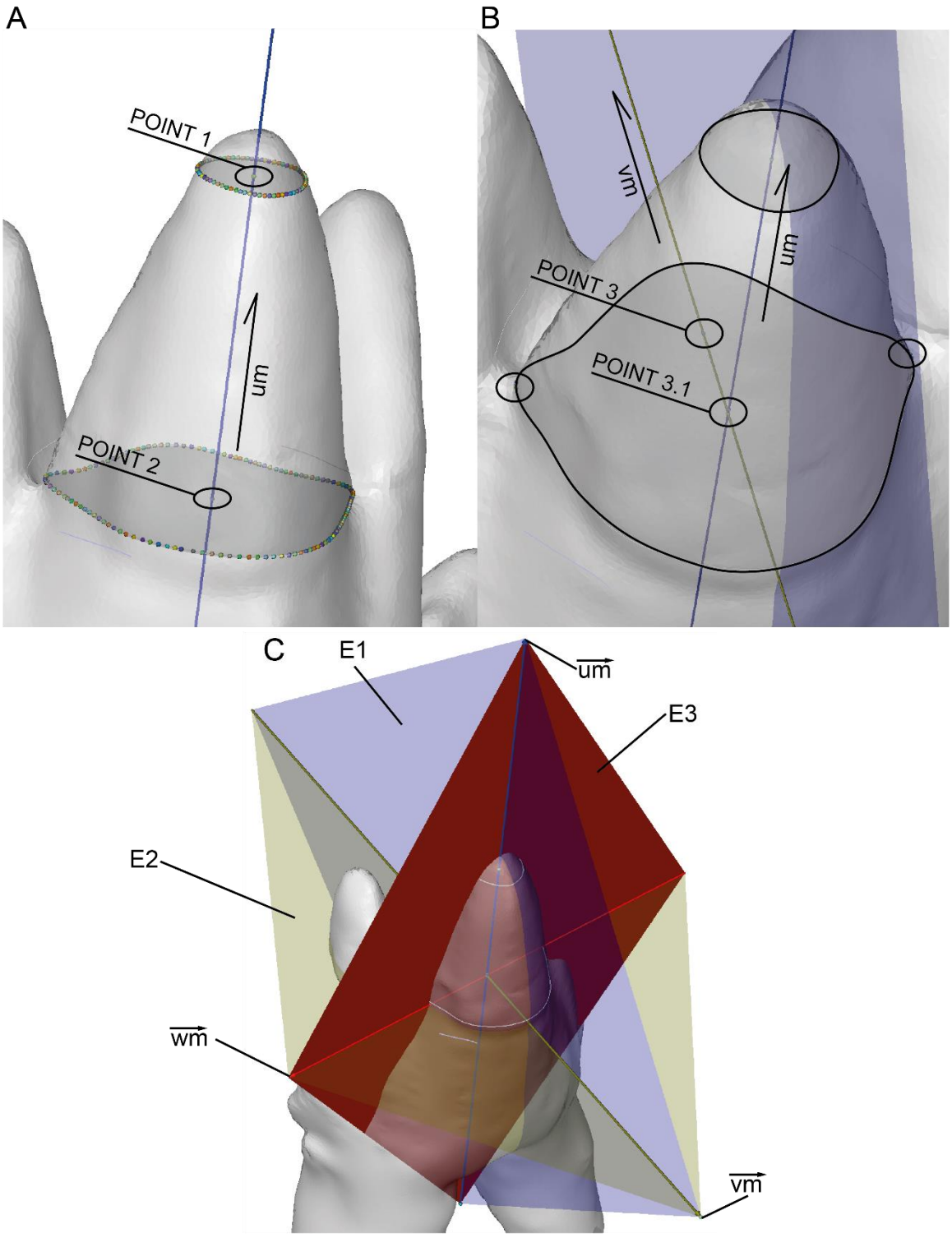

Fig. 7: Important steps in producing a reference plane for "symmetrodontan" molars using the example of *Maotherium sinense* (YFGP1724). A: POINT 1 and POINT 2 are average points of a series of points which were set onto each cross section outlines. The cross sections are depicted in darker grey. Using POINT 1 and POINT 2, vector um was created. B: POINT 3 is the average point of 20 points, which were set onto the most mesial and distal point of the lower cross section (unlabeled circles). POINT 3.1 is a duplicate of POINT 3, which was projected onto vector um. Both points were used to create vector vm. C: The resulting vectors and planes in combination. E1 is created with vector um and vm. Vector wm is perpendicular to E1. E2 is the result of vector vm and wm, whereas E3 was created by um and wm.

3.7 Occlusal Fingerprint Analyser (OFA)

The Occlusal Fingerprint Analyser (ZiFiLoX IT Ltd. & Co. KG) is a simulation software for virtually detecting tooth-to-tooth contact during mastication (Kullmer et al., 2009). To ensure that the results of each OFA project are comparable, the resolution of all 3D-models was standardized by reducing the number of polygon faces. This was done by setting the polygons' average edge length to 0.01 mm. Then, each set of molars was oriented according to the procedure described in chapter 3.6 and roughly brought into maximum mandibular closure. The reduction of the resolution and orientation of the molar sets was performed with Polyworks. Every set comprises one upper and two lower molars of one taxon. After that, a set of 3D-models was imported into OFA and further adjustments, concerning the orientation, were made. With the aid of the SEM and reflective light microscope studies, in which the orientation of striations was determined (see chapter 3.3, and 3.4), a theoretical chewing path (collision path) was implemented. This chewing path was developed by setting several path points into virtual space. These path points represent key positions of the lower molars along important trajectory time steps. During the simulation, the lower molars moved along this theoretical path. When the lower molars encountered the upper one, a deflection occurred, and the lower molars were redirected. Due to the deflection, a new, adjusted, chewing path was created by OFA. The adjusted collision path is influenced by the topographic reliefs of the teeth. In addition to the calculation of the adjusted collision path, the OFA recorded and documented the resulting collision areas of the upper and lower molars for each time step. To perform the analyses, the settings and commands of Schultz and Martin (2014) were adopted (see Tab. S3, Appendix). The same setting was used for each set to ensure the comparability of the data.

Due to the fact that OFA has been continuously developed, a new OFA version (Qt Version: 4.8.4), with an advanced collision path mode was released at the end of this project. The improvement in the advanced mode is the possibility to simulate the rotation of the (hemi) mandible. Instead of setting one point for each key position, there are now three points available for each position, which are at the corners of a triangle. In addition to the position, this triangle describes the orientation of the model in virtual space. With this option, a postulated roll (see chapter 2.2) of the hemimandible was simulated. Therefore, a triangle for each key position was produced by anchoring a point on the protoconid of the anterior lower molar and one on each two most posterior main cusps of the succeeding lower molar. If the inclination of the lower teeth changes from one key position to the next, OFA rotates the lower teeth around this inclination. For this purpose, the advanced mode was first used by Schultz et al. (2017a). [Remark: The OFA projects of this study are available either on the attached CD or in the appendix (online version); c.f. chapter 9]

3.8 Collision areas documented by the OFA

As mentioned in chapter 3.7, the OFA records the collision areas separately for each time step. To get an idea about the extent of the collision areas during the entire chewing cycle, each total collision area had to be mapped by hand. This was done by summing up every single collision area in which the same antagonistic tooth structure was involved. The summing up was done in Polyworks by creating an element for each total collision area from the oriented polygonal model. Each element was assigned to a different color. As far as possible, the same color coding was used for comparable collision areas of the different taxa (see Tab. S2, Appendix).

3.9 Mastication compass

A mastication compass is a 2D visualization of the mandibular movement (mastication path, trajectory path), and combines three aspects of the power stroke (Koenigswald et al., 2013). The first aspect is the number of shearing stroke phases, the second one is the occlusal direction, and the last aspect is the inclination of each phase. This visualization allows the comparison of the mastication modes of different taxa. The direction of an arrow represents the direction of the mandibular closure, and the arrow length displays the inclination of the mandibular movement. If a taxon has a second shearing stroke phase including a change in direction and/or inclination, a second arrow follows the first one (for details see Koenigswald et al., 2013). Due to the fact that in “symmetrodontans”, maximum intercuspation does not coincide with maximum mandibular closure (end of the shearing stroke; see chapter 2.6), the mastication compass as proposed by Koenigswald et al. (2013) was modified for this study. The center of the compass in the present study represents the maximum mandibular closure, whereas in Koenigswald et al. (2013) the center of the diagram defines the centric occlusion. Another modification is the inclusion of a time component into the compass. For this, the duration of the power stroke was equated with the arrow length (inclination). This was done to pinpoint the moment in which the maximum intercuspation occurred. The maximum intercuspation is represented by a horizontal line, which crosses the arrow. In addition, the equator starting point is not always 0° as proposed by Koenigswald et al. (2013), instead, it was individually fitted. The mastication compasses used in this study were therefore created as follows (see also Fig. 8):

Step one:

The OFA collision path was transferred into the Polyworks project, which contains the associated reference plane **E2** (see chapter 3.6).

Step two:

The beginning and the end of the power stroke were marked on the collision path, and a vector (**v-ps**) was fitted to these points (elements).

Step three:

A duplicate of vector **v-ps** (**v-ps(1)**) was projected onto plane **E2**.

Step four:

The declination angle was measured between **v-ps** and **wm**.

Step six:

The inclination angle was measured between **v-ps** and **v-ps(1)**.

Step seven:

The angles were converted into a polar coordinate by a Microsoft Excel template (Sheriff, 1998) and mapped onto a point plot (x/y diagram).

Step eight:

The point plot was transferred into Adobe Illustrator, and an arrow was drawn between the coordinate point and the center of the compass. The arrow points to the center.

Step nine:

A marker was set onto the arrow. This marker depicts the point of time when maximum intercuspation is reached. Its position was calculated as follows, and an example referring to the *Spalacotherium cretulablatta* OFA analysis with a roll is given in square brackets. First, the time step of the maximum intercuspation (**ts_{mi}**) is needed. For this, the time step of the lower molars maximum collision area was pinpointed in OFA [time step 166]. From this time step, the time step when the power stroke began [time step 36] was subtracted [**ts_{mi}** *(S. cret.)* = 166 - 36 = **130**]. Then the time step of the maximum mandibular closure (**ts_{mmc}**) was pinpointed [time step 222], and the shearing stroke's starting time step was subtracted from it [**ts_{mmc}** *(S. cret.)* = 220-36= **186**]. Next, the length of the arrow [**l_{arrow}**] was measured in Adobe Illustrator [**l_{arrow}** *(S. cret.)* = 16.21]. To calculate the point on the arrow (**l_{mi}**) which coincides with the maximum intercuspation, the following equation was used:

$$l_{mi=}\frac{l_{arrow}*ts_{mi}}{ts_{mmc}} \qquad [l_{mi}(Sp.cret.) = \frac{16.21*130}{186} = 11.33]$$

Step ten:

The point of the maximum intercuspation (**l_{mi}**) was marked onto the arrow with a horizontal line.

Step eleven:

The compass was improved for publication, including an adjustment of the equator's starting value.

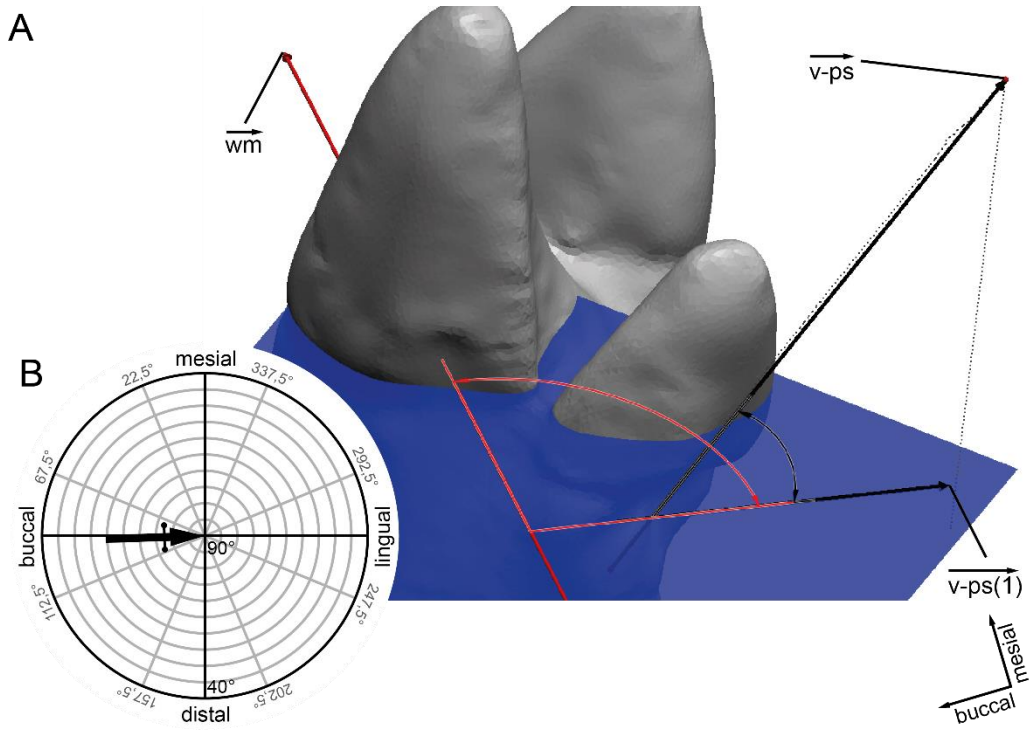

Fig. 8: The modified mastication compass employed in this study for the *Maotherium sinense* (YFGP 1724) power stroke without roll. A: The measurements of the inclination and declination. Vector v-ps was created by using the beginning and ending of the power stroke (dotted black line). Vector v- ps(1) is a duplicate of v-ps, and was projected onto plane E2. The inclination angle (black angle) is measured between v-ps and v-ps(1). The declination angle (red angle) is measured between v-ps(1) and wm. B: The resulting compass. The resulting compass depicts a one-phased shearing stroke with an inclination of 59° and a declination of 92°. The maximum intercuspation is reached in the last third of the power stroke (horizontal line, which crosses the arrow).

3.10 Overall collision area diagrams

The overall collision area diagrams describe the total surface area of both lower molars in relation to the total collision area of both lower molars and were produced in Excel. Therefore, the results for the lower dentition were exported from OFA into Excel. The data contain, among other information, every single resulting collision area at each time step in mm². The data were processed to the extent that the sum of the total collision area for each time step was calculated and converted into percent.

3.11 *Dryolestes leiriensis*

To put the research on the “symmetrodontan” chewing cycles into a broader evolutionary context, the results of this study were compared with *Dryolestes leiriensis* as a representative of the Dryolestidae. For comparison, the results of Martin (1999), Schultz (2012), and Schultz and Martin (2011, 2014), were used. The *Dryolestes* specimens, which were used by Schultz (2012) and Schultz and Martin (2014) to reconstruct the chewing cycle, are:

Dryolestes leiriensis	GuiMam 1150	Mx
Dryolestes leiriensis	GuiMam 1155	mx

The dentition, wear and chewing cycle of *D. leiriensis* was compared with those of the “symmetrodontans” to show the evolutionary development within the Mesozoic mammals. *D. leiriensis* branches off closely behind the spalacotheriids from the stem lineage of the tribosphenidans (Martin, 1999). *D. leiriensis* itself is a representative of a pretribosphenic cladotherian. Cladotherians acquired a neomorphic structure in their lower molars, the hypoflexid, which is not present in “symmetrodontans” (see chapter 1).

4 Results

A number of molar morphologies of Mesozoic mammals were included into the paraphyletic group “Symmetrodonta”. These molars have all in common, that their main cusps are arranged in a triangle and a talonid is not developed in the lower molars. These triangles, again, are arranged in a reversed-triangle tooth pattern with a two-to-one occlusion. To check, if the different molar morphologies have more in common than the features mentioned above, and to evaluate the efficiency of each dentition, the following “symmetrodontans” were studied in detail:

- *Woutersia butleri* (Woutersiidae)
- *Kuehneotherium praecursoris* (Kuehneotheriidae)
- *Maotherium sinense* (Zhangheotheriidae)
- *Spalacolestes cretulablatta* (Spalacotheriidae)

These taxa represent four major “symmetrodontan” molar morphologies from the Late Triassic to the Middle Cretaceous (Fig. 9).

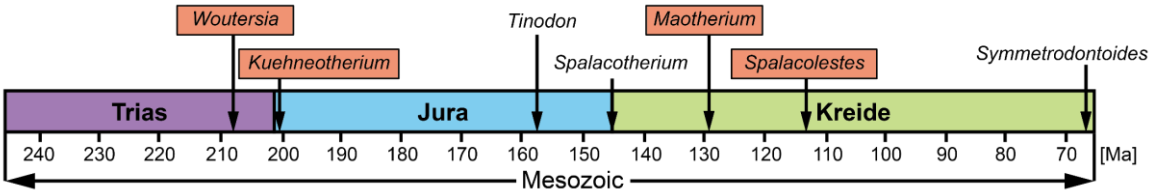

Fig. 9: A selection of “symmetrodontans” and their temporal occurrence in the fossil record. The highlighted taxa were studied in detail. They were chosen to cover a wide time span of the “symmetrodontan” fossil record. Another selection criterion was the availability of fossils.

Additionally, a brief summary of the studies on the *Dryolestes leiriensis* dentition, which has been done by Martin (1999), Schultz and Martin (2011, 2014), and Schultz (2012), is presented. The reason for that is to discuss the evolutionary development from the “symmetrodontans” towards the pretribosphenic cladotherians.

The descriptions of the molars (chapter 4.1), and the chewing cycle analysis (chapter 4.3) show that each taxon has a unique upper and lower molar morphology and mastication pattern.

The early diverging *W. butleri* has very bulky and massive molars with blunt and conical cusps. Of particular note is cusp X (CPX), which is situated on the lingual cingulum, as well as the centro-lingual cusp g (cpg). These cusps do not exist on other “symmetrodontan” molars. All cusps and crests of the available *Woutersia* specimen are strongly worn (chapter 4.2).

In general, the lower molars of *K. praecursoris* and *M. sinense* almost resemble each other. Both taxa have pointed, well separated, conical cusps, which are organized in the

same way. The centro-buccally situated protoconid (pr) is the largest cusp. Mesio-buccally to pr sits the paraconid (pa), and next to pa, at the base of the crown, is the small cuspule cpe. Disto-buccally to pr lies the metaconid (me), followed by the small cuspule cpd, which is located at the distal base of the crown. Nevertheless, there are some noticeable differences, like the acute trigonid, and the bulkier main cups of *M. sinense*. The cusps of the upper molars of *K. praecursoris* are similarly organized as the lower ones. The paracone (PA) is the largest cusp and is situated lingually in the middle of the crown. Next to the PA with a slight buccal shift are the stylocone (ST) and the metacone (ME). Distal to ME is the metastyle (MTS), whereas the parastyle (PAS) sits mesio-lingually to ST. Unlike the lower, the upper molars of *M. sinense* and *K. praecursoris* do not resemble each other. The upper molars of *M. sinense* are mesio-distal compressed, and there is an additional cusp B'. The wear of *M. sinense* and *K. praecursoris* is mainly restricted to the buccal flanks of the lower molars, and the lingual flanks of the upper ones (chapter 4.2).

The upper and lower molars of the most derived "symmetrodontan" *S. cretulablatta*, resemble that of *D. leiriensis*, (chapter 4.2). Both taxa have continuous, almost lingo-buccally oriented mesial and distal flanks (prevallum/id and postvallum/id surfaces) with prominent crests and a mesial protruding PAS. The PAS and MTS of both taxa are reduced to small cuspules and cpe is absent. Despite the similarities, there are important differences. The stylocone and metacone are absent in *S. cretulablatta,* while in *D. leiriensis* the stylocone is situated buccally in the middle of the crown, and the metacone is located distally between PA and MTS. The lower molar mesial, buccal, and distal part of the *S. cretulablatta* base is surrounded by a cingulid, which lacks in *D. leiriensis*. *D. leiriensis*, on the other hand, developed a hypoflexid, which separates cpd from the rest of the crown; cpd is absent in *S. cretulablatta*. In both taxa, striations occur mainly on the mesial and distal flanks (chapter 4.2). The striae of *S. cretulablatta* are almost parallel. The striations of *D. leiriensis*, in turn, are more inclined at the tip than at the base, but locally also parallel.

The reconstruction of the chewing cycles (chapter 4.3), which was done with the OFA, revealed that the lower dentition of *Woutersia*, *Kuehneotherium*, *Maotherium*, *Spalacolestes*, and *Dryolestes* performed a one-phased, transverse movement (yaw) during the shearing stroke. In addition, the transverse movement of the "symmetrodontans" lower dentition is accompanied by a slight mesial or distal shift.

Two different chewing cycles for each "symmetrodontan" were reconstructed. One with a roll (rotation) of the hemimandible (wr-cycle) and the other without a roll (wor-cycle). A comparison of these two cycles shows that they barely differ. The inclination and declination vary only to some degrees and the resulting collision areas are almost the same. Nevertheless, there are some minor differences. For example, Crompton and Jenkins

(1968), and Gill (2004b) identified a wear facet at the mesial base of the lower molar crown of *Kuehneotherium*. This area could only be reached by the chewing reconstruction with a roll.

During the shearing stroke, different tooth structures were used for comminuting the food particles (chapter 4.4). These structures performed different tasks, like piercing puncture-crushing, shear-cutting, and shearing. In each taxon, these tools are differently pronounced.

4.1 Molar morphology

The “symmetrodontans” and *Dryolestes leiriensis* molars, which were used to reconstruct the chewing cycle are briefly described in this chapter. The descriptions represent the principle molar morphology of each taxon.

4.1.1 *Woutersia butleri*

Two species are known for *Woutersia,* which are combined in the Woutersiidae.

- *Woutersia mirabilis* Sigogneau-Russell, 1983
- *Woutersia butleri* Sigogneau-Russell and Hahn, 1995

The upper molar, as well as the lower molar morphology of both taxa, hardly differ, except for the size, which is smaller in *W. butleri*. The crowns are very bulky, sturdy, compact in shape, and the cusps are blunt. (Fig. 10).

Averianov and Lopatin (2006) recognized Woutersiidae as early diverging Docodonta. However, the structural pattern of their molars is “symmetrodontan” with an obtuse trigonid angle.

Upper molar, specimen SNP 720

The exact position of SNP 720 within the upper molar series of *W. butleri* is unknown, but due to its morphology, it must be somewhere in the middle of the postcanine tooth row. Sigogneau-Russell and Hahn (1995) described SNP 720 in detail and compared this molar with other *Woutersia* molars. Whereas the anterior molars are almost symmetrical, in sense of the angulation and distance between paracone, stylocone, and metacone, the more posterior molars, such as SNP 720, are asymmetrical. The asymmetry results in a bucco-mesial shift of the stylocone within the molar series. Therefore, the more anterior upper molars are mesio-distally broader than bucco-lingually wide, and the more distal ones are almost as broad as wide. The angle of the triangulation between paracone, stylocone, and metacone is obtuse, and the trigon is widely open.

The most prominent molar cusp is the blunt paracone, which is situated centrally (Fig. 10). Its buccal and lingual faces are convex and mesially as well as distally pinched. Due to that pinching, there is a mesial and distal dull crest at the contact zones of the faces. Immediately next to the distal flank of the paracone sits the metacone. The metacone is a relatively small blunt cusp and is separated from the paracone by a faint indentation. At the mesial flank of the metacone, there is a small crest, which leads to the distal crest of the paracone. Due to the intense wear of the distal portion of the metacone, the original appearance of this area cannot be described, but there is a faint crista which leads distally towards a cuspule, which in turn is disto-buccally connected with cusp D ([C]ME~CPD). Mesio-buccally to the paracone, and with some distance, the stylocone (ST) is present. The ST is a prominent, solitary, conical, blunt cusp, and half as high as the paracone. A blunt crest originates mesially from the paracone, curves mesio-buccally and leads to the lingual crest of ST. Both crests are distinguishable due to an indentation at the base of the stylocone. The well-separated cusp X lies disto-lingually of the paracone on a cingulum ([CG]CPE_CPZ_ME). The blunt CPX is much smaller than PA and ST. At the mesial and distal portion of CPX are crests. The distal crest goes into the distal portion of the cingulum, which ends in turn somewhat below the metacone. The mesial crest of CPX converts into the distal portion of the cingulum, which extends lingo-mesially and ends at the lingual side of cusp E. CPE sits well separated at the base of the crown, but is only slightly elevated. Another small, blunt, conical cuspule (CPD) sits disto-buccally at the base of the crown. A cuspule connects ME and CPD. There is a short buccal cingulum mesially to CPD, which ends beneath the stylocone ([CG]CPD_ST). This cingulum is distally well separated from CPD by an indentation, whereas it is fading beneath ST.

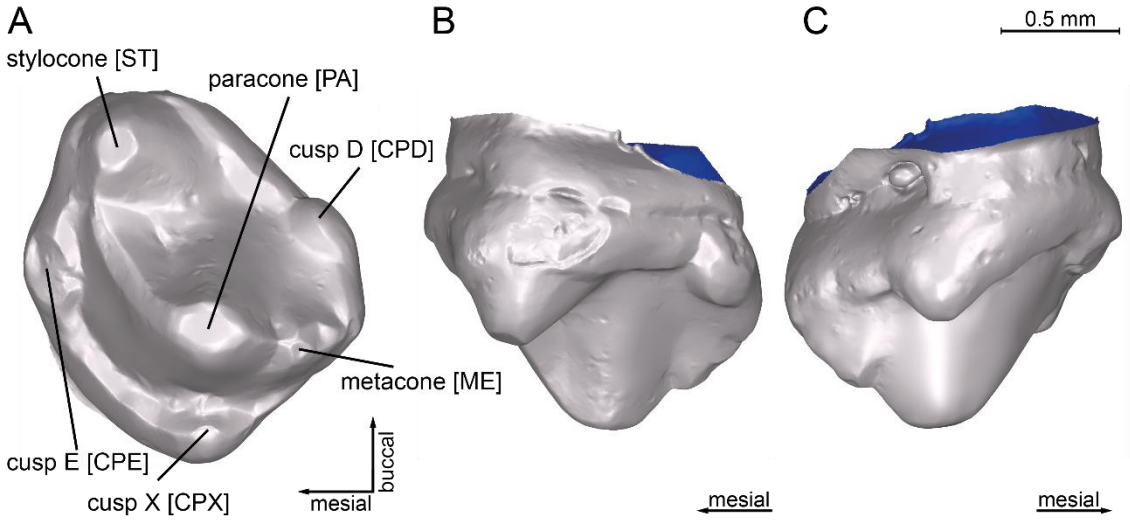

Fig. 10: An upper molar of *Woutersia butleri* (SNP 720, right M, mirrored) in occlusal (A), buccal (B), and lingual (C) views.

Lower molar, specimen SNP 517

The exact position of SNP 517 within the tooth row is unknown. But due to the comparison with a molariform tooth (presumably premolar), done by Sigogneau-Russell and Hahn (1995), it can be concluded, that SNP 517 was situated somewhere in the middle of the molar series.

The largest cusp of the lower molar is the bucco-central situated protoconid (Fig. 11). Its lingual and buccal flank is subequally convex and anterior as well as posteriorly pinched. This pinching results in mesial and distal crests. Closely to the protoconid are the paraconid and the metaconid. Both cusps are slightly shifted lingually. This shift results in an obtuse triangulation of pr, pa, and me. The paraconid and metaconid are approximately half as tall as the protoconid. Lingo-central, in the wide open trigonid basin, cpg is located. Mesial to cpg, also at the base of the crown, cpe is present. Protoconid, pa, me, cpg, and cpe are conical, bulky and blunt. Cusps e and cpg are well separated from the adjacent cusps by deep indentations. At the molars lingual side a faint cingulid is present, which is separated by cpg ([cg]cpe_cpg and [cg]cpg_cpd). [cg]cpg_cpd ends distally in a small cuspule (cpd).

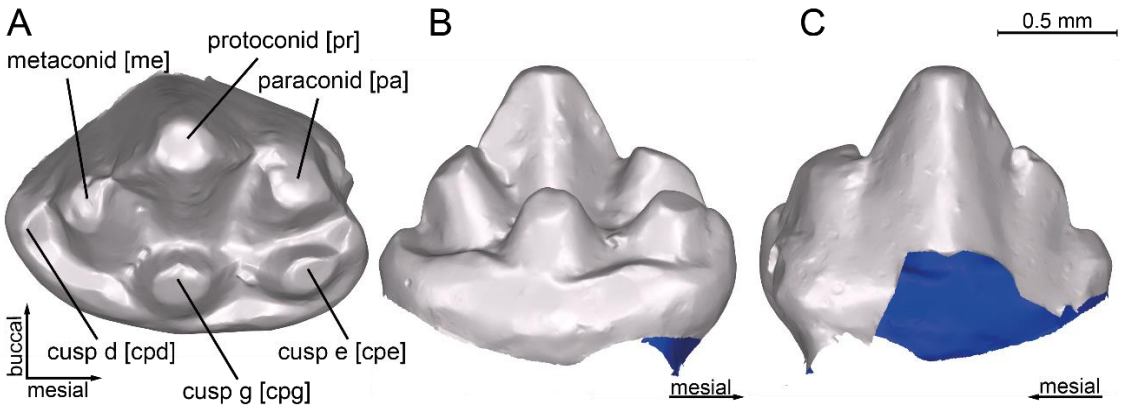

Fig. 11: A lower molar of *Woutersia butleri* (SNP 517, right m, mirrored) in occlusal (A), lingual (B), and buccal (C) views.

4.1.2 *Kuehneotherium praecursoris*

Two species of *Kuehneotherium* have been formally described yet.

- *Kuehneotherium praecursoris* Kermack, Kermack, and Mussett, 1968
- *Kuehneotherium stanislavi,* Debuysschere, 2017

Nevertheless, Gill (2004b) differentiated the fossil findings of *Kuehneotherium* in two further species, *Kuehneotherium* B and *Kuehneotherium* C. This differentiation is based on small morphological differences. Kuehneotheriids are obtuse-angled “symmetrodontans”.

Upper molar, specimen PV M 19771

This specimen has been classified as an M4 (Kermack, 1954b). A comparison with molars of the reconstructed upper *Kuehneotherium* tooth row (Gill, 2004b) validates this classification.

The paracone is the largest cusp of the upper molar and is centro-lingually situated (Fig. 12). The buccal and lingual faces are convex. Both faces are mesially and distally pinched. This pinching results in the development of slender, but sharp mesial and distal cristae. According to Gill (2004b), there are often notches on these cristae. These notches are not present at PV M 19771. At the paracones lingual face, as well as at the buccal face, next to the cristae, are vertically oriented, elongated depressions. With the crests and the elongated depressions, the mesio-buccal, as well as the disto-buccal portions of the cusp, resemble a hollow ground blade. The habitus of the much smaller ME is comparable with that of the PA but without the hollow ground blade feature. The cristae of PA are almost mesio-distally oriented. The ME cristae are rather bucco-mesially and lingo-distally orientated. The MTS sits lingually, at the base of the crown, is smaller, and more conical than ME. The cristae of MTS are in line with the cristae of ME. The stylocone is antero-posteriorly almost in line with the MTS, much more conical, and slightly larger than MTS. Whereas the [C]ST-d is bucco-distally oriented, [C]ST-m is bucco-mesially oriented. The parastyle is the smallest cusp, and disto-buccally and mesio-lingually connected with a cuspidated cingulum, which surrounds almost the entire base of the crown. The cingulum is only interrupted at the bucco-distal flank of the MTS. It can be categorized in [CG]PAS_MTS and [CG]MTS_ST_PAS. All cusps are well detached by deep indentations. The molar is asymmetrical due to the more lingual position of ST, in relation to ME, and the buccal position of PAS. Due to the obtuse angle of PA, ME, and ST, the trigon is buccally wide open.

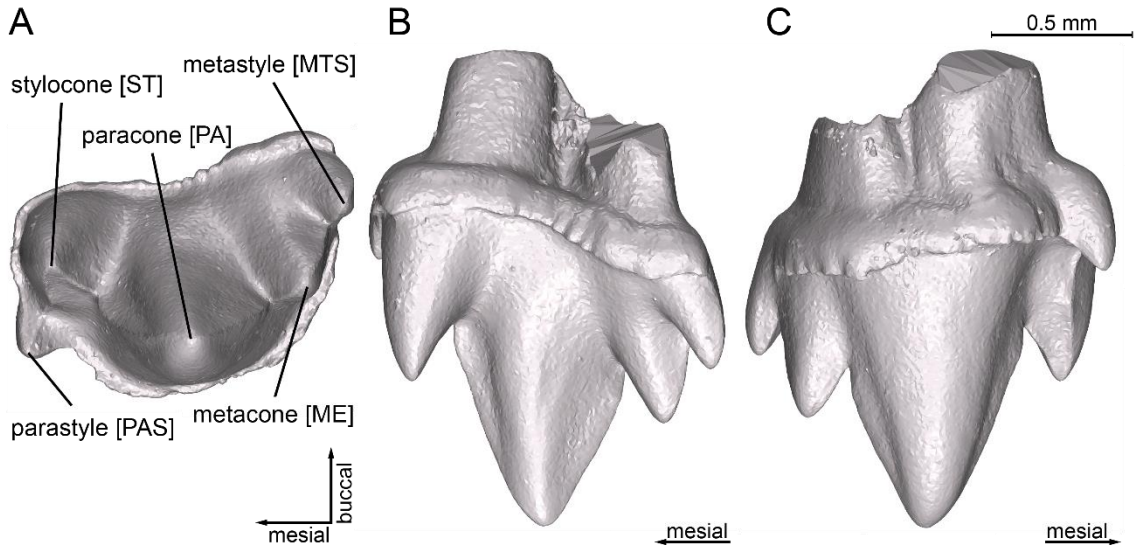

Fig. 12: An upper molar of *Kuehneotherium praecursoris* (PV M 19771, right M4, mirrored) in occlusal (A), buccal (B), and lingual (C) views.

Lower molar, specimen PV M 19143

This specimen has been described as an m3 (Kermack, 1954a). This classification is confirmed due to the comparison of the molars of the lower *Kuehneotherium* tooth row, which was reconstructed by Gill (2004b).

The protoconid, which is the largest cusp of the lower molars, is almost centrally located in sense of the molar base (Fig. 13). Whereas the pr buccal flank is convex, the lingual flank is almost planar, but with a faint lingo-posterior as well as lingo-anterior hollow ground blade feature. [c]pr-m and [c]pr-d originate at the contact zone between the buccal and lingual flank. While the orientation of the [c]pr-m is almost mesio-distal, the orientation of [c]pr-d is disto-lingual. The paraconid is conical, much smaller than pr, and its apex points slightly mesially. [c]pa-d is continuously prominent, whereas the [c]pa-m is faint at the tip, but becomes more prominent towards basal. The metaconid points slightly distally, is conical, and of the same size but lower situated as pa. The [c]me-m orientation is bucco-mesial, whereas the [c]me-d is disto-buccally oriented. The paraconid and me are more lingually situated than pr. Mesio-lingually to pa, and at the base of the crown is cpe. This cusp is much smaller than the three main cusps and has three faint crests. The [c]cpe-d starts apically at the buccal flank of cpe but curves and ends at the distal flank. [c]cpe-b and [c]cpe-l bands into a cingulid. This cingulid extends lingually and mesio-buccally and is interrupted by cpe. It can be divided into the lingual section [cg]cpe_pa_pr_me_cpd and into the buccal section [cg]cpe_cpf_pa. At the mesio-buccal portion of the cingulid, a small cingular cuspule (cpf) is located. Cusp d is conical and located distally of the metaconid at the base of the crown. It is slightly larger than cpe, and has three faint crests, [c]cpe-m, [c]cpe-d, and [c]cpe-b. All cusps are well separated by deep indentations, and the trigonid basin is lingually widely open, due to the obtuse triangulation of pr, pa, and me.

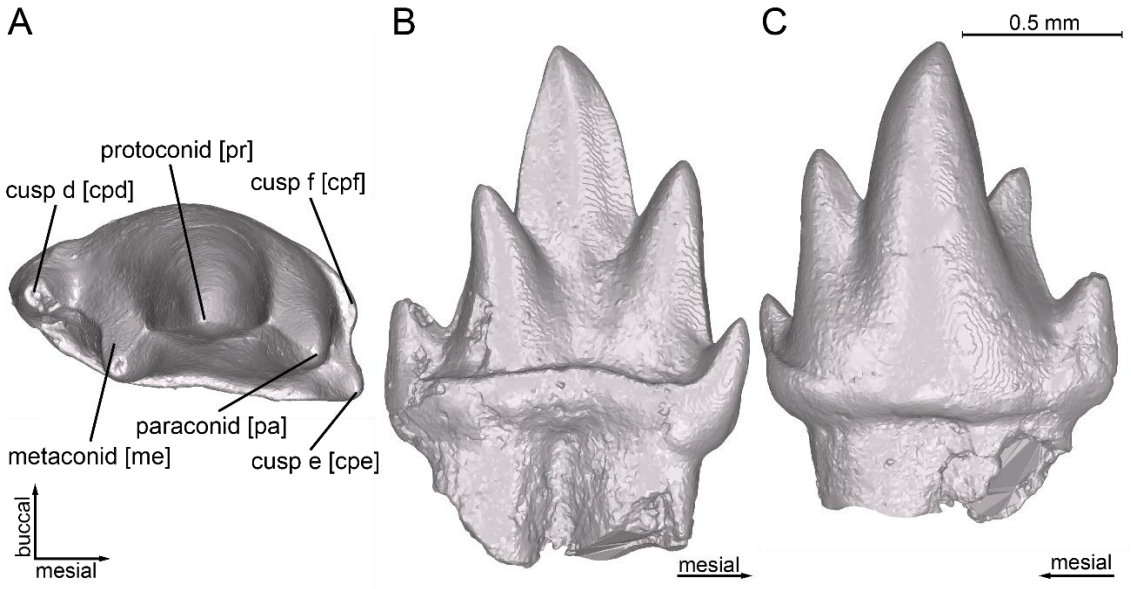

Fig. 13: A lower molar of *Kuehneotherium praecursoris* (PV M 19143, left m3) in occlusal (A), mesial (B), and buccal (C) views.

4.1.3 *Maotherium sinense*

The taxon *Maotherium* includes two species:

- *Maotherium sinense* Rougier, G.W., Q. Ji, and M.J. Novacek, 2003
- *Maotherium asiaticum* Ji, Q., Z.-X. Luo, X. Zheng, C.-X. Yuan, and L. Xu, 2009

The following description is based on the molars of specimen YFGP 1724 (Plogschties and Martin, 2019). Further molar descriptions of other *Maotherium* specimens were made by Rougier et al. (2003), and Ji et al. (2009). The main cusps triangulation of *M. sinense* is intermediate, and the molar morphology represents the general molar structure of the zhangheotheriids.

Upper molar, specimen YFGP 1724

Herein, the better preserved second upper molar is described. Its crown is almost as broad as wide (Fig. 14). The largest cusp is PA, which is situated lingo-centrally. The paracone lingual flank is convex, while the buccal flank is almost planar, but with a small, and faint, vertical centered elevation. This buccal elevation gives the bucco-anterior as well as the bucco-posterior portion a dull single hollowed blade feature. The tip of CPB' is missing, nevertheless CPB' had to be much smaller, and more conical than the paracone. The paracone, and CPB' are connected via a small, blunt crest. The conical ME and PA are well separated by a deep indentation. CPB' and ME should have had roughly the same size. The bucco-distal, as well as the bucco-mesial, portion of the crown is badly damaged, so that ST, PAS, and MTS are missing. The base of MTS protrudes distally. Buccally a deep u-shaped ectoflexus is present. Lingually, at the base of the crown, [CG]CPB'_PA_ME is

situated which is centrally interrupted by an indentation. The triangulation of the PA, CPB', and ME is obtuse. The trigon is wide open, with a broad basin at its bottom.

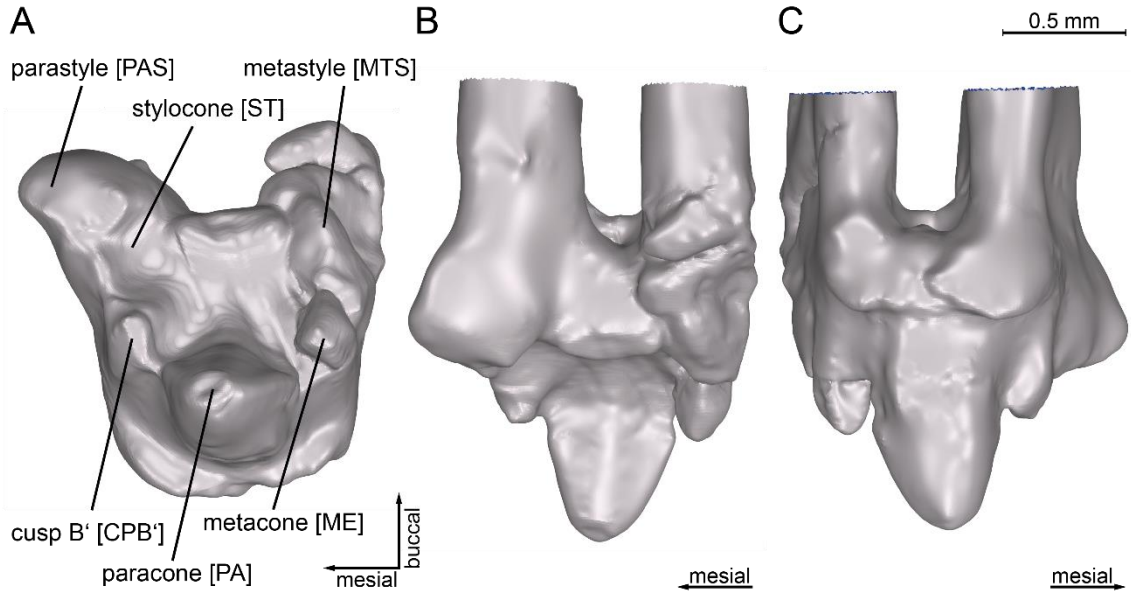

Fig. 14: An upper molar of *Maotherium sinense* (YFGP 1724, right M2, mirrored) in occlusal (A), buccal (B), and lingual (C) views.

Lower molar, specimen YFGP 1724

Due to the fact that the habitus of m2 and m3 are almost the same, only the better-preserved m3 is described herein (Fig. 15). The large conical protoconid is situated centro-buccally. The protoconid buccal face is convex, whereas the lingual side is almost flat but with a horizontal elevation in the middle. This elevation causes a faint lingo-mesial as well as a lingo-distal hollow blade feature. The paraconid is around two thirds as high as pr and mesio-lingually tilted. The shape of the pa is conical, but bucco-distally/lingo-mesially compressed. The habitus of me resembles that of pa, but is somewhat smaller, bucco-mesially/lingo-distally compressed and disto-lingually slightly tilted. The protoconid, pa, and me are well separated by deep indentations. The conical, but bucco-distally elongated cpe is located at the mesial base of the crown. Buccally, between cpe and the base of pa, is a channel-like depression. At the distal base of the crown, cpd is located. The conical cpd is smaller than cpe. Both cusps are well separated from their adjacent cusps by deep indentations. The triangulation between pr, pa, and me is acute. The acute triangulation induces, that the trigonid basin is much narrower than in *Kuehneotherium*, but also lingually open.

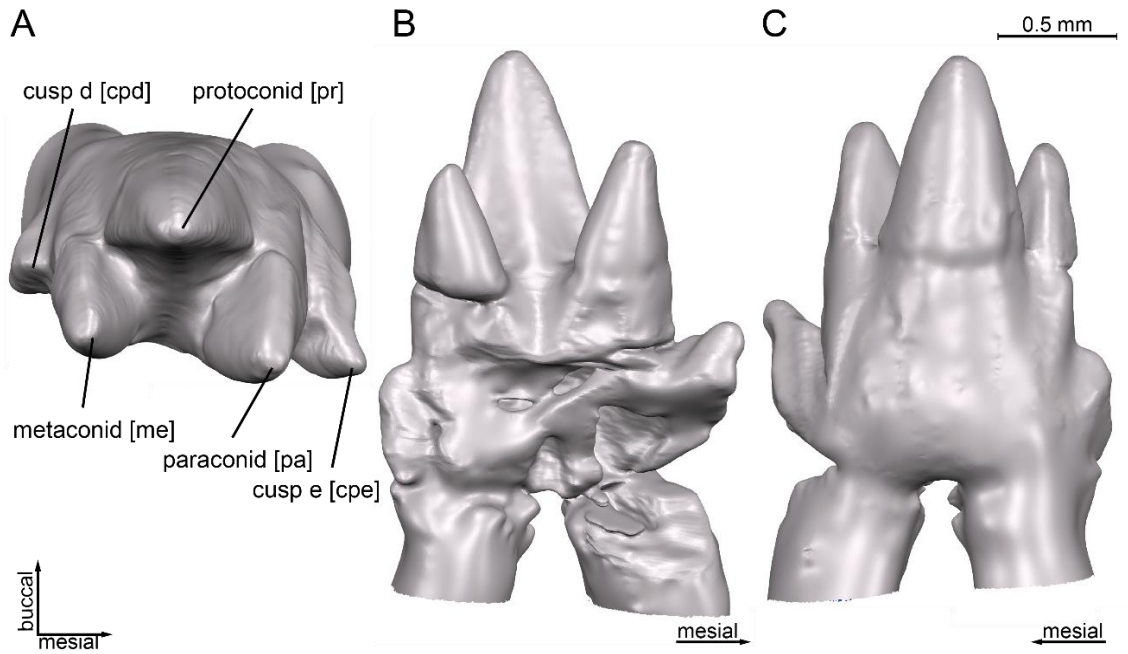

Fig. 15: A lower molar of *Maotherium sinense* (YFGP 1724, right m2, mirrored) in occlusal (A), lingual (B), and buccal (C) views.

4.1.4 *Spalacolestes cretulablatta*

The taxon *Spalacolestes* includes two species:

- *Spalacolestes cretulablatta,* Cifelli and Madsen 1999
- *Spalacolestes inconcinnus* Cifelli and Madsen 1999

The molars of both species resemble each other in most characteristics. The main difference is the larger size of *S. inconcinnus*. A detailed description of both taxa can be found in Cifelli and Madsen (1999). *Spalacolestes* is assigned to the spalacotheriids, which are acute-angled “symmetrodontans”. The molar morphology of *S. cretulablatta* is representative of the molars of the Spalacotheriidae.

Upper molar, specimen OMNH VP 033231

Cifelli and Madsen (1999) categorized this upper molar as M4. The crown of this molar has a triangular shape, in which PA, PAS, and MTS are developed at the edges as high points on the occlusal surface (Fig. 16). The paracone is the largest cusp and erects symmetrical. The ME protrudes slightly distally, while the PAS protrudes slightly mesially. Mesial to the MTS an elongated distal stylar cusp is located. PA and PAS are connected via a sharp preparacrista ([C]PA~PAS), while a sharp postparacrista ([C]MTS~PA) connects paracone and metastyle. Continuous pre- and postvallum surfaces (PA*PAS, MTS*PA) occupy the complete anterior and posterior flanks of the cusp. Due to a ridge, which is between the distal stylar cusp and PAS, the trigon is almost closed.

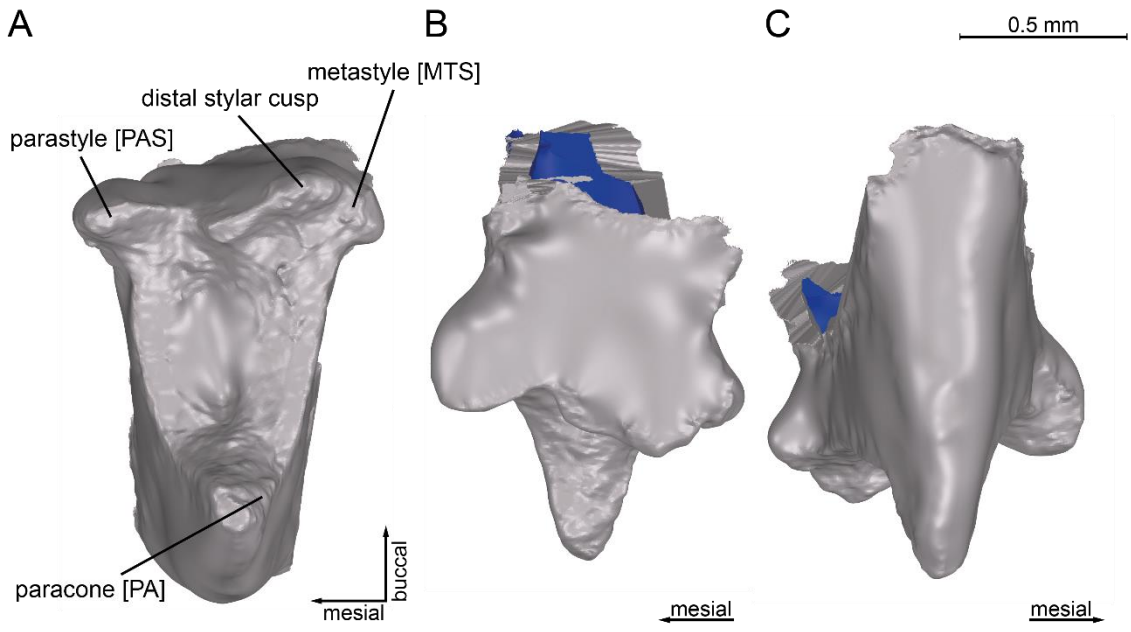

Fig. 16: An upper molar of *Spalacolestes cretulablatta* (OMNH VP 033231, left M4) in occlusal (A), buccal (B), and mesial (c) views.

Lower molar, specimen OMNH VP 027421 (mandibular fragment)

Specimen OMNH VP 027421 includes two successive molars. Cifelli and Madsen (1999) identified these molars as m4 and m5. Both teeth are very similar in shape; this description refers to m4 (Fig. 17). The crown has a triangular outline with a pr, pa, and me at the edges. All three cusps are pointed and marginally tilted towards lingual. Cusp e and cpd are reduced. The paraconid and me are each connected via a sharp crest with pr (paracristid = [c]pa~pr; protocristid = [c]pr~me). [c]pr~me is higher situated than [c]pa~pr, and me is taller than the more lingually situated pa. The pre- and postvallid surfaces (pa*pr; pr*me) are continuous and extend over the whole anterior and posterior face of the cusps. At the base of the crown, a prominent cingulid ([cg]pa_pr_me) is present, which surrounds the mesial, buccal, and distal flank. The rim of the [cg]pa_pr_me forms a sharp ridge. At the most mesial and distal points of [cg]pa_pr_me are small cuspules situated (mesial-, distal cingular cusp). Due to the acute trigonid angle, the trigonid is open but narrow.

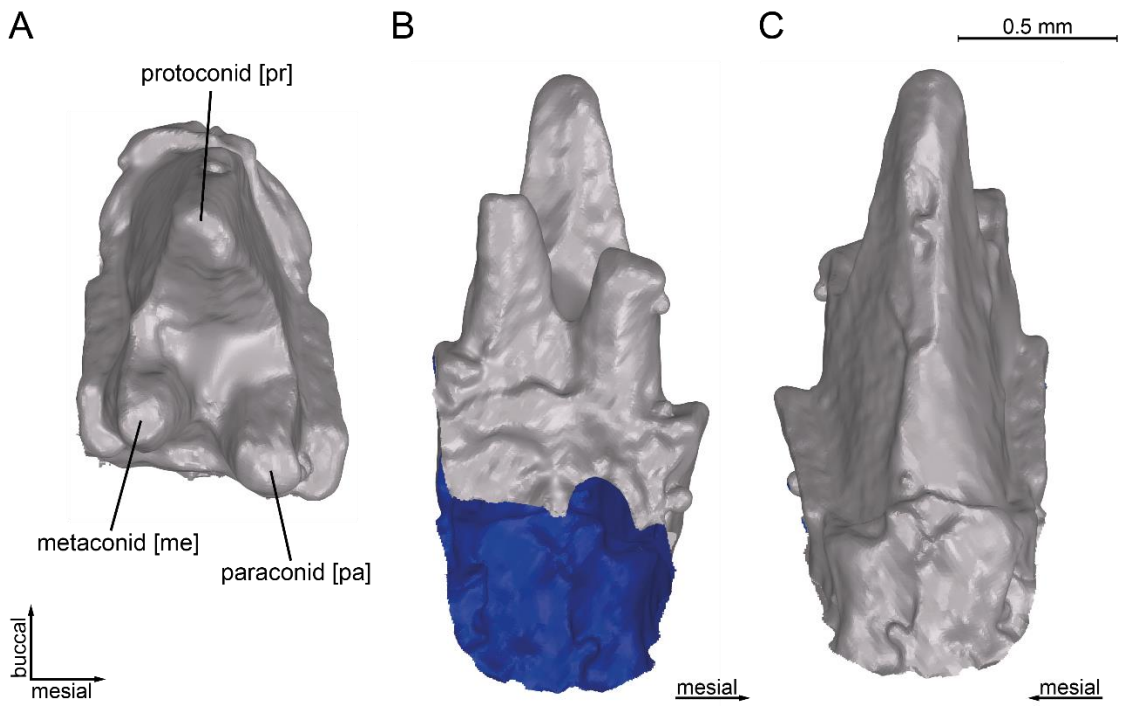

Fig. 17: A lower molar of *Spalacolestes cretulablatta* (OMNH VP 027421 ,left m4) in occlusal (A), lingual (B), and buccal (C) views.

4.1.5 *Dryolestes leiriensis*

Two taxa of *Dryolestes* are listed in the fossil record:

Dryolestes priscus Marsh, 1878

Dryolestes leiriensis Martin, 1999

A detailed description of the *Dryolestes leiriensis* dentition was provided by Martin (1999) and Schultz (2012). The *Dryolestes* molars of both taxa differ only in detail.

Upper molar, specimen Gui Mam 1150

The exact position of this upper molar is unknown. The largest cusp is the paracone, which is supported by the lingual root (Fig. 18). The lingual side of PA is convex, whereas the buccal side is almost flat, but a faint single hollow ground blade feature is mesio-buccally as well as disto-buccally present. The conical ST is almost as high as PA and is situated centro-buccally. [C]PA-m originates at the mesial flank of the paracone and continues in a buccal direction. At first [C]PA-m slopes down, but then ascends, and encounters two other crests. The first crest ([C]ST-bm) originates at the mesial side of ST, continuing inclined towards mesial, and crosses [C]PA-m. The second crista ([C]PAS-ld) arises at the distal side of PAS, ascends towards distal, and meets [C]PA-m and [C]ST-bm. The parastyle is situated at the base of the crown and protrudes mesially. At the mesial flank of PAS originates [C]PAS-lb, which slopes down towards lingual as well as towards buccal. At the distal side of the crown, the conical ME and MTS arise. They are situated lower than ST, but higher than PAS. Paracone, ME and MTS are connected via crests. The [C]PA~ME is convex, whereas [C]ME~MTS is sloping down from the metacone to the hardly elevated MTS. The trigon is almost closed due to the central located ST.

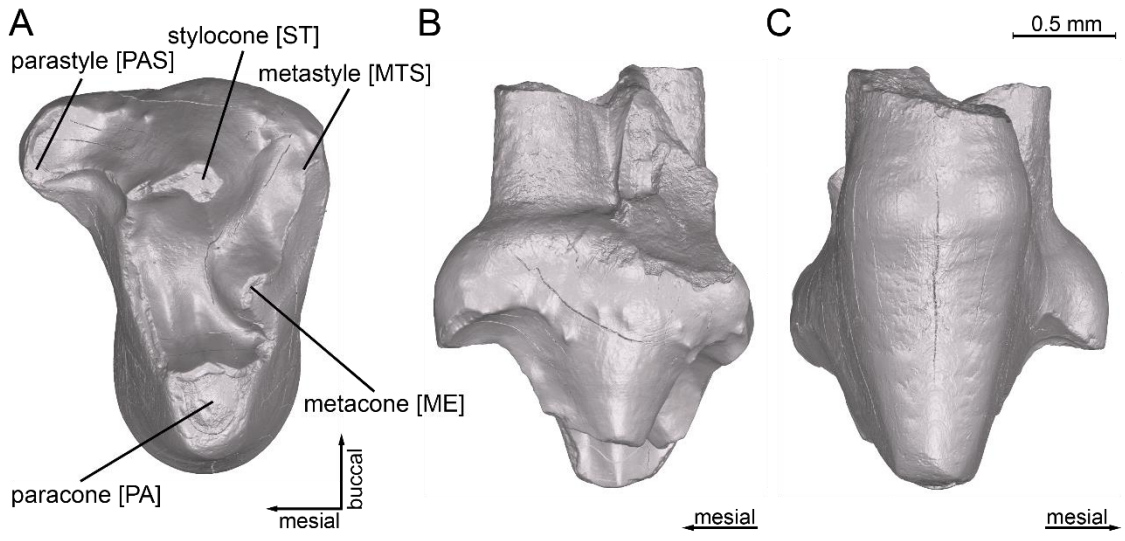

Fig. 18: An upper molar of *Dryolestes leiriensis* (Gui Mam 1150, right M, mirrored) in occlusal (A), buccal (B), and lingual (C) views.

Lower molar, specimen Gui Mam 1155

The position of this molar is unknown. The protoconid, pa, and me define the edges of an acute triangle. The protoconid and me are almost equal in height. The buccal side of pr is convex, whereas the lingual side is almost flat, but with a lingo-mesial as well as lingo-distal faint single hollow ground blade feature. The protoconid and the conical me are connected via [c]pr~me. [c]pr~me flexes cervical with its bottom half the way. The protoconid and pa are also connected by a curved crest ([c]pa~pr). The paraconid and me are separated by a deep indentation, so the trigon is lingually open. At the distal base of the crown, the hypoflexid protrudes, from which in turn cpd is situated disto-lingually. The hfd slopes towards buccal.

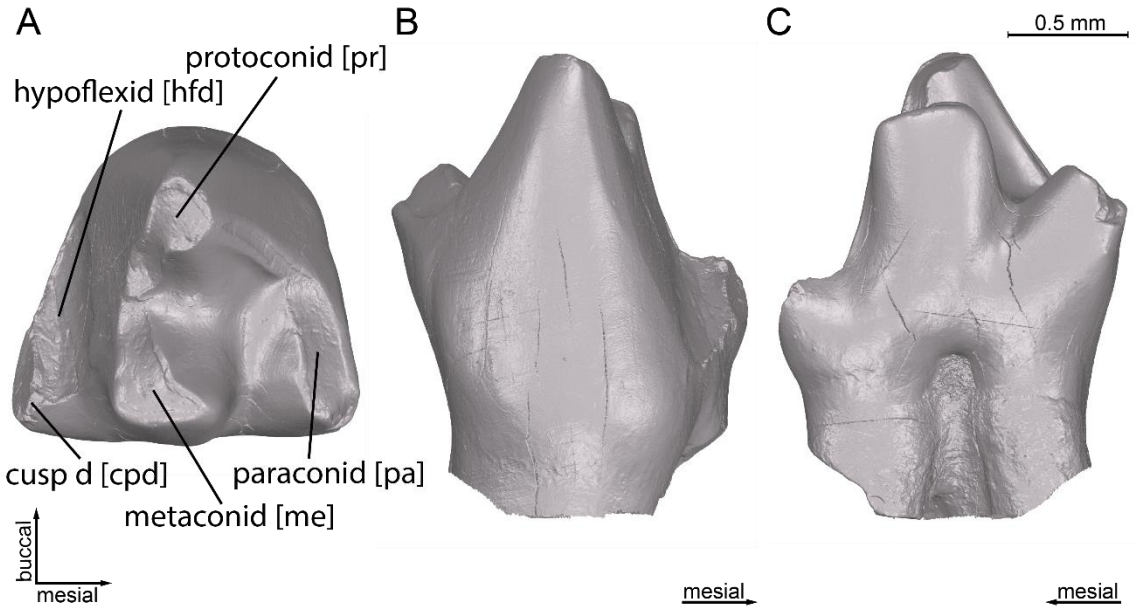

Fig. 19: A lower molar *of Dryolestes leiriensis* (Gui Mam 1155, left m) in occlusal (A), buccal (B), and mesial (C) views.

4.2 Tooth Wear

This is a summary of the tooth wear in “symmetrodontans” from personal observations as well as from the literature because only some of the accessible examined specimens showed wear.

4.2.1 *Woutersia butleri*

The wear of *Woutersia butleri* has been described in detail by Sigogneau-Russell (1983), Sigogneau-Russell and Hahn (1995), and Butler (1997). The following paragraph is a combination of personal observations and the descriptions mentioned above.

Upper molars

Most striking is the apical wear of PA, ST, ME, CPE, and CPX (Fig. 20). In some specimens wear has removed the complete tip of the cusps. The apical wear surface of the SNP 720 cusps are oriented as follows:

- paracone: mesially
- stylocone: bucco-mesially
- metacone: disto-lingually
- cusp X: lingually
- cusp E: mesio-lingually

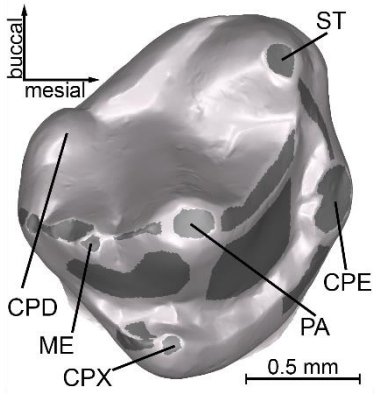

Fig. 20: A schematic summary of the wear facets, which was described and found on the upper molars of *Woutersia butleri*. The wear is sketched in dark grey onto SNP 720 (3D-model, right M).

In most specimens [C]ST~PA, [C]PA~ME and [C]ST~CPE are heavily affected by wear. In some specimens [C]ST~CPE is completely scuffed and instead of a crest, only a facet is visible. Another crest area, which is affected by wear, is located distally to the metacone ([C]ME-d). Wear facets occur on the disto-lingual and mesio-lingual side of PA and ME, and on the distal flank of CPX. Another prominent facet protrudes mesial from the apical wear of CPE on the mesio-lingual flank of the cingulum. In some specimens, CPE is worn-off to its base.

Striae on the facets have not been described in the literature but were found on some specimens that are present in the study (SNP 719, SNP 884). The striations occur on the mesio-lingual portion of the paracone and extend to the cingulum (Fig. 21). They are orientated bucco-lingually with a steep inclination. Interestingly, some striae are in a depression, which could not be reached by a lower molar structure, so they had to be caused by food-tooth contact.

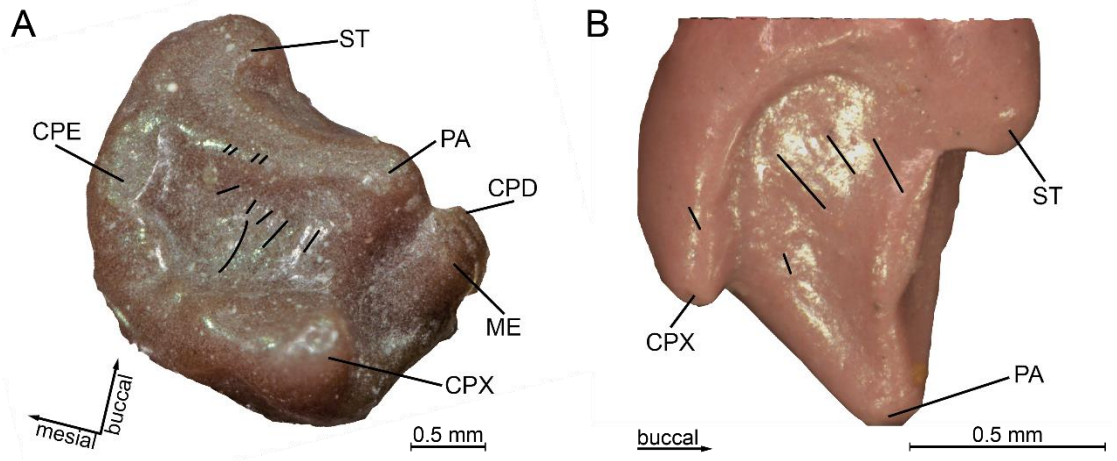

Fig. 21: Right upper molar molds of *Woutersia* sp. Representative striae are traced in black (figures are mirrored). A: SNP 719, striations are concentrated on the mesio-lingual side (occlusal view). B: SNP 884, upper molar, mesial view.

Lower molars

As for the upper molars, the most striking wear for the lower molars is the apical wear, which flattened the tips of pr, me, pa, cusp d, cpg, and cpe, as well as cuspules on the lingual cingulid (Fig. 22). The apical wear surfaces of the SNP 517 cusps are sloping as follows:

- protoconid: almost horizontally
- metaconid: disto-lingually
- paraconid: mesio-buccally
- cusp d: disto-buccally
- cusp g: lingually
- cusp e: mesio-lingually
- mesial cingulid cuspule: lingo-mesially
- distal cingulid cuspule: lingo-distally

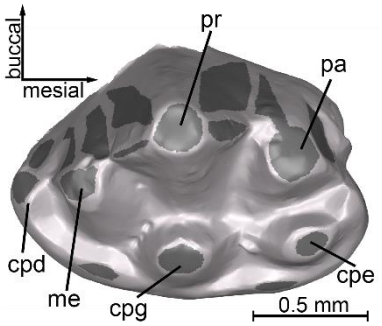

Fig. 22: A schematic summary of the wear facets, which was described and found on the lower molars of *Woutersia butleri*. The wear is sketched in dark grey onto SNP 720 (3D-model, right m, mirrored).

The [c]pr~pa and [c]me~pr are also affected by wear, whereby the mesial crest is more worn than the distal one. Wear facets occur on the mesio-buccal and disto-buccal flanks of pr and pa, as well as on the mesio-buccal portions of cpd and me. Sigogneau-Russell (1983) described wear facets on the disto-buccal flanks of me and mesio-buccal side as the apex of cpd.

4.2.2 *Kuehneotherium praecursoris*

The herein described distribution of *Kuehneotherium* tooth wear is mostly a summary of the observations by Crompton and Jenkins (1968), Crompton (1971), Mills (1984), Godefroit and Sigogneau-Russell (1999), Gill (2004b), and Conith et al. (2016). The most remarkable difference compared to *Woutersia* is the much weaker apical wear in *Kuehneotherium*. Only molars in a very advanced stage of wear have worn-off tips. Striations could not be identified on the accessible specimens and are not documented in the literature.

Upper molars

Wear facets occur at the mesio-buccal and disto-buccal flanks of PA and ME (Fig. 23, A). Furthermore, at the lingo-distal flank of ST, the lingo-mesial side of MTS, and the lingo-distal portion of PAS wear can be seen. The wear of PAS extends lingo-distally onto [CG]PAS_PA. In addition, wear has been described for a small disto-lingual area of [CG]ME_MTS.

Lower molars

The mesio-buccal and disto-buccal flanks of pr and pa are affected by wear (Fig. 23, B). In some specimens, these areas of wear extend almost to the molar base. Wear occurs also at the mesio-buccal flank of cpd, as well as the buccal side of me. Another area of wear has been described for the mesio-buccal portion of cpf, which extends to the buccal area below [cg]cpf-mb.

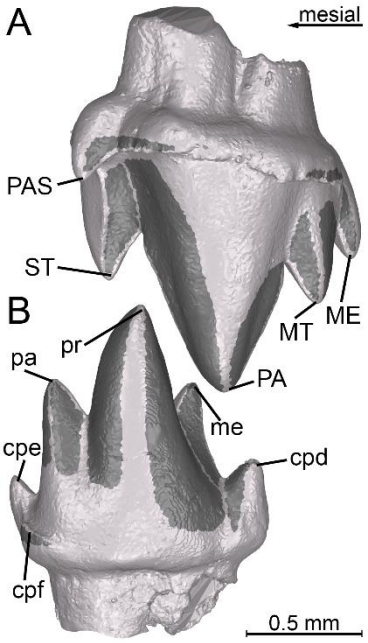

Fig. 23: The distribution of wear facets of *Kuehneotherium praecursoris,* schematically summarized. The wear is marked in dark grey. A: Upper molar (3D-model of PV M 19771, right M4); B: Lower molar (3D-model of PV M 19143, left m3).

4.2.3 *Maotherium sinense*

On the studied *Maotherium sinense* specimen (YFGP1724) some striations, but no facets could be identified, and there is just little information on *Maotherium* tooth wear documented in the literature. Nevertheless, there is a character coding for some facets of *Maotherium sp.* in Ji et al. (2009) (c.f. Fig. 24):

- "128. Topographic relationships of wear facets to the main cups: [...] (2) Lower cusps a, c support a single wear facet (facet 4) that contacts the upper primary cusp B. (this facet extends onto cusp A as wear continues, but 1 and 4 do not develop simultaneous in these taxa); [...]."
- "130. Wear facet 1 (a single facet supported by cusp a and cusp c) and facet 2 (a single facet supported by cusp a and cusp b) [...] (1) Present."
- "131. Upper molars - development of facet 1 and the preprotocrista (applicable to molars with reversed triangulation): (0) Facet 1 (prevallum crest) short, not extending to the stylocone area; […]".

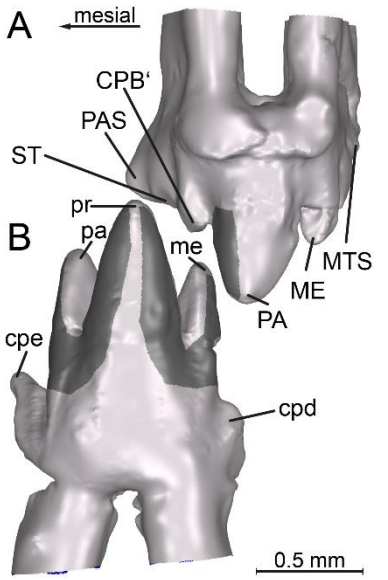

Fig. 24: The distribution of wear facets based on the description of Ji et al. (2009). The wear is sketched in dark grey onto 3D-models of *Maotherium sinense* molars A: right M2 (YFGP 1724); B: right m2, mirrored (YFGP 1724).

Some striations are visible on the ultimate premolar and on m1 of specimen YFGP 1724. These striations have a steep inclination. Their orientation is not uniform, but the main direction extends from mesio-lingual to bucco-distal (Fig. 25).

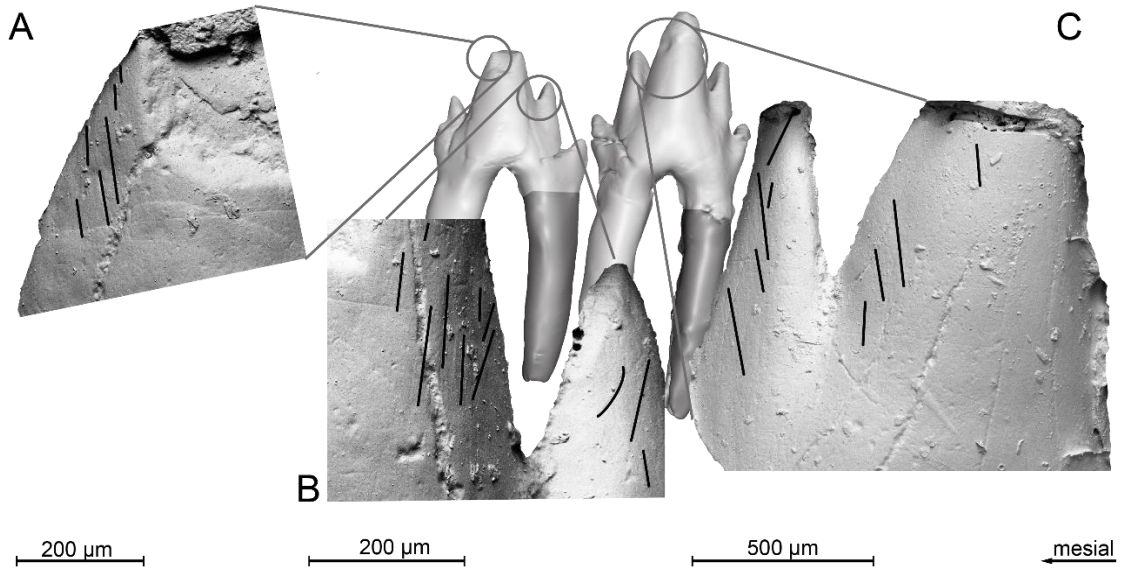

Fig. 25: SEM pictures of striations, which are on the right lower ultimate premolar and m1 of *Maotherium sinense* (YFGB 1724). The striae are traced in black. The pictures are mirrored for the ease of comparison. A: Striae at the mesio-buccal side of the ultimate premolar apex. B: Striae next to the indentation between the metaconid and cusp d. C: Close up of striae next to the indentation between the m1 paraconid and cusp e. Background: 3D-models of the ultimate premolar and first molar.

4.2.4 *Spalacolestes cretulablatta*

Cifelli and Madsen (1999) documented the wear of *Spalacolestes cretulablatta* in detail.

Upper molars

On the upper molars wear occurs mainly on [C]PAS~PA, [C]PA~MTS, and on the pre- and postvallum surfaces (PAS*PA, PA*MTS) (Fig. 26, A). In advanced stages of wear, the cristae are flattened, although the outer edges of the cristae remain sharp. With progress of wear, the apices got worn-off.

Striae are present all over PAS*PA and PA*MTS surfaces. They have a steep inclination (about 45°) and proceed almost parallel in an oblique bucco-lingual direction. In advanced wear stages, there are steps between the dentine and enamel on the occlusal surface.

Lower molars

On the lower molars wear affect [c]pa~pr, [c]pr~me, the pre- and the postvallid surfaces (pa*pr, pr*me), as well as the cingulid (Fig. 26, B). The outer edges of the cristids stay sharp with the progress of wear, whereas the tips of the three main cusps became blunter. In addition, steps between dentine and enamel occur on the occlusal area, and a continuous, concave, triangular worn surface has been developed on the crown. This surface dips slightly mesially. The sharp ridges of [cg]pa_pr and [cg]pr_me were beveled off into flat, obliquely oriented facets in advanced wear stages.

Parallel striae occur all over the pa*pr and pr*me (Fig. 27). They are obliquely, lingo-buccally oriented with a steep inclination (about 45°). The inclination of striae reflects the slope of the [cg]pa_pr and [cg]pr_me.

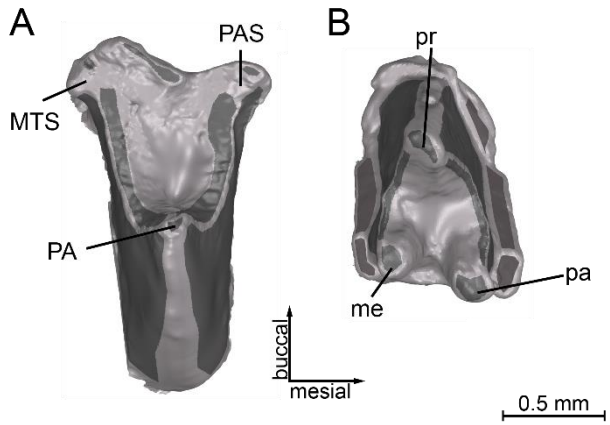

Fig. 26: The distribution of wear facets on *Spalacolestes cretulablatta* molars. The facets are sketched in dark grey onto 3D-models. A: left M4, mirrored (OMNH VP 033231); B: left m4 (OMNH VP 027421).

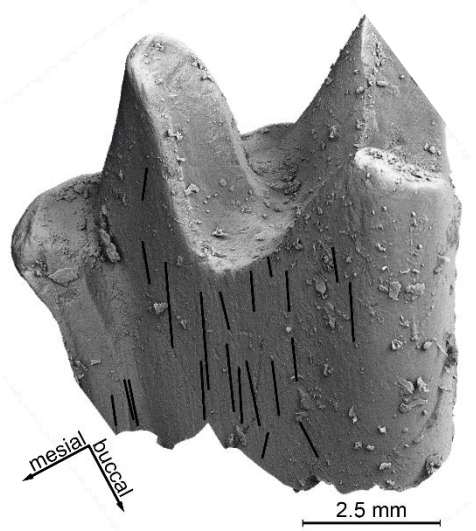

Fig. 27: Left lower m4 of *Spalacolestes cretulablatta* (OMNH VP 030627, SEM picture). The striae orientation is almost parallel to each other, and to the slope of [cg]pa_pr and [cg]pr_me.

4.2.5 *Dryolestes leiriensis*

The wear of *Dryolestes leiriensis* has been described in detail by Schultz and Martin (2011) and Schultz (2012).

Upper molars

Most striking is the apical wear of the PA, ST, PAS, and MTS as well as the wear on the crests (Fig. 28, A). These areas of wear are oriented as follows:

- paracone: almost horizontally
- stylocone: mesio-buccally
- metacone: disto-lingually
- metastyle: disto-lingually
- parastyle: disto-buccally
- [C]ME~MTS: disto-lingually
- [C]PAS~ST: mesio-lingually

In advanced stages of wear, there is a step between the enamel and the dentine of the cusps, and crests, due to the exposure of the softer dentine. These steps are typical for abrasion. Furthermore, there are attrition facets on PA*ME*MTS and PAS*PA as well as on the lingual portion of the PAS.

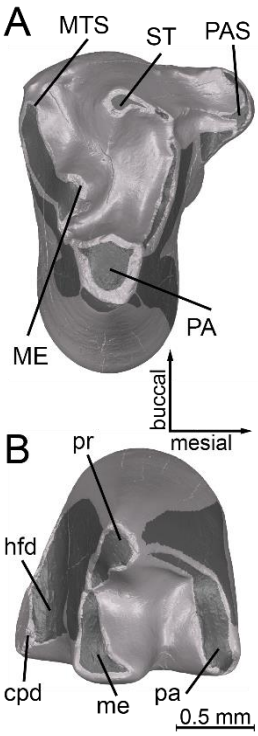

Fig. 28: Distribution of wear facets sketched onto 3D-models of *Dryolestes leiriensis* molars based on the description of Schultz and Martin (2011) and Schultz (2012). The wear facets are marked in dark grey. A: right M, (Gui Mam 1150); B: left m (Gui Mam 1155).

Striations are common on the entire PA*ME*MTS and PAS*PA facets. They run parallel from bucco-apical towards lingo-cervical. The most apical located striae are slightly steeper than the more cervical ones, and less parallel aligned (Fig. 29, A).

Lower molars

The lower molars show extensive apical wear on the pr, pa, and me as well as on [c]pr~me, and [c]pa~pr (Fig. 28, B). The apical wear facets are oriented as follows:

- protocone: disto-lingually
- metacone: bucco-distally
- paracone: mesio-buccally

The cusps and crests show the typical abrasion steps, in which the dentine is more deeply excavated than the adjacent enamel. In addition, there are attrition facets on pr*me, and pa*pr as well as on the hypoflexid.

Striae occur on the lower pr*me and pa*pr facets. They run parallel from bucco-cervical to lingo-apical. The most apically situated striations are around 10° more steeply inclined than the more cervical ones, which are oriented parallel to the hypoflexid (Fig. 29, B). It is noticeable that the more apical striae are less parallel aligned than the more cervical ones.

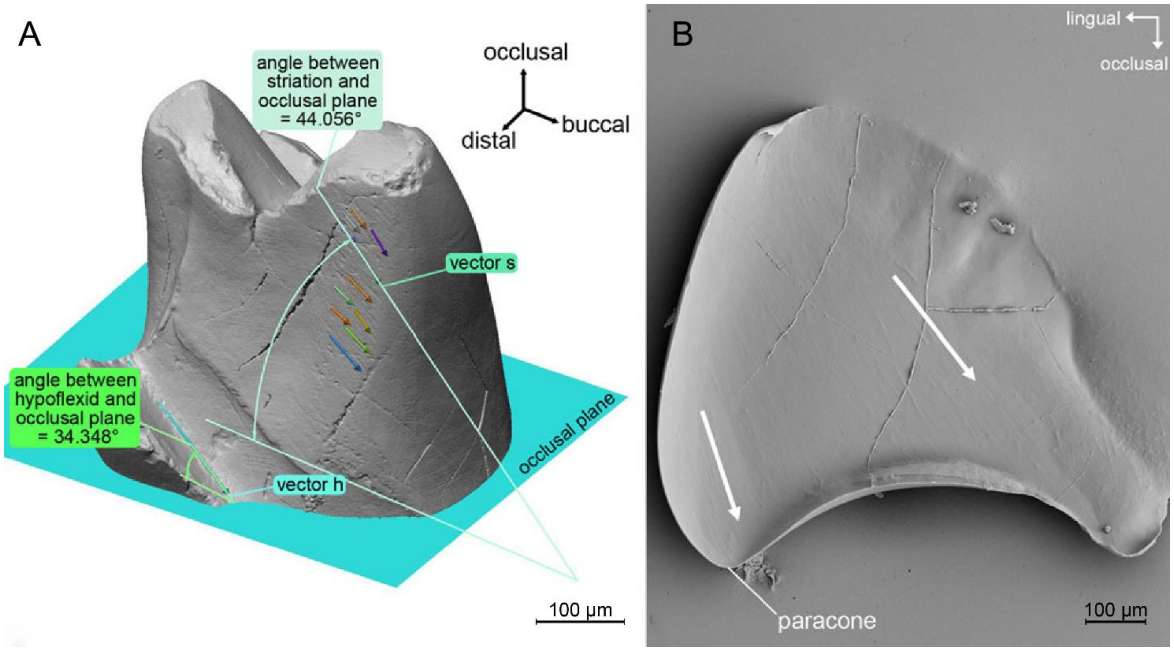

Fig. 29: A: High resolution 3D-model of a lower *Dryolestes leiriensis* molar (Gui Mam 1163). The more apical striae on pr*me are steeper inclined (around 10°) as the more cervical ones. The more cervical ones run parallel to the hypoflexid. The arrows represent the two striae directions. B: SEM image of an upper *Dryolestes leiriensis* molar (mesial). The white arrows show the two striae orientations. (Modified from Schultz and Martin, 2011)

4.3 Occlusal Fingerprint Analyser (OFA)

The chewing cycles of *Woutersia butleri*, *Kuehneotherium praecursoris*, *Maotherium sinense*, and *Spalacolestes cretulablatta* were reconstructed with the OFA. As mentioned in chapter 3, these taxa were chosen, because they represent major “symmetrodont” molar pattern. For each taxon, one cycle without a roll (wor-cycle), and one cycle with a roll (wr-cycle) of the lower dentition were performed. All taxa have in common that their shearing strokes have a single phase (phase I), in which the lower molars slide into interdental spaces of the upper molars. During each shearing stroke, there is no change in direction.

There are minor differences in the wr-cycle and wor-cycle. For all taxa, the highest overall contact area values between the upper and lower molars were slightly higher in the wor-cycles. For some taxa, the wr-cycle reconstruction showed additional collision areas, which correspond to observed wear facets. These areas are lacking in the wor-cycle.

The inclination and declination of the wr-cycle and wor-cycle differ only by a few degrees. Table 6 shows the specimens, which were used to reconstruct and analyze the chewing cycles. For easier comparison, all right teeth were mirrored for the OFA, so that each set of teeth corresponds to a left dentition.

Tab. 6: Sets of molars, which were used to reconstruct the chewing cycle.

Taxon	Collection number	Tooth position
Woutersia butleri	SNP 720	mirrored right Mx
	SNP 517	mirrored right mx
	SNP 517	mirrored right mx
Kuehneotherium praecursoris	PV M 19771	mirrored right M4 (left M3 substitute)
	PV M 19143	left m3
	PV M 19143	left m3 (m4 substitute)
Maotherium sinense	YFGP 1724	mirrored right M2
	YFGP 1724	mirrored right m2
	YFGP 1724	mirrored right m3
Spalacolestes cretulablatta	OMNH VP 033231	left M4
	OMNH VP 027421	left m4
	OMNH VP 027421	left m5
Dryolestes leiriensis	Gui Mam 1150	mirrored right Mx
	Gui Mam 1155	left mx
	Gui Mam 1155	left mx

4.3.1 The chewing cycle of *Woutersia butleri*

Based on the results of the molar wear study and the illustration of a tentative occlusion, proposed by Sigogneau-Russell (1983), the chewing cycle was virtually reconstructed. For the reconstruction, one right upper and one right lower molar were used (SNP 720, SNP 517). The morphology of both teeth indicates that they were situated somewhere in the middle of the upper and lower tooth row, but the exact molar positions are unknown. In order to have two consecutive lower molars, the lower molar SNP 517 was duplicated.

The general movement of the lower dentition of the wr-cycle and of the wor-cycle is almost identical (Fig. 30). During the shearing stroke, the lower dentition performs an upward and transverse movement with a slight shift towards distal until the maximum mandibular closure is reached, and the recovery stroke begins. The inclination for the chewing cycle with a roll is 39° (wor-cycle = 52°), and the declination is 80° (wor-cycle = 79°). A rotation of 10° towards lingual was performed by the OFA simulation with a roll.

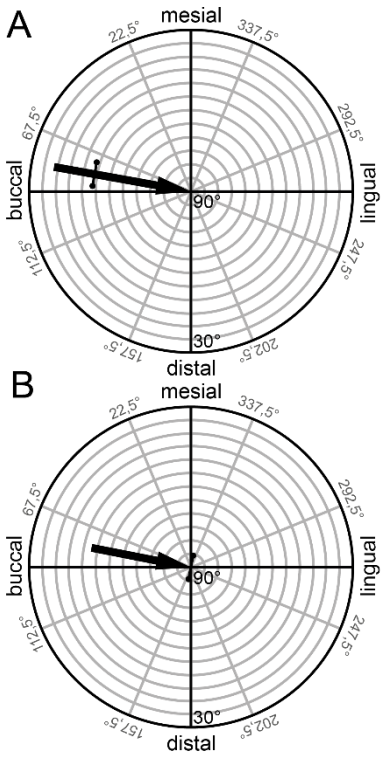

Fig. 30: The mastication compasses for *Woutersia butleri*. In both scenarios, the lower teeth perform a transverse upward movement with a slight mesio-distal shift. The marker (line perpendicular to the arrow) depict the moment of the maximum mandibular closure. The length of the arrow is equated with the duration of the shearing stroke. A: Compass of the chewing cycle with roll (wr-cycle); B: Without roll (wor-cycle).

The shearing stroke of the wr-cycle ends at time step (t-s) 98, whereas it is 25 time steps longer for the wor-cycle. At first (t-s 0) the overall contact area of the wr-cycle rises until t-s 29 is reached, whereas it rises up to t-s 36 in the wor-cycle. Afterward, the overall contact area of the wr-cycle decreases until about t-s 54 and stays at the same level until the maximum mandibular closure is reached (t-s 98). The wor-cycle decreases until t-s 80, and increases again until the maximum mandibular closure is reached (t-s 123). Whereas the maximum intercuspation of the wr-cycle is reached at t-s 29, the maximum intercuspation of the wor-cycle coincides with the maximum mandibular closure (t-s 123). The overall contact area of the maximum intercuspation, as well as the maximum mandibular closure (end of the shearing stroke), is higher for the wor-cycle (Fig. 31).

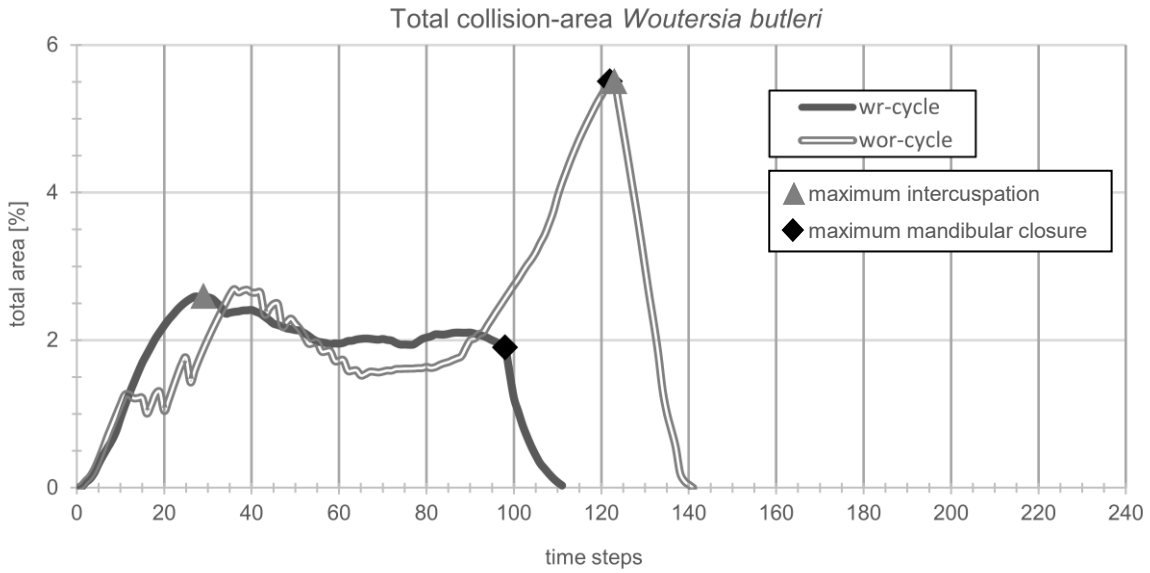

Fig. 31: Change of total collision area over time in *Woutersia butleri* lower molars, during one chewing cycle. The total collision area is a percentage of the total collision area of the lower molar relative to the total area of the lower molars. The dark grey graph shows the course of the wr-cycle, the light grey double-line graph that of the wor-cycle. Whereas the wr-cycle maximum intercuspation is reached in the beginning of the shearing stroke, it coincides with the end of the wor-cycle shearing stroke (maximum mandibular closure).

At the beginning of the shearing stroke pa-mb-a (pa-bm-a; wor cycle) contacts [C]PA~ME (Fig. 32, A; see also Fig. 33). In addition, pr-bm occludes with ME-ld. At the same time, me-d-a gets in contact with the most apical portion of [C]PA~ST. Furthermore, pr-bd-a occludes with a more buccal portion of [C]PA~ST. With the aforementioned occlusal contact areas, restricted interdental spaces originate. The first space is restricted by the [c]pr~me/[C]PA~ST, the second one is limited by [c]pr~pa/[C]PA~ME. While the lower molars slide past the upper molar, these spaces close, and the collision areas shift to the molar flanks. At this time the wr-cycle shows an extensive contact of me-db/PA-ml(1) as well as of pr-db(2)/PA*ST. These contacts are marginal in the wor-cycle (me-db/PAml; pr-d/PAml(2)). As the closure of the dentition progresses, a second set of interdental spaces originates between [c]pa~pr/[C]CPX-d as well as between [c]pr~me/[C]CPX-m. Concurrently pr-db(1) (pr-db; wor-cycle) slides past a small area of [CG]_ml. At the end of the shearing stroke, the second set of interdental spaces closes, and CPX occupies the interdental space between me and pa (Fig. 32, B). The remarkable difference between the wr-cycle and wor-cycle is the intense contact of me-db/CPX ml, pa-b*pa-mb/ PA*ME-ld, and pa-mb/CPX d in the wor-cycle, which is not developed to that extent in the wr-cycle (Fig. 33). On the other hand, there is a large contact area between pr-db(2)/PA-ml(2), as well as between me-db/PA-ml(1) in the wr-cycle, which is not developed to that extent in the wor-cycle.

The resulting collision areas of the lower dentition and their upper molar antagonists for both scenarios are summarized in Figure 33.

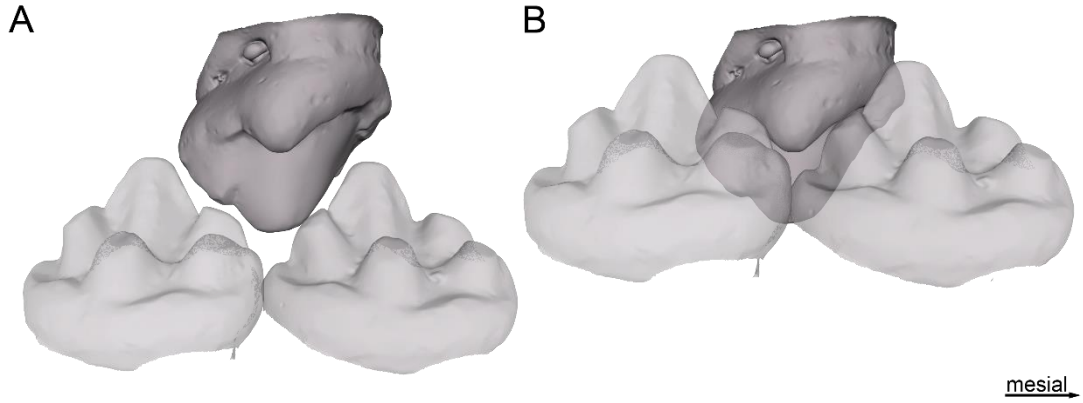

Fig. 32: Important molar positions of *Woutersia butleri* during the shearing stroke. A: At the beginning of the shearing stroke. B: At the end of the shearing stroke.
3D-models of SNP 720 (upper molar) and SNP 517 (both lower molars).

A

Collision areas, wr-cycle, *Woutersia butleri*

	lower coll. areas	upper antagonists	add. upper antagonists
	pr-db(2)	PA-ml(2)	
	pr-db(1)	[CG]-ml	
	me-db	PA-ml(1)	PA-m-a
	me-d-a	PA-ml(1)	PA-m-a
	pr-bd-a	[CG]-ml	
	pr-bm	ME-ld	
	pa-mb(1)		CPX-dl
	pa-mb(2)	CPX-dl	PA*ME
	pa-bm	PA*ME	
	pa-mb-a		PA*ME

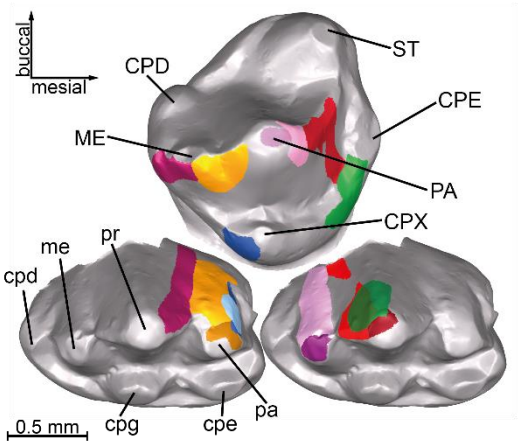

B

Collision areas, wor-cycle, *Woutersia butleri*

	lower coll. areas	upper antagonists	add. upper antagonists
	pr-d	PA-m	
	pr-db	[CG]-ml	
	me-db	CPX-ml	PA-ml,PA-m-a
	me-d-a	CPX-ml	PA-ml,PA-m-a
	pr-bd-a	[CG]-ml	
	pr-bm	ME-ld	
	pa-mb	CPX-d	PA*ME
	pa-b	PA*ME	
	pa-bm-a		PA*ME

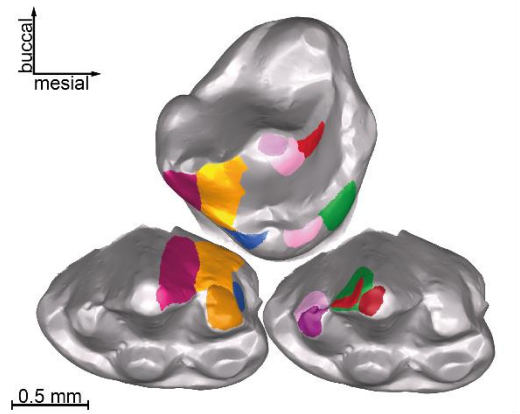

Fig. 33: The resulting OFA collision areas of the shearing stroke of *Woutersia butleri* in summary. A: Collision areas of the chewing cycle with a roll. B: Collision areas of the chewing cycle without a roll. Basically both cycle produce the same areas, but there are some exceptions. First, the more extensive pr-db(2)/PA-ml(2), and pr-db(1)/[CG]-ml wr-cycle contact zones. Second, the presence of the CPX-ml contact area, and the more extensive pa-b/PA*ME contact facet of the wor-cycle. Upper molars correspond to right ones, whereas lower molars correspond to left ones.
3D-models of SNP 720 (upper molar) and SNP 517 (both lower molars).

4.3.2 The chewing cycle of *Kuehneotherium praecursoris*

The chewing cycle of *Kuehneotherium praecursoris* was reconstructed with the wear facets analyses from Crompton (1971), Godefroit and Sigogneau-Russell (1999), and Gill (2004b). For the reconstruction 3D-models were used, which were provided by Prof. Richard Cifelli. The original molars are a right M4 (PV M 19771) and a left m3 (PV M 19143), of which the M4 was mirrored and the m3 was duplicated in order to have two consecutive lower molars for the OFA reconstruction. Because no striations were observed on the available specimens or have been described in the literature, the OFA reconstruction was performed without a striation analysis.

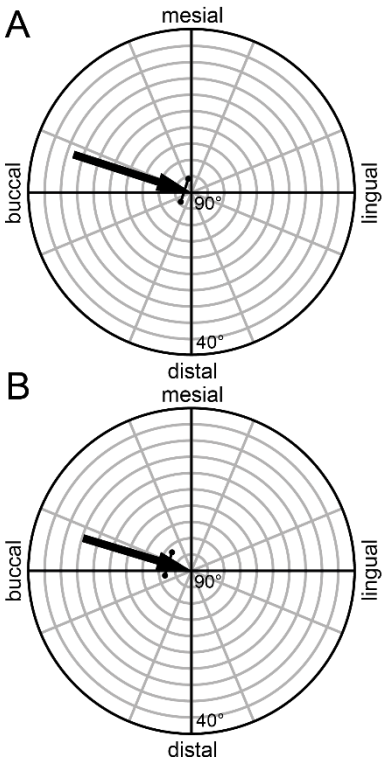

Fig. 34: The mastication compass of both *Kuehneotherium praecursoris* chewing cycle scenarios. Both cycles performing a transverse chewing motion with a mesio-distal shift. The length of the arrow is equated with the duration of the shearing stroke. The marker perpendicular to the arrow, represents the maximum inter-cuspation. A: The compass for the cycle with roll. B: The compass for the cycle without roll.

The general movement of the lower dentition of the wr-cycle and wor-cycle are very similar (Fig. 34). The shearing stroke of both scenarios exerts an upward transverse movement with a distal shift. Whereas the inclination of the wr-cycle is 52°, it is 55° for the wor-cycle. The declination of both cycles is around 73°. The reconstruction with a rotation of the mandible results in a roll rate of six degrees towards lingual.

The shearing stroke of the wr-cycle has a duration of 134 time steps, whereas that of the wor-cycle is 13 time steps shorter (Fig. 35). The overall contact area of the wr-cycle increases until t-s 74, whereas that of the wor-cycle increases till t-s 95. Time step 95 of the wor-cycle coincides with the maximum intercuspation, and the value of the overall collision area stays almost the same until the end of the shearing stroke (maximum mandibular closure, t-s 121). On the contrary, the value of the overall wr-cycle contact area stays almost the same from t-s 74 to t-s 100 and then rises again until the maximum intercuspation is reached (t-s 126). Afterward, the wr-cycle contact area decreases slightly until the end of the shearing stroke (maximum mandibular closure, t-s 134). The total overall contact area at maximum intercuspation is higher for the wor-cycle than for the wr-cycle, whereas at the end of the shearing stroke it is higher for the wr-cycle.

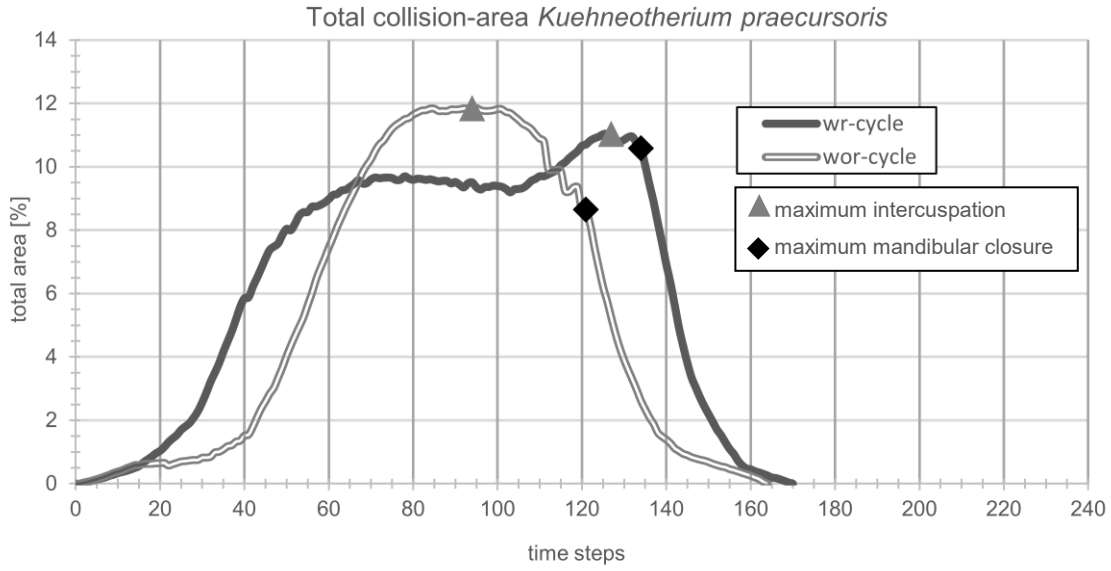

Fig. 35: Change of the total collision area over time of the *Kuehneotherium praecursoris* lower molars, during one chewing cycle. The total collision area is a percentage of the total collision area of the lower molars relative to the total area of the lower molars. The dark grey graph shows the course of the wr-cycle, the light grey double-line graph that of the wor-cycle. Whereas the wr-cycle maximum intercuspation is reached around 100 t-s before the shearing stroke ends, it almost coincides with the end of the wor-cycle shearing stroke (maximum mandibular closure).

At the beginning of the shearing stroke me-db occludes with PA-ml (Fig. 36, A; see also Fig. 37). With further closing, the buccal face of pr slides into the lingual intercuspal area of PA and ST, which results in a contact of pr-d/PA-m as well as pr-b/ST-l (pr-mb(1)/ST-dl; wor-cycle). Furthermore, the lingual portion of PA occludes with the buccal intercuspal area of me and cpd. Thereby me-db/PA-ml, as well as cpd-b/PA-l, come into contact. Concurrently the bucco-mesial portion of pr moves into the disto-lingual area between ME and MTS, and the mesio-buccal portion of pa slides into the lingual intercuspal area of PA and ME. The dents of the intercuspal areas lead the antagonistic cusps during the further upward movement of the lower dentition. Additionally, [c]pr-d slides towards [C]PA-m, and [c]pr-m (posterior m) moves towards [C]ME-d. While the cusps continue to interlock, restricted spaces between [c]pr~me/[C]ST~PA as well as between [c]pa~pr/[c]PA~ME originate, which are getting narrower over the time and finally close (Fig. 36, B).

Shortly before the end of the shearing stroke pr-d occludes with the notched area between PAS-l and [CG]ST_PA (Fig. 36, C). At the same time pr-bm(2) (pr-mb(2); wor-cycle) occludes with the distal portion of [CG]PA_ME. At the end of the wr-cycle, the tip of PA comes into contact with cpf, which is not the case in the wor-cycle.

The resulting overall collision areas of the wr-cycle and the wor-cycle almost resemble each other, except for the additional [cg]-mb/PA-dl contact in the wr-cycle.

The shearing stroke collision detections for both scenarios are summarized in Figure 37.

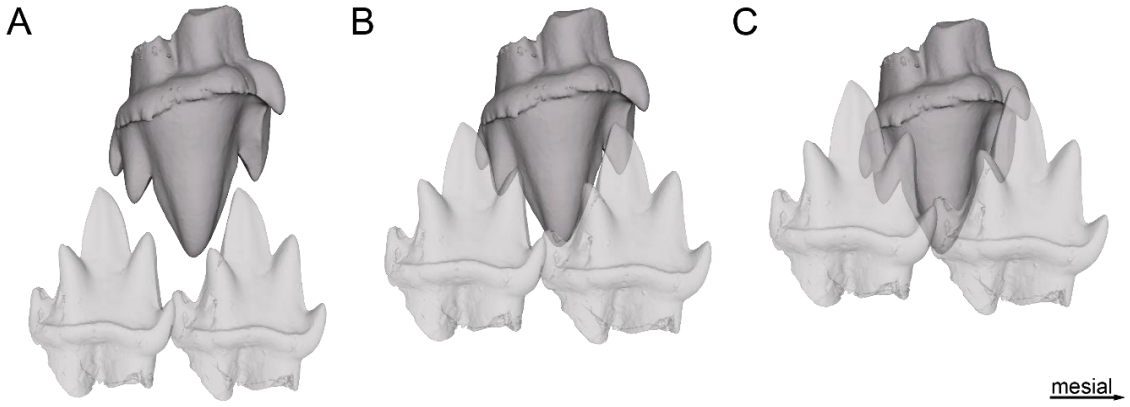

Fig. 36: Important molar positions of *Kuehneotherium praecursoris* during the shearing stroke. A: At the beginning of the shearing stroke. B: Shortly before closing the interdental spaces. C: At the end of the shearing stroke.
3D-models of NHM PV M 19771 (M4) and NHM PV M 19143 (m3).

A Collision areas, wr-cycle, *Kuehneotherium praecursoris*

	lower coll. areas	upper antagonists	add. upper antagonists
	pr-d	PA-m	[CG]ST_PA
	me-db	PA-ml	
	cpd-b	PA-l	
	pr-bm(1)	MTS-dl	
	pr-bm(2)	ME-ld	[CG]PA_ME
	pr-b	ST-l	PAS-l
	pa-bd	ME-lm	
	pa-mb	PA-dl	[CG]PA_ME
	[cg]cpf-mb	PA-dl	

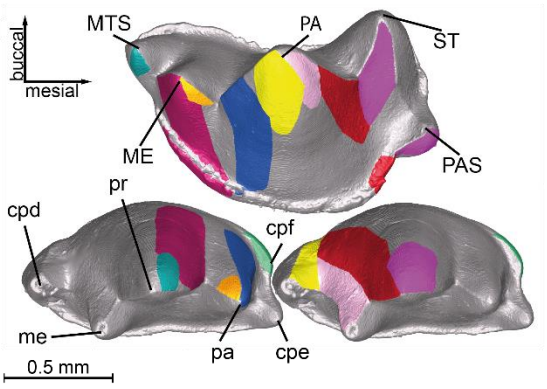

B Collision areas, wor-cycle, *Kuehneotherium praecursoris*

	lower coll. areas	upper antagonists	add. upper antagonists
	pr-d	PA-m	[CG]ST_PA
	me-db	PA-ml	
	cpd-b	PA-l	
	pr-bm	MTS-dl	
	pr-mb(2)	ME-dl	[CG]ME_MTS
	pr-mb(1)	ST-dl	PAS-dl
	pa-d	ME-m	
	pa-m	PA-d	[CG]PA_ME

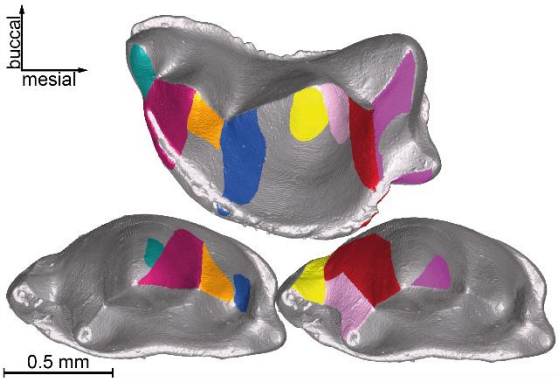

Fig. 37: The resulting OFA collision areas of the shearing stroke of *Kuehneotherium praecursoris* in summary. A: The collision areas of the wr-cycle. B: The collision areas of the wor-cycle. The contact areas of both scenarios are very similar except that PA-dl is reaching [cgf]-mb in the wr-cycle. Upper molars correspond to right ones, whereas lower molars correspond to left ones.
3D-models of NHM PV M 19771 (M4) and NHM PV M 19143 (m3).

4.3.3 The chewing cycle of *Maotherium sinense*

The chewing cycle of *Maotherium sinense* was reconstructed with two successive right lower molars (m2, m3) and with their antagonist (M2). The molars are from a partial skull including a mandible with complete dentition (except for incisors and canine), and the maxilla with two molars (YFGP 1724, Plogschties and Martin, 2019). The striations, which were observed on the lower ultimate premolar and m1 of YFGP 1724 were used for the reconstruction.

The general movement of the wr-cycle as well as of the wor-cycle is a transverse movement with a slight shift towards mesial (Fig. 38). In both scenarios, the inclination is around 60° and the declination is around 92°. The lower dentition rolled with a resulting rotation of 8° towards lingual in the wr-cycle.

The duration of the shearing stroke for the wr-cycle is 150 t-s, while that of the wor-cycle is 25 time steps longer (Fig. 39). In both cycles, the overall collision area increases until the maximum intercuspation is reached (wr-cycle = t-s 75; wor-cycle = t-s 104) and decreases afterward until the end of the shearing stroke. The total overall contact area at the maximum intercuspation is slightly higher in the wr-cycle as in the wor-cycle, whereas it is vice versa at the end of the shearing stroke (maximum mandibular closure). The curves of both scenarios are similar, with the exception that the diagram of the wor-cycle is somewhat protracted.

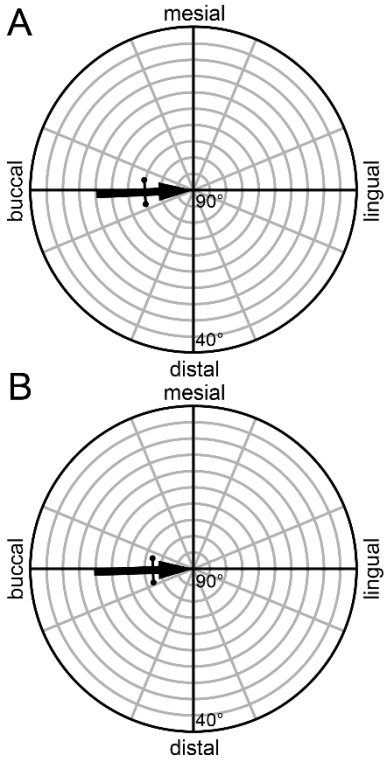

Fig. 38: The mastication compass of both *Maotherium sinense* chewing cycle scenarios. Both cycles perform a transverse chewing motion with a slight mesial shift. A: The compass for the cycle with roll. B: The compass for the cycle without roll. The length of the arrow is equated with the duration of the shearing stroke. The wr-cycle reaches the maximum intercuspation (line perpendicular to the arrow) almost in the middle of the shearing stroke, whereas the wor-cycle reaches it somewhat in the last third of the shearing stroke.

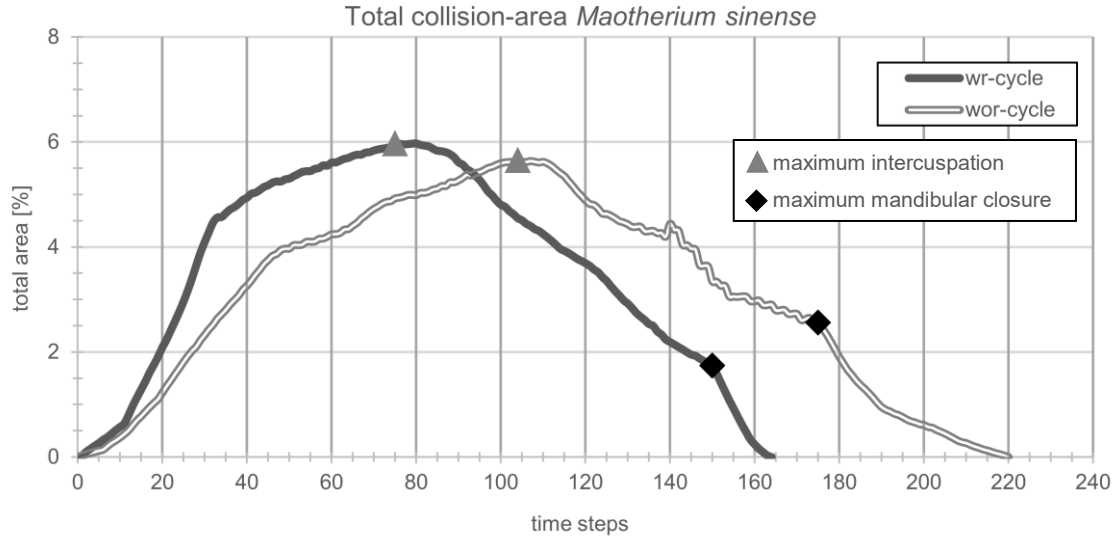

Fig. 39: Change of the total collision area over time of the *Maotherium sinense* lower molars, during one chewing cycle. The total collision area is a percentage of the total collision area of the lower molars relative to the total area of the lower molars. The dark grey graph shows the course of the wr-cycle, the light grey double-line graph that of the wor-cycle. Both curves resemble each other, but the wor-cyle graph is somewhat protracted.

At the beginning of the shearing stroke, the intercuspal area between me and pa moves towards PA (Fig. 40, A). At this time me-d/PA-m, as well as pa-m/PA-d, come into contact (Fig. 41). Concurrently, pr-mb/ME-dl, as well as pr-db/CPB'-ml get also in contact, and interdental spaces originate between the cusps. The mesial interdental space is restricted by [c]pr~pa/[C]PA~ME, and the distal interdental space is restricted by [c]pr~me/[C]PA~CPB'. With further progress of the shearing stroke, the interdental spaces close. Concurrently, the me/PA, pa/PA, pr/CPB' as well as pr/ME contact regions become more extensive, and each area expands to the basal region of the respective cusp.

In addition, the contact areas cpe-mb/PA-dl, as well as cpd-bd/PA-lm, arise in the wr-cycle. Soon afterward, me-db occludes with [CG]PA_CPB', and pa-m comes into contact with [CG]PA_ME. By that, a second set of interdental spaces originates, which are restricted by [c]pr~me/[CG]PA_CPB' as well as by [c]pa~pr/[CG]PA_ME (Fig. 40, B). These interdental spaces close at the end of the shearing stroke (Fig. 40, C), and the contact areas between pr*me/[CG]PA_CPB', as well as pr*pa/[CG]PA_ME increase, whereas all other contact areas decrease (Fig. 40, D).

The resulting collision areas for the wr-cycle as well as for the wor-cycle are summarized in Figure 41. The distribution of the collision areas for both scenarios is similar.

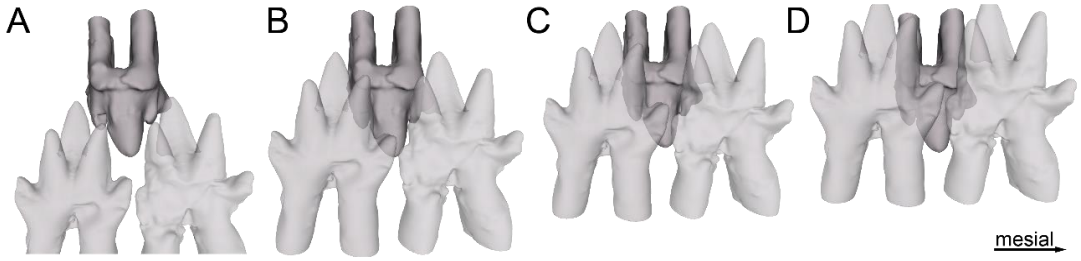

Fig. 40: The molar positions of the power stroke of *Maotherium sinense*. A: The beginning of the power stroke. The first set of interdental spaces originate. B: The position, in which the second set of interdental spaces originate. C: The position, in which the second set of interdental spaces are closed. D: The end of the power stroke. 3D-models of YFGP 1724 (M2, m2, and m3).

A Collision areas, wr-cycle, *Maotherium sinense*

	lower coll. areas	upper antagonists	add. upper antagonists
	pr-db	CPB'-ml	[CG]PA_CPB'-m
	pr-db(1)	[CG]PA_CPB'-m	[CG]PA_CPB'-d
	me-bd	[CG]PA_CPB'-d	
	me-d	PA-m	PA-lm
	cpd-bd	PA-lm	PA-m
	pr-mb	ME-dl	[CG]PA_ME-d
	pr-m	[CG]PA_ME-d	ME-dl
	pa-m	PA-d	[CG]PA_ME-m
	pa-bm	[CG]PA_ME-m	PA-d
	cpe-mb	PA-dl	

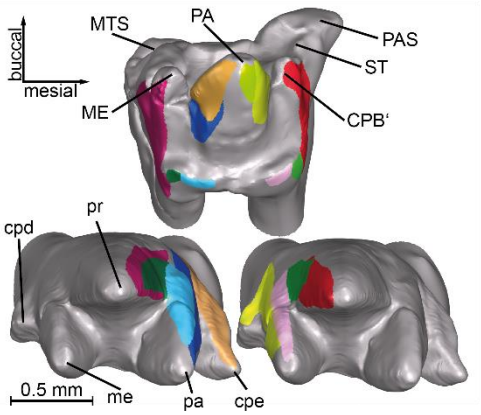

B Collision areas, wor-cycle, *Maotherium sinense*

	lower coll. areas	upper antagonists	add. upper antagonists
	pr-db	CPB'-ml	[CG]PA_CPB'-m
	pr-d	[CG]PA_CPB'-m	[CG]PA_CPB'-d
	me-bd	[CG]PA_CPB'-d	
	me-d	PA-m	
	pr-mb	ME-dl	[CG]PA_ME-d
	pr-m	[CG]PA_ME-d	ME-dl
	pa-m	PA-d	[CG]PA_ME-m
	pa-b	[CG]PA_ME-m	PA-d
	cpe-mb	PA-dl	

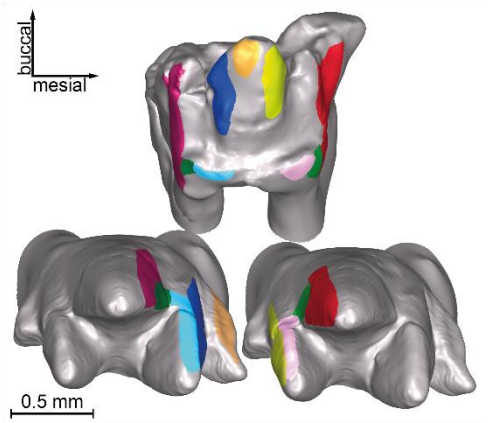

Fig. 41: The resulting OFA collision areas of the power stroke of *Maotherium sinense* in summary. A: The collision areas of the wr-cycle. B: The collision areas of the wor-cycle. The contact areas of both scenarios are similar. Upper molars correspond to right ones, whereas lower molars correspond to left ones.
3D-models of YFGP 1724 (M2, m2, and m3).

4.3.4 The chewing cycle of *Spalacolestes cretulablatta*

The chewing cycle of *Spalacolestes cretulablatta* was reconstructed based on the results of the SEM wear study. For the reconstruction of the cycle 3D-models of two left lower molars from one specimen (OMNH VP 027421), and one left upper molar (OMNH VP 033231) from another specimen was used. The molars were classified as m4, m5, and M4 by Cifelli and Madsen (1999).

The general movements of the wr-cycle and wor-cycle resemble each other (Fig. 42). The lower dentition performs a transverse movement with a slight shift towards distal. Whereas the declination for the wr-cycle is 88° and the inclination is 48°, the declination and inclination for the wor-cycle are 86° and 52°. For the wr-cycle the rate of roll is around 7°.

The duration of the wr-cycle is 186 time steps, while it is 17 time steps longer for the wor-cycle (Fig. 43). The wr-shearing stroke reaches the maximum intercuspation at t-s 130, and the wor-cycle at t-s 142. During the shearing stroke, the total collision area of both scenarios increases until the maximum intercuspation and decreases afterward. The total overall contact area at the maximum intercuspation is slightly higher for the wor-cycle as for the wr-cycle, whereas it is vice versa at the end of the shearing stroke (maximum mandibular closure).

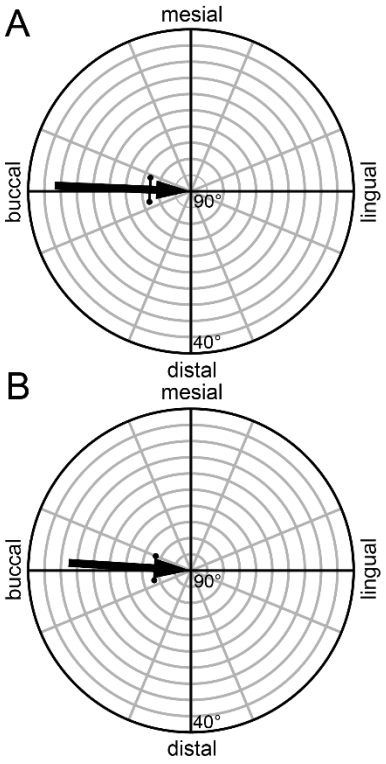

Fig. 42: The mastication compass of both *Spalacolestes cretulablatta* chewing cycle scenarios. The cycles perform a transverse chewing movement with a slight mesial shift. A: The compass for the cycle with roll. B: The compass for the cycle without roll. The marker (line perpendicular to the arrow) depicts the moment of the maximum mandibular closure. The length of the arrow is equated with the duration of the power stroke.

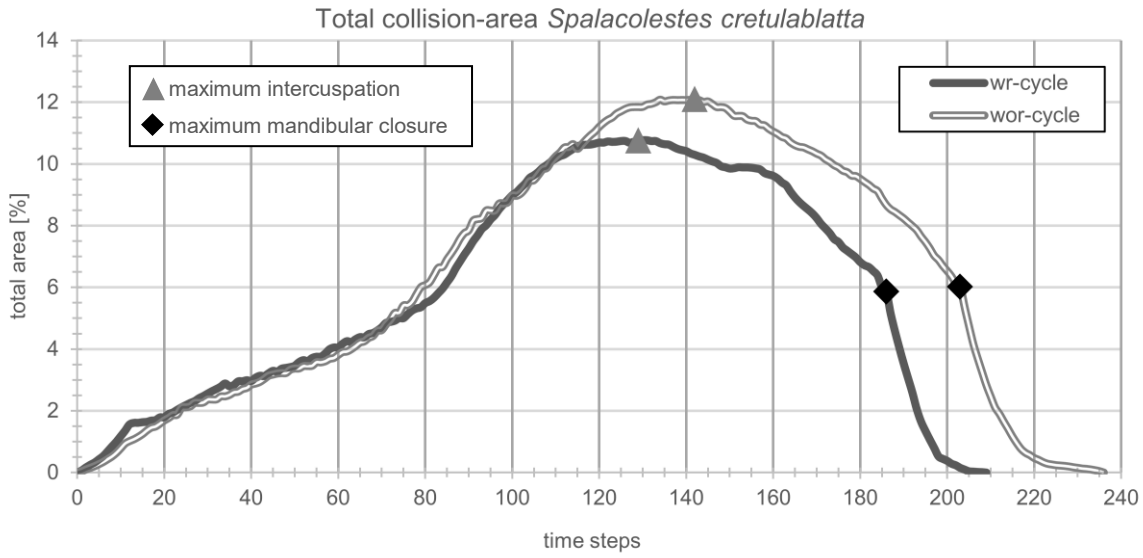

Fig. 43: The diagram of the *Spalacolestes cretulablatta* lower molars total collision area in temporal relation, during one chewing cycle. The total collision area is a percentage of the total collision area of the lower molars relative to the total area of the lower molars. The dark grey graph shows the course of the wr-cycle, the light grey double-line graph that of the wor-cycle.

At the beginning of the shearing stroke pr-bd (pr-b; wor-cycle) contacts PAS-lm (PAS-m; wor-cycle), and pr-bm occludes with MTS-ld (Fig. 44, A; see also Fig. 45). At the same time me-d/PA-m(1) as well as pa-m/PA-d(1) come into contact. In this way, mesial and distal elliptical interdental spaces originate. The mesial interdental space is restricted by [c]pr~me/[C]PAS~PA and [C]PA~MT/[c]pa~pr. With a further upward movement of the lower dentition, the interdental spaces close, and the collision areas expand to the prevallid/postvallum surfaces (pa*pr/PA*MTS) as well as to the postvallid/prevallum surfaces (pr*me/PAS*PA) (Fig. 44, B). In addition, the paracone occludes with the [cg]pr_me as well as with the [cg]pa_pr. From this point on, the cingulids guide the movement of the lower dentition via the PA contact, until the end of the shearing stroke, so that the pa*pr and pr*me surfaces pass along their antagonists (PA*MTS, PAS*PA) (Fig. 44, C).

The distribution of the collision areas of the wr-cycle and wor-cycle equals each other. They are summarized in Figure 45.

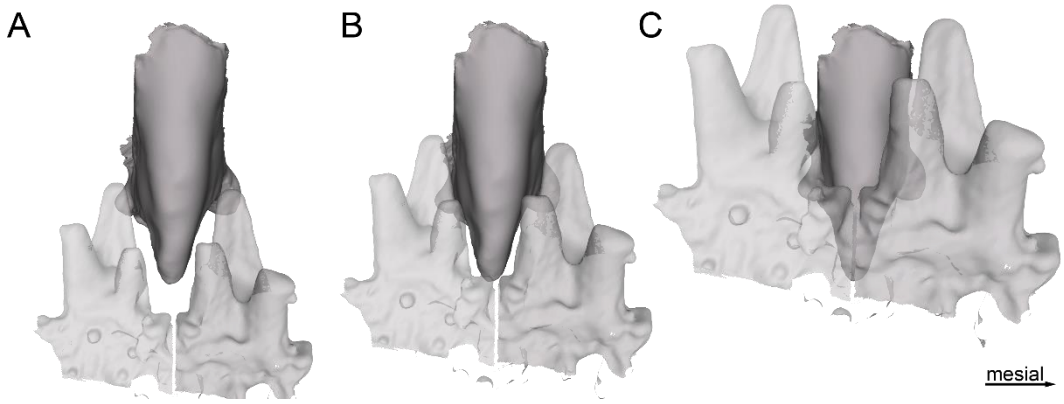

Fig. 44: Key positions during the power stroke of *Spalacolestes cretulablatta*. A: The beginning of the power stroke. The interdental spaces originate. B: The position, in which PA comes into contact with the cingulids. The interdental spaces are almost closed. C: The end of the power stroke.
3D-models of OMNH VP 033231 (M4) and OMNH VP 027421 (m4, m5).

A Collision areas, wr-cycle, *Spalacolestes cretulablatta*

	lower coll. areas	upper antagonists	add. upper antagonists
	pr-bd	PAS-lm	
	me-d	PA-m(1)	PAS*PA
	pr*me	PAS*PA	PA-m(1)
	pr-bm	MTS-ld	
	pa-m	PA-d(1)	PA*MTS
	pa*pr	PA*MTS	PA-d(1)
	[cg]pr_me	PA-m(2)	
	[cg]pa_pr-l	PA-d(2)	
	[cg]pa_pr-b	PA-d(2)	

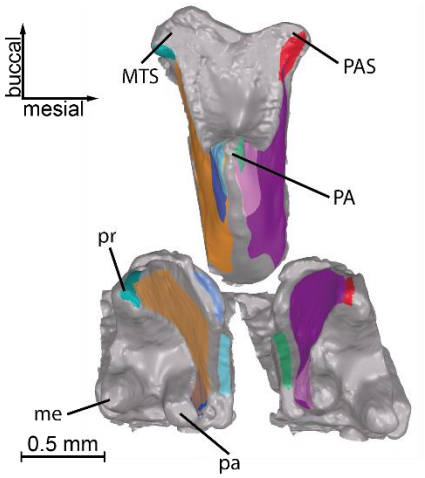

B Collision areas, wor-cycle, *Spalacolestes cretulablatta*

	lower coll. areas	upper antagonists	add. upper antagonists
	pr-b	PAS-m	
	me-d	PA-m(1)	PAS*PA
	pr*me	PAS*PA	PA-m(1)
	pr-bm	MTS-ld	
	pa-m	PA-d(1)	PA*MTS
	pa*pr	PA*MTS	PA-d(1)
	[cgd]pr_me	PA-m(2)	
	[cgd]pa_pr-l	PA-d(2)	
	[cgd]pa_pr-b	PA-d(2)	

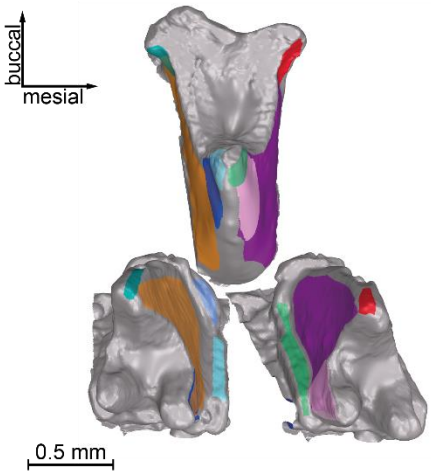

Fig. 45: The resulting OFA collision areas of the power stroke of *Spalacolestes cretulablatta* in summary. A: The collision areas of the wr-cycle. B: The collision areas of the wor-cycle. The contact areas of both scenarios are very similar. Upper molars correspond to right ones, whereas lower molars correspond to left ones.
3D-models of OMNH VP 033231 (M4) and OMNH VP 027421 (m4, m5).

4.3.5 The chewing cycle of *Dryolestes leiriensis*

The chewing cycle of *Dryolestes leiriensis* was studied in detail by Schultz (2012) and Schultz and Martin (2014). In this chapter, the results of these studies are summarized.

The time step division of the *Dryolestes leiriensis* OFA project from Schultz and Martin (2014) has been adjusted to Lambda = 0.01, and the total collision area was converted into percent. These modifications were made in order to make the results comparable to the results of the present study.

For the reconstruction of the chewing cycle, Schultz (2012) and Schultz and Martin (2014) used 3D-models of a right upper (Gui Mam 1150), and a left lower molar (Gui Mam 1155). To complete the set of teeth the left lower molar was duplicated, and the right upper was mirrored. The molars derive from the middle part of the tooth row, but their exact position is unknown. A chewing cycle with a roll has not been reconstructed.

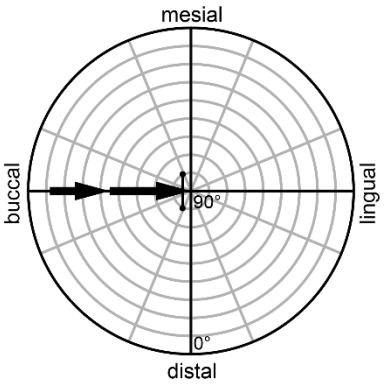

Fig. 46: The wor-cycle mastication compass of *Dryolestes leiriensis*. The chewing cycle performs an upward transverse movement. At first with an inclination of 45° (right arrow), but when the paracone is led by the hypoflexid the inclination decreases to 35°(left arrow). The marker (line perpendicular to the arrow) depicts the moment of the maximum mandibular closure, which is almost at the end of the power stroke.

Generally, the lower dentition performs a transverse movement without a lateral shift (Fig. 46). Whereas at the beginning of the shearing stroke the inclination is 45°, it declines to around 35° at the time when the paracone is guided by the hypoflexid.

The duration of the shearing stroke is 101 t-s (Fig. 47). The total collision area increases until the maximum intercuspation (t-s 95) and is almost at the same level until the end of the shearing stroke. The paracone gets in contact with the hypoflexid (hfd) at t-s 34. At this time, the inclination changes as mentioned above.

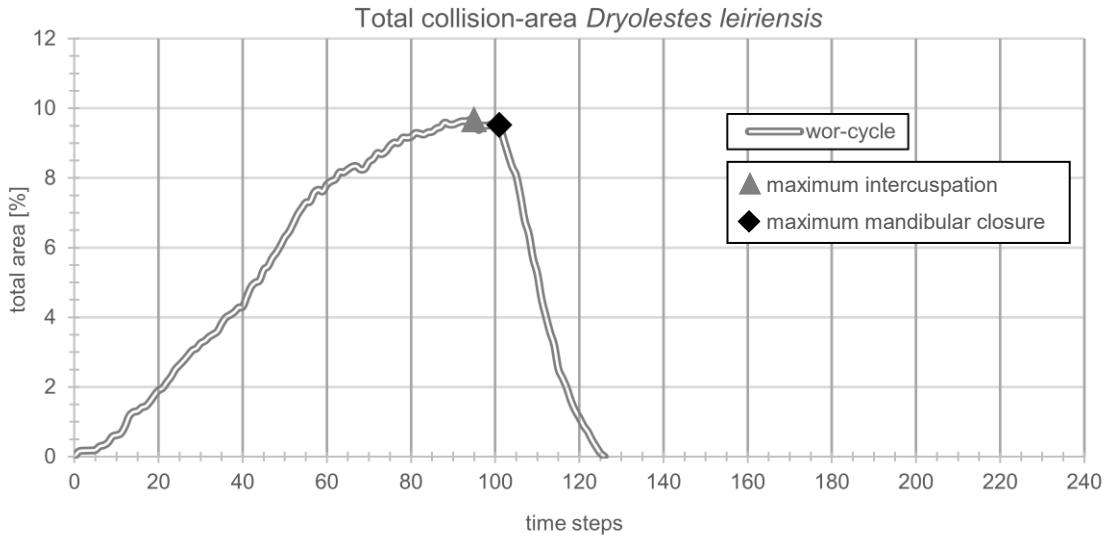

Fig. 47: The diagram of the *Spalacolestes cretulablatta* lower molars total collision area in relation to time, during one chewing cycle. The total collision area is a percentage of the total collision area of the lower molars relative to the total area of the lower molars. The maximum intercuspation almost coincides with the end of the power stroke.

At the beginning of the shearing stroke me-d comes in contact with Pa-m (Fig. 48, A; see also Fig. 49). With further closing, the distal portion of the pr comes in contact with the mesio-buccal part of PA*PAS. Due to the contact of me-d/PA-m as well as pr-d/PA*PAS, an interdental space originates. This space is restricted by [c]me~pr/[c]PA~PAS, gets narrower during the upward movement of the lower dentition, and finally closes. Almost at the time when the interdental space closes, the PA-m-a comes into contact with hfd-bd (Fig. 48, B). This contact results in the deflection of the lower dentition (see above). During PA is led by the hfd, pr*me slides past PA*PAS and pr*pa slides past PA*ME*MTS. The contact areas of pr*me/PA*PAS and pr*pa/PA*ME*MTS increase until the end of the shearing stroke (maximum mandibular closure) (Fig. 48, C).

The resulting overall collision areas are summarized in Figure 49.

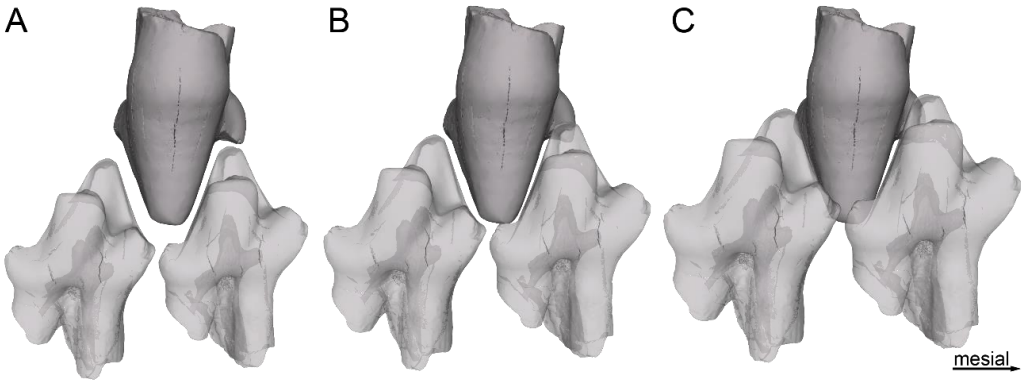

Fig. 48: The important positions during the power stroke of *Dryolestes leiriensis.* A: The beginning of the power stroke. A mesial interdental space originates. B: The position, in which PA-m-a comes into contact with the hfd-bd. The inclination decreases from 45° to 35°. The interdental space is almost closed. C: The end of the power stroke.
3D-models of Gui Mam 1150 (upper molar) and Gui Mam 1155 (both lower molars).

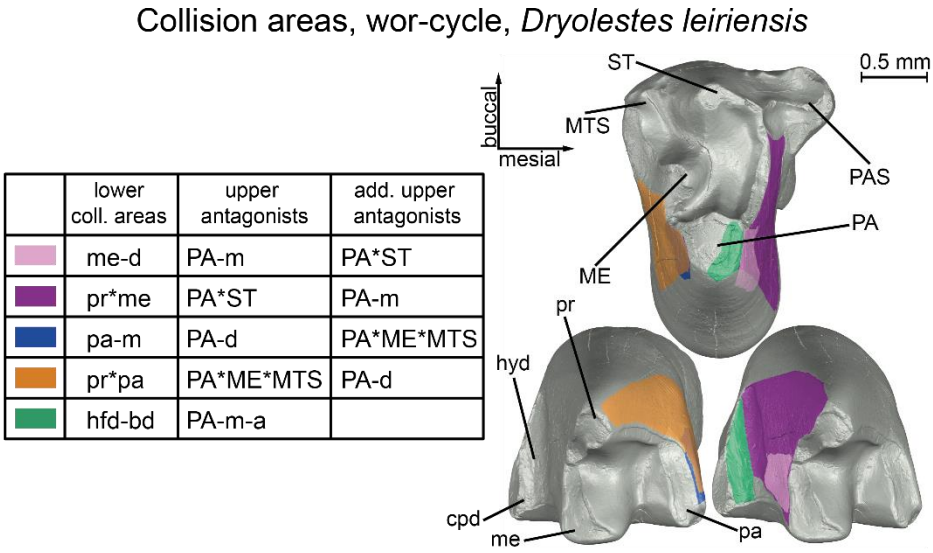

	lower coll. areas	upper antagonists	add. upper antagonists
	me-d	PA-m	PA*ST
	pr*me	PA*ST	PA-m
	pa-m	PA-d	PA*ME*MTS
	pr*pa	PA*ME*MTS	PA-d
	hfd-bd	PA-m-a	

Fig. 49: The resulting OFA collision areas of the power stroke of *Spalacolestes cretulablatta* in summary. Upper molars correspond to right ones, whereas lower molars correspond to left ones.
3D-models of Gui Mam 1150 (upper molar) and Gui Mam 1155 (both lower molars).

4.4 Tooth structure types (“tools”)

The OFA reconstructions of the chewing cycles show that various lower tooth structures, in combination with their upper antagonists, were involved in comminuting food. The interaction between the lower tooth structures and their antagonists can be abstracted into "tools". These “tools” are presented schematically in this chapter.

The Crushing-Tool

The Crushing-Tool performs actions like piercing and crushing (Fig. 50). There are two realizations of this tool. The first type is a cusp, which encounters a chunk of food, whereas the second type is a cusp, which slides into an embayment with food particle in-between. In both scenarios, the material collapses due to the force of the cusp, and cracks originate (Lucas, 2004).

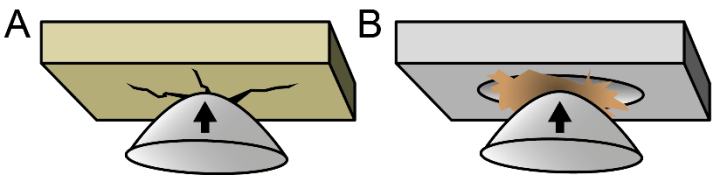

Fig. 50: A cusp encounters a material. By increasing the force, the material collapses, and cracks originate and extend. Thereby, a food particle gets pierced and crushed. A: A cusp encounters food (type I) B: A cusp slides into an embayment with food in-between (type II). (Modified from Lucas, 2004)

The Cracking-Tool

During this process, chunks get trapped and bent between the three cusps (Fig. 51). The bending results in a failure of the food material and cracks originate remotely of the cusps (Berthaume, 2016). The Crushing-Tool can occur simultaneously.

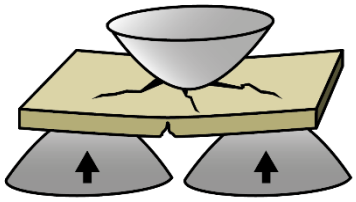

Fig. 51: The material bends between the three cusps, by increasing the force. The result are cracks remote of the cusps. The Crushing-Tool can occur simultaneously. (Modified from Berthaume, 2016)

The Crest-Crest-Tool

This tool includes two straight crests, which move past each other (Anderson and La Barbera, 2008) (Fig. 52). Depending on crest sharpness the food gets shear-cut or blunt-sheared.

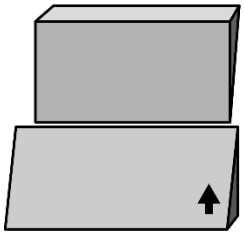

Fig. 52: The Crest-Crest-Tool. The food gets shear-cut or blunt-sheared in-between the crests edges. (Modified from Anderson and LaBarbera, 2008)

The Notch-Fang-Tool

This type of tool consists of two different antagonists, whereas the first is a triangular indented edge, the other one is a fanged crest or a cusp (Fig. 53). Food comminuting through this configuration includes crushing, puncturing, shear-cutting, blunt-shearing and puncture-shearing. The comminuting process depends on the sharpness of the crests or cusps. In addition, this tool includes a “Crushing-Tool” component (Anderson and La Barbera, 2008).

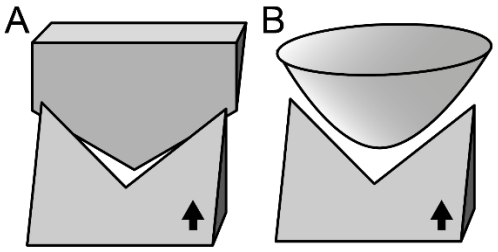

Fig. 53: Two versions of the Notch-Fang-Tool. In both versions food gets pierced, crushed, shear cut and/or ripped apart, depending of the crest, fang sharpness. In A, a fanged crest is involved, while in B it is a cusp. (Modified from Anderson and LaBarbera, 2008)

The Cusp-Groove-Tool

During this process, a cusp moves along a channel, groove or crest (Fig. 54). Food particles in-between the cusp and its antagonists get squeezed and crushed. The dentition movement is largely influenced by this tool.

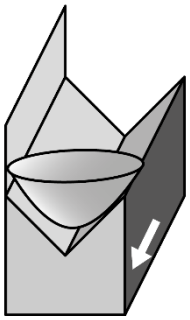

Fig. 54: The Cusp-Groove-Tool. The cusp moves along a channel groove or crest, and food particles in-between these structures get squeezed and crushed.

The Straight-Notch-Tool

This tool includes one straight, and one triangular indented crest (Anderson and La Barbera, 2008) (Fig. 55). When the crests move past each other the restricted space closes and the food particles get trapped in-between. With further closing, the particles get shear-cut, or blunt-sheared, depending on the sharpness of the crests.

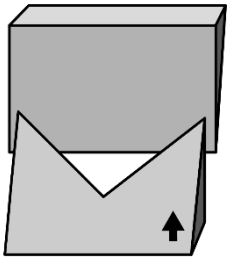

Fig. 55: In this tool the food particles get shear-cut, pinched-off or blunt-sheared by a triangular crest, which moves past a straight crest. (Modified from Anderson and LaBarbera, 2008)

The Notch-Notch-Tool

There are two general versions of this tool (Evans and Sanson, 2003; Schultz, 2012) (Fig. 56). The first version is two opposite edges, in which each edge has a triangular notch. The other version has two curved notches. The principle procedures of these two tools are the same. Food particles get trapped in-between the edges and, depending on the sharpness of the crests, get shear-cut or blunt-sheared.

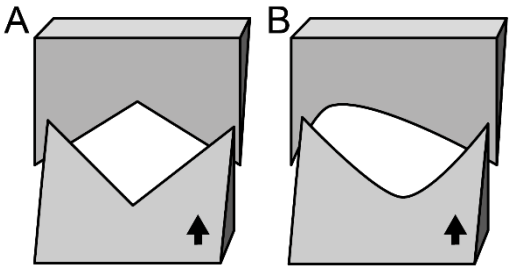

Fig. 56: Both designs of the Notch-Notch-Tool. The triangle inflection (A), and the curved inflection (B). Both designs have the same procedure, they shear-cut, blunt-shear or pinch-off food material. (Modified from Evans and Sanson, 2003)

The Two-Surfaces-Tool

This tool consists of two plane surfaces, which move past each other (Fig. 57, A). During this movement food particles get plane-sheared (Thiery et al., 2017). If there is a groove at one surface, compressional-shearing can occur additionally (Fig. 57, B).

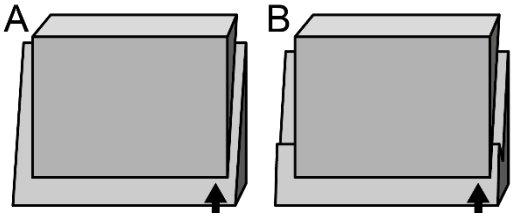

Fig. 57: The Two-Surface-Tool. Food particles get sheared and crushed in-between two surfaces, which past each other. In version B compressional shearing can occur within a groove. (Modified from Thiery et al., 2017)

5 Discussion

In the past, there have been several studies about “symmetrodontan” molars. Most of them were comprehensive descriptions of the occlusion on the base of wear facets of *Kuehneotherium* molars, sometimes with a wear facet homologization of other early diverging and more derived taxa (Crompton and Jenkins, 1967, 1968; Crompton, 1971; Crompton and Jenkins, 1973; Mills, 1984; Godefroit and Sigogneau-Russell, 1999; Gill, 2004b). Other studies set the focus on the dietary specialization of *Kuehneotherium*. According to Gill et al. (2014), *Kuehneotherium* preferred a “soft” prey diet. Their study is based on a quantitative textural microwear analysis of the molars, and a finite element method, which was applied to the mandible. This result was corroborated by an experimental study by Conith et al. (2016), in which simplified models of the *Kuehneotherium* dentition “chewed” different “food” items. Another research approach is the reverse-engineering of an ideal insectivore molar. In these studies, theoretical teeth were generated after certain functional parameters. The shape of one of these theoretical teeth, called the protoconoid (Evans and Sanson, 2003, 2006), is comparable to the structure of “symmetrodontan” molars. Any of these studies gives an insight view into the comminuting process of “symmetrodontan” molars in detail. In the current study, for the first time, the mastication of four different “symmetrodontan” taxa was studied in detail based on the OFA analysis.

Crompton and Hiiemäe (1969, 1970) recognized in a cineflourographic study of the *Didelphis marsupials* mastication two types of power strokes, the crushing-puncturing stroke and the shearing stroke. The crushing-puncturing stroke occurs immediately after ingestion. During that stroke, the ingested prey is fractured (puncture-crushed) without tooth-tooth contact. After the food is adequately comminuted the shearing stroke starts, in which tooth-tooth contact is involved. This observation can also be postulated for the mastication of “symmetrodontans”. The fragmentation process of the crushing-puncturing stroke is comparable to the Crushing-Tool and Cracking-Tool (see chapter 4.4). The crushing-puncturing mode may last some cycles before the shearing stroke starts (Hiiemäe, 1976).

5.1 The roll of a hemimandible in “symmetrodontans”

That “symmetrodontans” and Mesozoic mammals in general rolled the active hemimandible during the shearing stroke has been postulated by various researchers (Crompton and Hylander, 1986; Crompton, 1995; Cifelli and Madsen, 1999; Grossnickle, 2017; Bhullar et al., 2019). Due to this assumption and the possibility to simulate the roll with the current

OFA version, a chewing cycle with roll-rotation was reconstructed for *Woutersia butleri*, *Kuehneotherium praecursoris*, *Maotherium sinense,* and *Spalacolestes cretulablatta*. The comparison of the wor-cycle (without roll cycle) result with the wr-cycle (with roll cycle) result of the respective taxon shows that there are only minor differences. Almost all wear facets, which were described for each taxon in the literature, could be reconstructed without a roll rotation. Clear evidence for a roll could not be found. However, there are two indications, which support a roll. The first hint is the collision areas me-db and pr-db(2) of the *W. butleri* chewing cycle. These areas are much more pronounced in the reconstruction of the wr-cycle and correspond to the described facets of Sigogneau-Russell (1983) and Sigogneau-Russell and Hahn (1995). The second exception is the extension of the *K. praecursoris* wr-cycle collision area PA-m onto the lingo-mesial part of the cingulum. Crompton (1971), as well as Gill (2004), recognized wear at this cingulum area. Nevertheless, the resulting angle of the roll rate in all taxa is relatively modest and ranges between 10° to 6°, whereby a theoretical roll rate of 10° was assumed for all taxa. This range is comparable to the results of the roll rate of *Docodon victor* (~12°; Schultz et al., 2017a), a Late Jurassic docodontan, and the extant marsupial *Monodelphis domestica* (~7°; Bhullar et al., 2019). The OFA analysis showed that the degree of the roll is influenced by the morphology of the molars, and with this observation, it can be postulated, that the roll was passively triggered. Furthermore, the comparison of both cycles points out that the roll did not influence the type of comminution in “symmetrodontans”, because the “tools” remain the same. However, presumably, the roll had a positive effect on the efficiency of the chewing process at least for zhangheotheriids and spalacotheriids. For both taxa OFA calculated a lesser amount of time steps, in connection with a lesser percentage of the total collision area, for the shearing stroke with a roll rotation (wr-cycle), compared to the shearing stroke without a rotation (wor-cycle) of the respective taxon (c.f. Fig. 39 and Fig. 43, and chapter 5.5).

5.2 Interpretation of the OFA chewing cycles in relation to prey comminution

The OFA chewing cycle reconstructions show that the dentition of the studied taxa (*Woutersia butleri*, *Kuehneotherium praecursoris*, *Maotherium sinense*, and *Spalacotherium cretulablatta)* differs in the function of the comminuting process, despite the fact that their chewing path is almost the same. In this chapter, the different chewing cycles will be interpreted, with regard to the comminuting process. Due to the fact, that the OFA only detects collision areas of the tooth-tooth contact, the chewing cycle can be equated with the shearing stroke. But it should be noted, however, that some cycles of the crushing-puncturing mode must have been preceded, in which the Crushing-Tool and Cracking-Tool

came in use. The following interpretation of the mastication processes is a combination of the wor- and wr-cycle.

5.2.1 Mastication of *Woutersia butleri*

The chewing cycle (shearing stroke) of *Woutersia butleri* can be separated into three stages of food reduction. At the beginning of the first stage, a chunk of food got trapped between the notched crest [c]pr~me and [c]pa~pr and their straight antagonists [C]PA-mb and [C]PA~ME (Fig. 58, A). With further closing, the crests moved past each other, and the trapped food was blunt-sheared. The crest structures are comparable to the Straight-Notch-Tool, with the specialty, that the straight crests are inclined. At the time when the crests passed each other the second stage was initiated. During this stage, particles, which were trapped in-between PA-m/pr*me and PA*ME/pa*pr got plane-sheared and crushed. The fragmentation process of this stage is matching the Two-Surfaces-Tool. At the same time, a puncture-crushing between the metaconid of the mesial molar, the paraconid of the distal molar, and CPX took place (Cracking-Tool). In the last stage, two different “tools” came in use. The first one was the Straight-Notch-Tool with a combination of cusps and crests ([CG]CPE_CPX/[c]pr~me; [CG]CPX-d/pa-b) (Fig. 58, B). The second “tool” was the Two-Surfaces-Tool but with the specialty, that there was a compressional-shearing, which took place between PA-ml/me-db and PA-dl/pa-mb. Food got plane-sheared at the lingual flank of the paracone, but then gets stuck at the lingual cingulum. With further closing of the mandible, more and more food particles got accumulated and compressed below the cingulum. Another plane-shearing with a Two-Surfaces-Tool took place at PA-m/pr*me, CPX-d/pa-m, and ME-l/pa*pr. Interestingly, a roll of the mandible would have increased the compressional-shearing activity. The *W. butleri* shearing stroke stages are summarized in Figure 59.

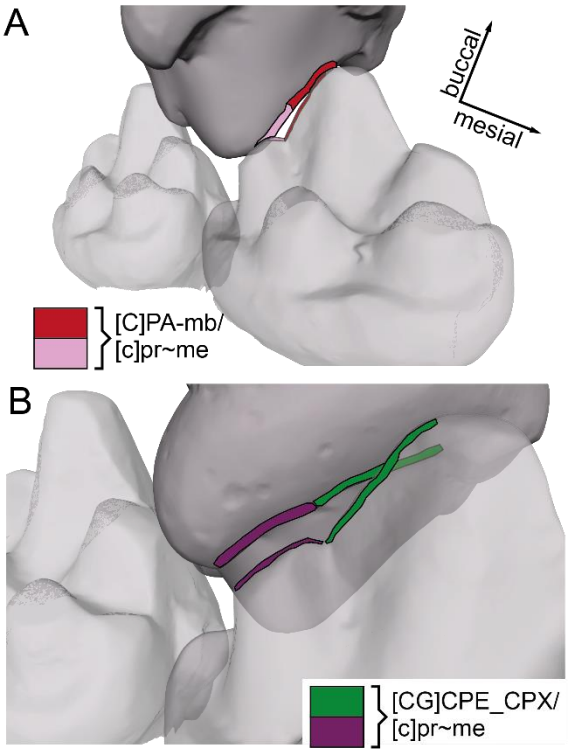

Fig. 58: Snapshots of the shearing stroke of *Woutersia butleri* (mesio-lingual view). The highlighted crests performed a blunt-shearing. A: At the beginning of the first stage. B: During the third stage.
(Upper molar: SNP 720 W, lower molars: SNP 517 W)

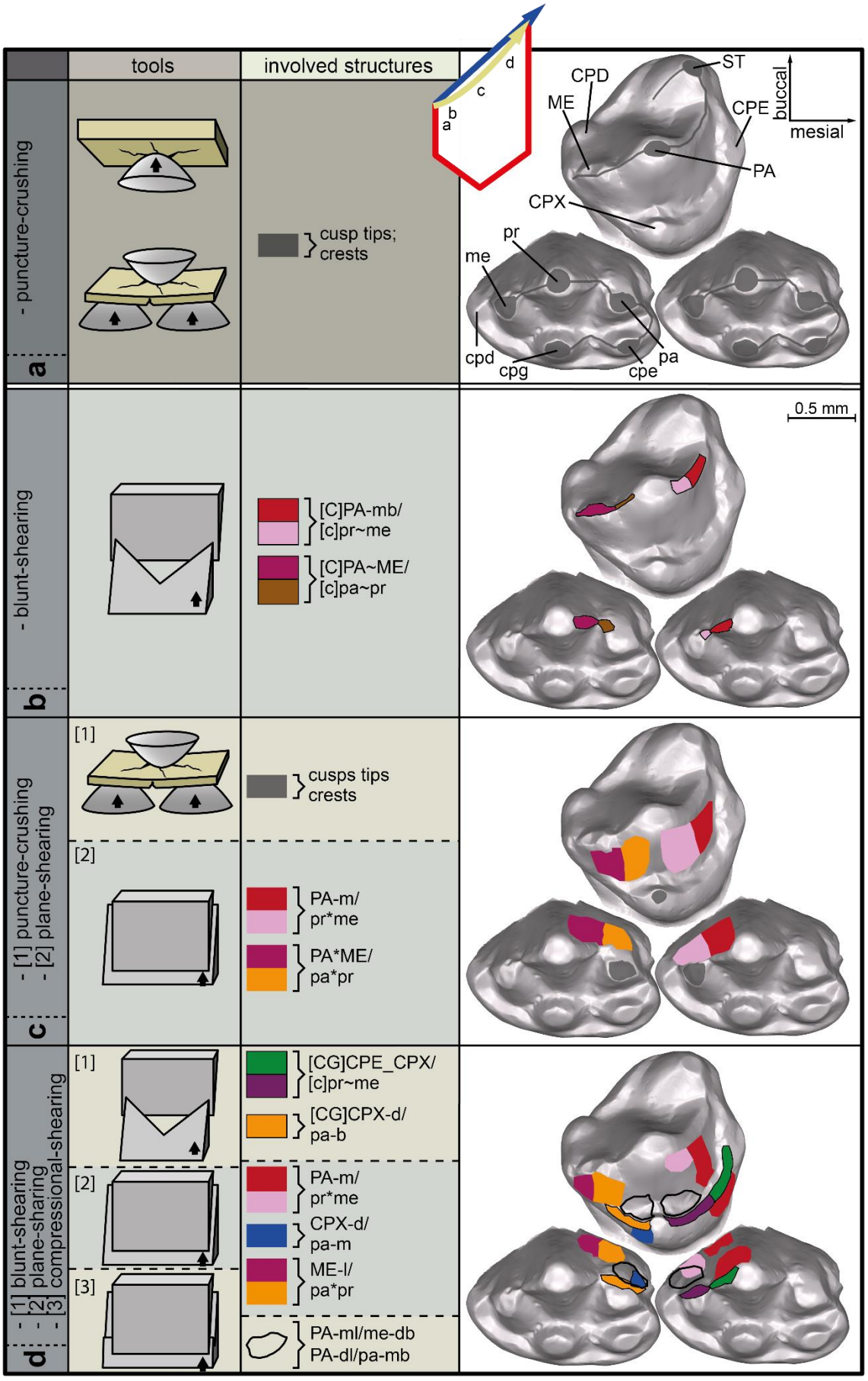

Fig. 59: A summary of the chewing cycle of *Woutersia butleri* and the involved molar structures. The puncture-crushing mode preceded the shearing stroke (a). The shearing stroke can be divided into three stages (b-d). Blue arrow: predicted OFA trajectory path, yellow arrow: calculated OFA trajectory path, red line: recovery stroke.
(Upper molar: SNP 720 W, lower molar: SNP 517 W)

5.2.2 Mastication of *Kuehneotherium praecursoris*

Subsequently to the crushing-puncturing stroke, three shearing stroke stages were recognized for the chewing cycle of *Kuehneotherium praecursoris*. In the first stage, the functional units [C]ST~PA/pr and ME/[c]pa~pr trapped and puncture-sheared the prey, by moving the cusps past the notched crests (Notch-Fang-Tool). At the same time [C]PA-m/[c]pr~me, as well as [C]ME~MTS/[c]pr-m, moved past each other and performed a shear-cutting action. In each of these functional units, one straight crest and one notched crest was involved. Additionally, a plane-shearing started in-between PA-ml/me-db. This plane-shearing took place until the end of the shearing stroke. During the second stage another puncture-shearing was performed, in which the paracone and the notched [c]me~cpd, as well as the paraconid and the notched [C]PA~ME moved past each other (Fig. 60, A). Concurrently, almost all lower buccal cusp flanks started a plane-shearing with their upper antagonists (Fig. 61). It is to point out, that the functional units PA-dl/[cgd]-mb only get into collision if a roll of the mandible is involved. In the course of the third stage, the plane-shearing was continued until the end of the shearing stroke. Shortly before the end of the shearing stroke, a compressional-shearing, additionally to a plane-shearing of ST-l/pr-b, took place, in which food particles got trapped and accumulated in a lingo-distal embayment next to the stylocone and below the cingulum (Fig. 60, B). With further progress, the paracone moved past the embayment, and the chewing cycle was completed. A roll of the mandible would simplify the moving past the cingulum without losing the contact of the flanks. Figure 61 summarizes the different stages of *K. praecursoris.*

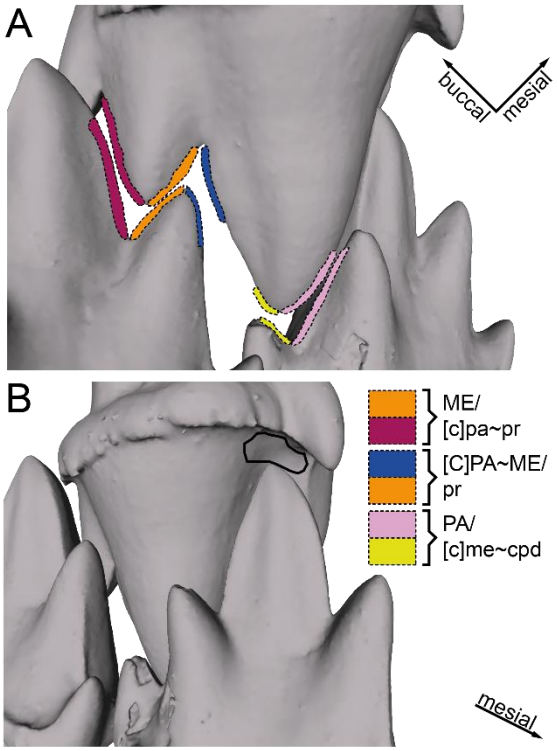

Fig. 60: Two stages of the shearing stroke of *Kuehneotherium praecursoris*. A: Molar position at the beginning of the second stage. Highlighted crest executed a puncture-shearing (lingo-distal view). B: Molar position at the end of the third stage. The encircled area indicates the region, in which a compressional-shearing took place (lingual view).
(Upper molar: PV M 19771, lower molars: PV M 19143)

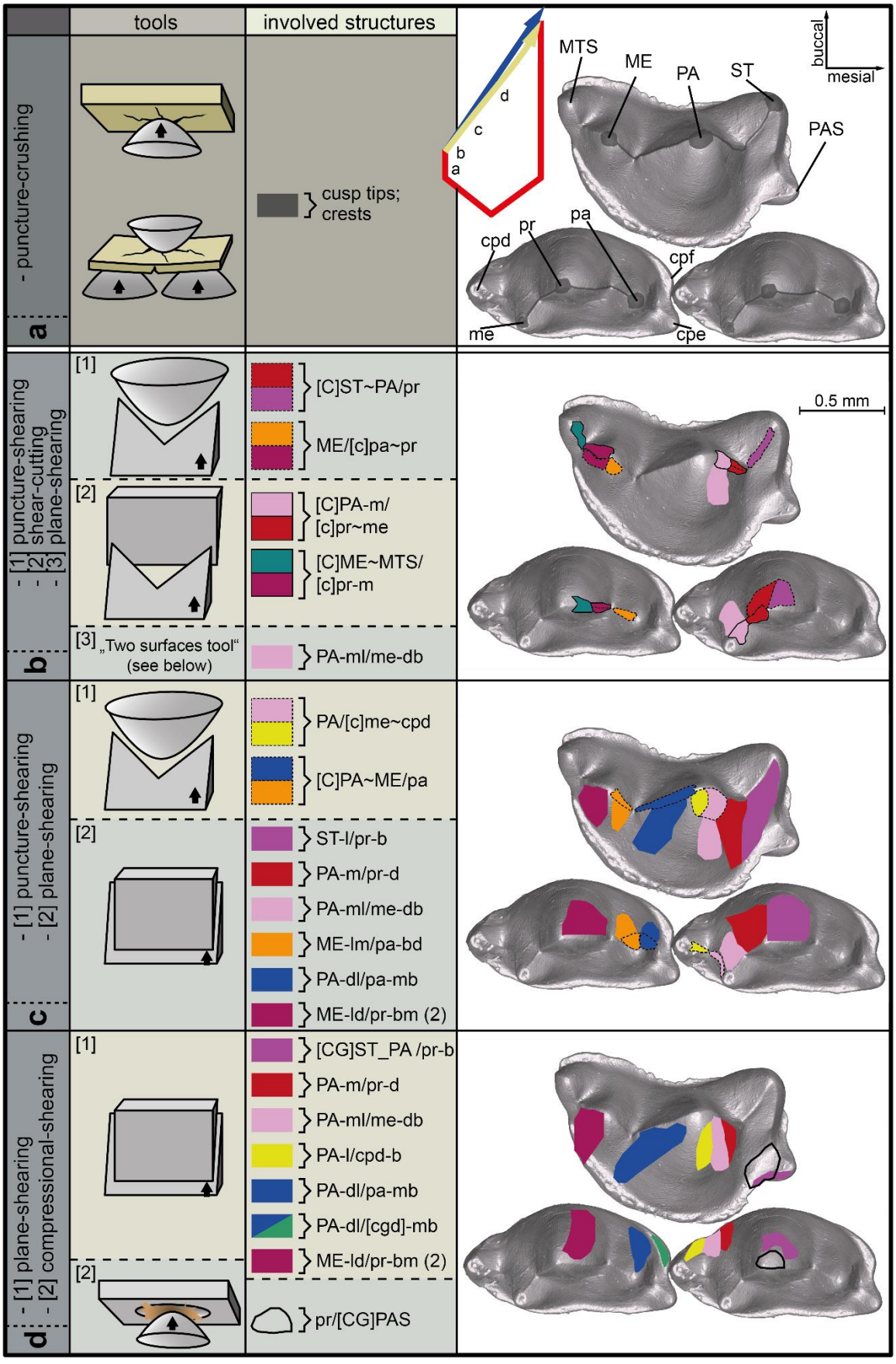

Fig. 61: A summary of the chewing cycle of *Kuehneotherium praecursoris* and the involved molar structures. The puncture-crushing mode preceded the shearing stroke (a). The shearing stroke can be divided into three stages (b-d). Blue arrow: theoretical chewing path, yellow arrow: path resulting from the OFA analysis, red line: recovery stroke.
(Upper molar: PV M 19771, lower molar: PV M 19143)

5.2.3 Mastication of *Maotherium sinense*

The shearing stroke of *Maotherium sinense* can be separated into three stages. The first stage started with a blunt-shearing, in which the functional units [C]CPB'-m/[c]pr-d and [C]PA-m/[c]me-d as well as [C]PA-d/[c]pa-m and [C]CPC-d[c]pr-m were involved (Fig. 62, A). This comminuting action is comparable to the Notch-Notch-Tool. With further closing, the collision zone shifted towards the cusp flanks and a plane-shearing (Two-Surfaces-Tool) took over the blunt-shearing. The involved flanks, are CPB'-m/pr-db, PA-m/me-d, PA-d/pa-m, and CPC-dl/pr-mb. This plane-shearing process was continued in the second stage, and further flanks started a plane-shearing (PA-dl/cpe-mb, PA-ml/cpd-db). Another comminuting process of the second stage was a second blunt-shearing, in which [CG]PA_CPB'/[c]pr~me and [CG]PA_ME/[c]pa~pr were implicated (Fig. 62, B). These functional units have the appearance of the Straight-Notch-Tool. Whereas the plane-shearing contacts of the first stage lost their contact in the third stage, the plane-shearing contacts of the second stage shifted towards basal. With further closing of the mandible a compressional shearing occurs below [CG]PA_CPB' and [CG]PA_ME. Food particles got trapped below the cingulum and were accumulated. A summary of the important stages of the *M. sinense* chewing cycle is summarized in Figure 63.

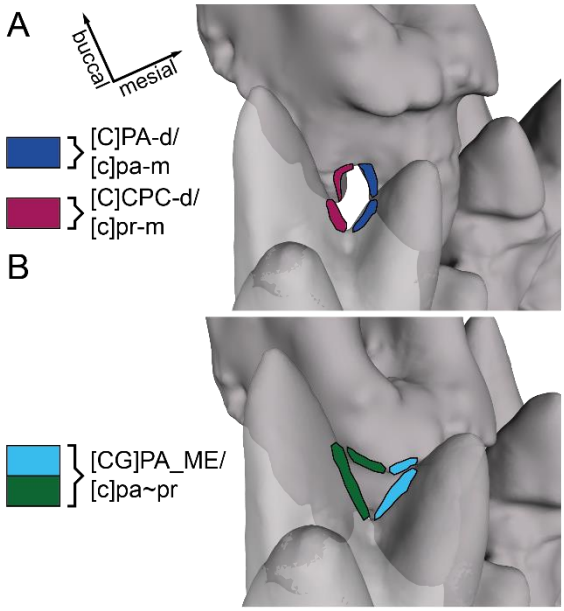

Fig. 62: Two stages of the shearing stroke of *Maotherium sinense* (lingo-mesial view). The highlighted crests performed a blunt-shearing A: At the beginning of the first stage. B: At the beginning of the third stage.
(Upper and lower molars: YFGP 1724)

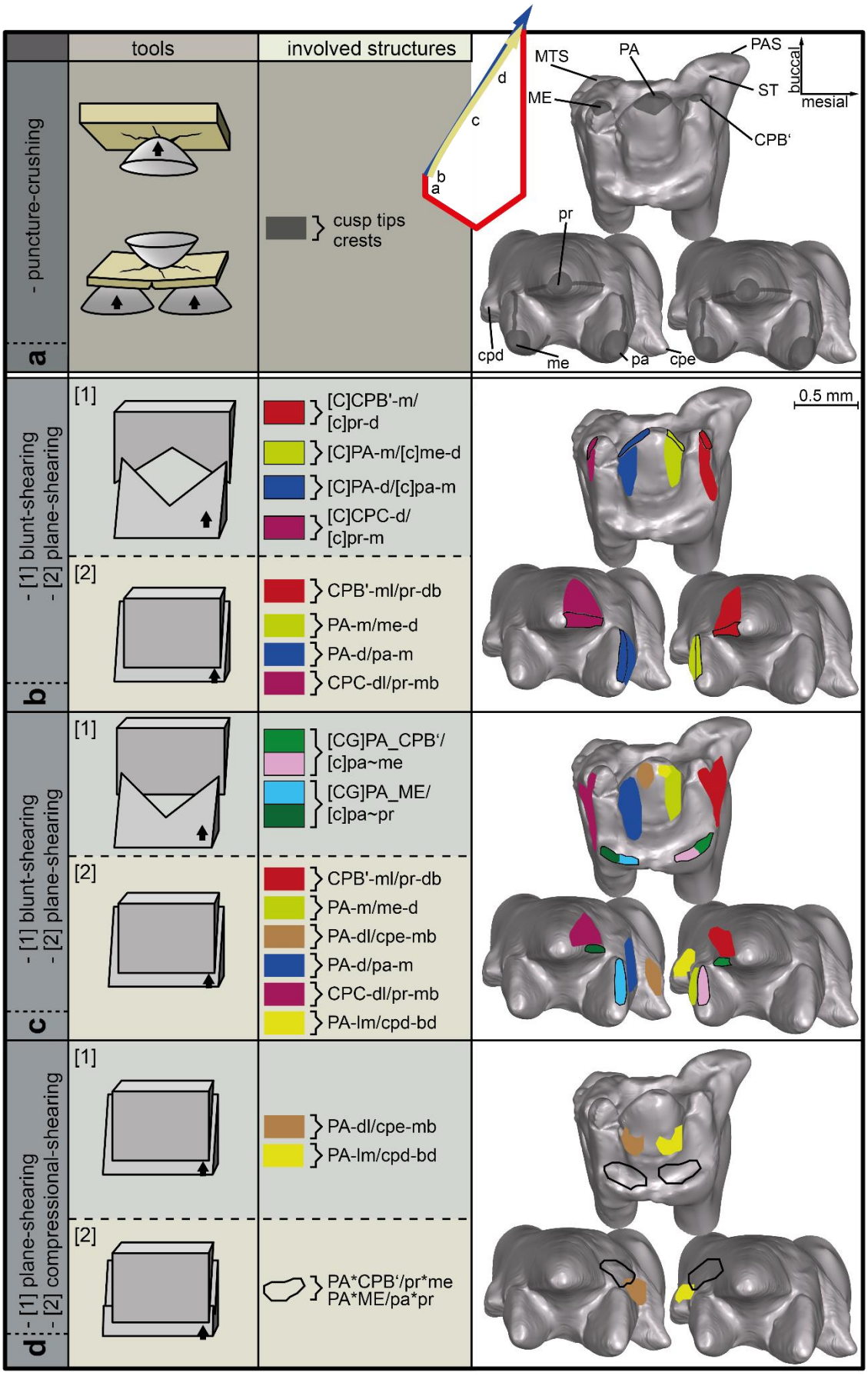

Fig. 63: A summary of the chewing cycle of *Maotherium sinense* and the involved molar structures. The puncture-crushing mode preceded the shearing stroke (a). The shearing stroke can be divided into three stages (b-d). Blue arrow: theoretical chewing path, yellow arrow: path resulting from the OFA analysis, red line: recovery stroke.
(Upper and lower molars: YFGP 1724)

5.2.4 Mastication of *Spalacotherium cretulablatta*

The shearing stroke of *Spalacolestes cretulablatta* can be divided into two principal stages. With the closing of the mandible, a shear-cutting process was performed by the functional units [C]PAS~PA/[c]pr~me and [C]PA~MTS/[c]pa~pr (Fig. 64, A). This cutting action is comparable to the Notch-Notch-Tool, but with two concave crests. With further closing of the mandible, trapped food between the sharp crest was cut similar to a cigar cutter. After the crest units moved past each other, a plane-shearing started, in which PAS*PA/pr*me and PA*MTS/pa*pr were involved. This plane-shearing continued until the end of the second stage. During the second stage, a compressional-shearing took place between PA-m and [cgd]pr_me as well as PA-d and [cgd]pa-pr (Fig. 64, B). These occlusal contacts guided the mandible during further closure. The different stages are summarized in Figure 65.

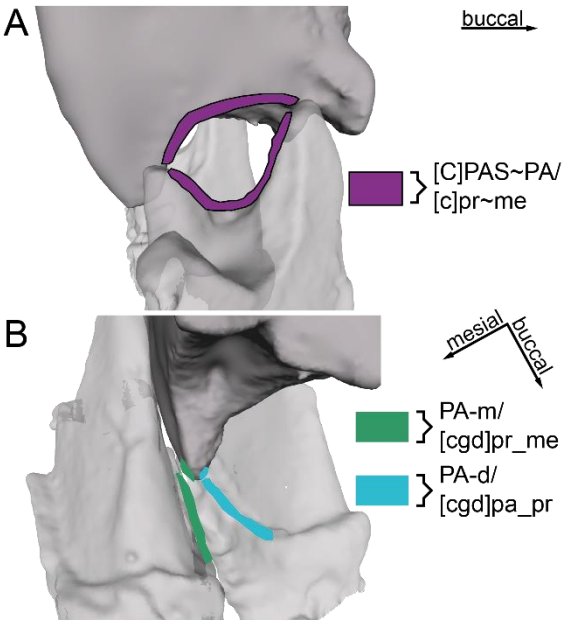

Fig. 64: Two stages of the shearing stroke of *Spalacolestes cretulablatta* A: At the beginning of the first stage. Highlighted crests executed a shear-cutting (distal view). B: At the beginning of the second stage: Highlighted areas performed a compressional-shearing (bucco-lingual view). (Upper molar: OMNH VP 033231, lower molars: OMNH VP 027421)

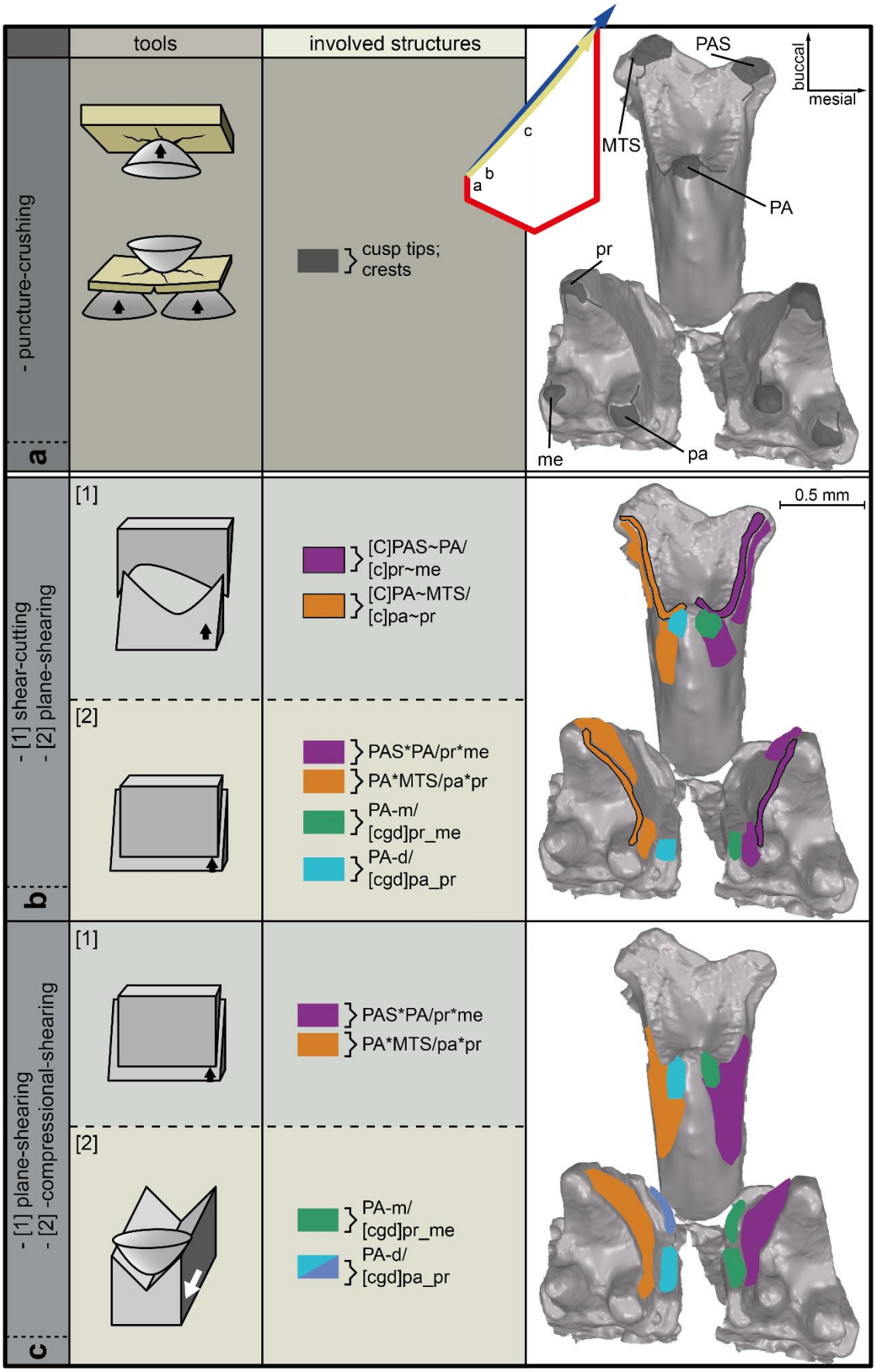

Fig. 65: A summary of the chewing cycle of *Spalacolestes cretulablatta* and the involved molar structures. The puncture-crushing mode preceded the shearing stroke (a). The shearing stroke can be divided into two stages (b and c). Blue arrow: theoretical chewing path, yellow arrow: path resulting from the OFA analysis, red line: recovery stroke.
(Upper molar: OMNH VP 033231, lower molars: OMNH VP 027421)

5.2.5 Mastication of *Dryolestes leiriensis*

There are three stages within the *Dryolestes leiriensis* shearing stroke. At the beginning of the first stage, food particles were shear-cut between [C]PA~PAS and [c]me~pr (Fig. 66, A). This shear-cutting is comparable to the Notch-Notch-Tool, but with concave crests. At the same time, there was a plane-shearing process between PA*PAS and me*pr, as well as a compressional-shearing between PA-m-a and hfd-bd (Fig. 66, B). Both processes were continued until the end of the shearing stroke. With the contact of PA-m-a and hfd-bd, a change of the inclination angle of about -10° occurred. Until the end of the shearing stroke, the contact between PA-m/hfd-bd led the occlusal movement of the mandible. At the beginning of the second stage, the shear-cutting of the functional unit [C]PA~PAS/ [c]me~pr ended, and a shear-cutting of [C]PA-d/[c]pa-m started (Notch-Notch-Tool). As mentioned above, the plane-shearing and compressional-shearing processes were continued but shifted slightly. At the end of the second stage, and with the beginning of the third stage, the [C]PA-d/[c]pa-m shear-cutting ended and a plane-shearing started below their flanks (PA-d/pa-m). Figure 67 is a summary of the three stages.

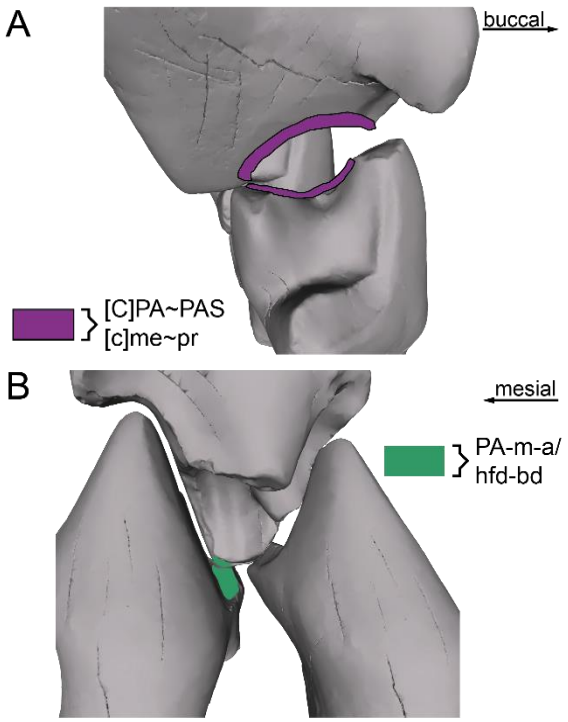

Fig. 66: Two stages of the shearing stroke of *Dryolestes leiriensis*. A: At the beginning of the first stage. Highlighted crests executed a shear-cutting (mesio-occlusal view) B: At the beginning of the second stage. Highlighted areas performed a compressional shearing (buccal view).
(Upper Molar: Gui Mam 1150, lower molars: Gui Mam 1155)

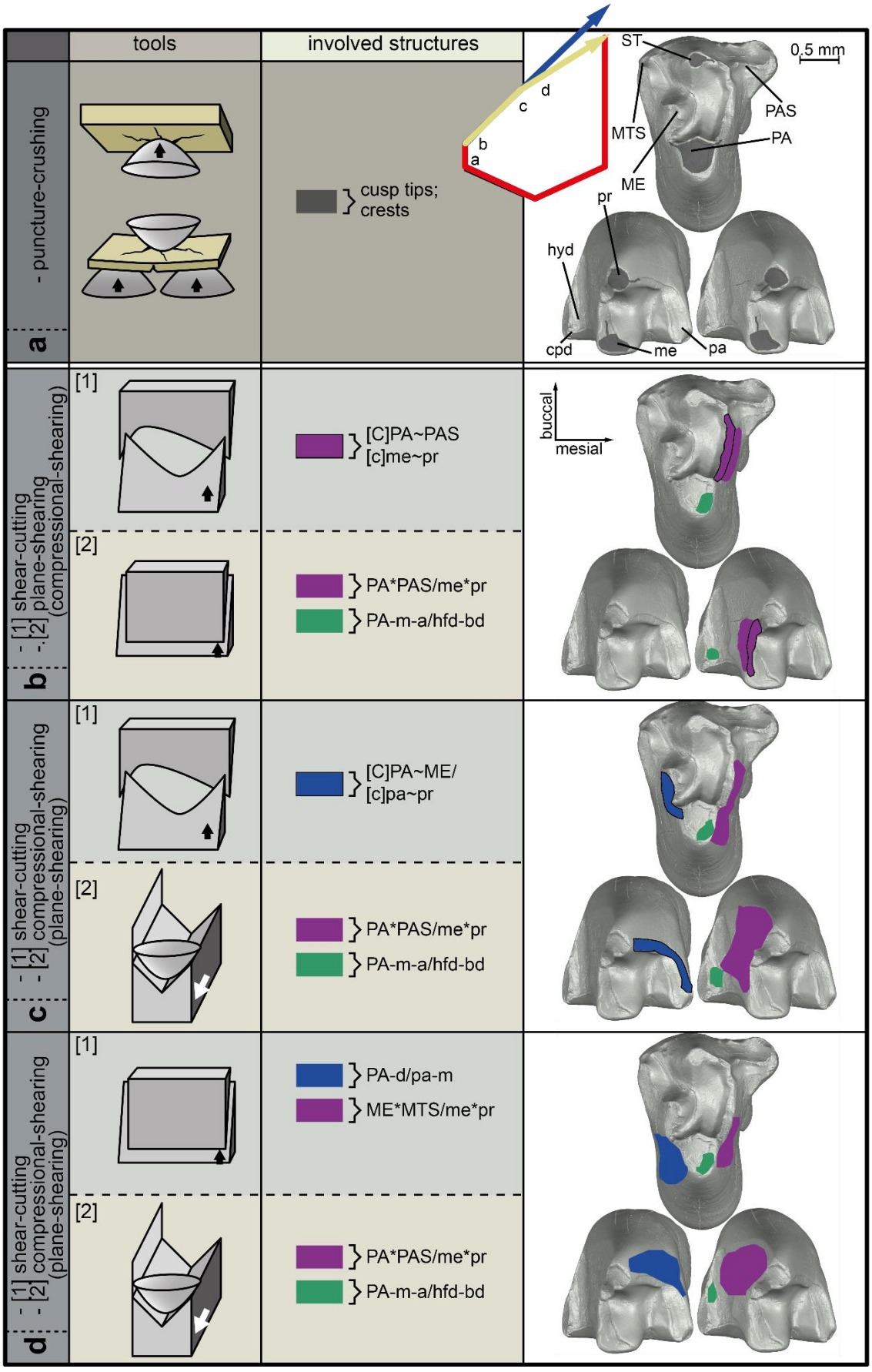

Fig. 67: A summary of the chewing cycle of *Dryolestes leiriensis* and the involved molar structures. The puncture-crushing mode preceded the shearing stroke (a). The shearing stroke can be divided into three stages (b-d). Blue arrow: theoretical chewing path, yellow arrow: path resulting from the OFA analysis, red line: recovery stroke.
(Gui Mam 1150, lower molars: Gui Mam 1155)

5.3 The molar occlusion of “symmetrodontans” in comparison

The interpretation of the “symmetrodontans” food comminuting showed that the fragmentation process is different, despite the fact that the principle movement of each mandible (transversal upward with a slight mesial or distal shift) resembles each other. But there is one basic feature, which can be identified in all taxa, the embrasure shearing (Fig. 68). The embrasure shearing is characterized by an arrangement of tooth structures, which are like a three-sided pyramid wedge that moves upwards and transversely in an embayment. The embayment has the same form as the wedge, only negative. The advantage of this configuration is that the sides of the pyramids, which are embraced by the embayment, are in constant contact with its opposing embayment surfaces, during the whole time of the movement (Crompton et al., 1994).

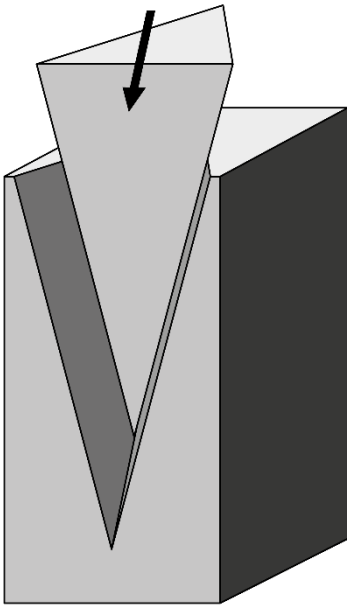

Fig. 68: The principle of the embrasure shearing. The advantage of the embrasure shearing is to provide a constant contact of the collision areas. (Modified from Schultz and Martin, 2014)

The food comminution of *Woutersiidae* was dominated by crushing and puncturing, in which the cusp tips were involved (Crushing-Tool, Cracking-Tool). This observation is supported by the abrasive origin of the heavily worn cusp tips (Sigogneau-Russell, 1983). In the course of this, the inclination of the occlusal wear surface is interesting. Most of the occlusal wear is a result of tooth-food or tooth-food-tooth interaction. Exceptions are the lingually inclined wear facets of cpg, cpe, and the lingual cingulid cusples. Due to the lingual orientation of these wear facets, they must have been originated by a tooth-food-tongue interaction. A shear-cutting component as proposed by Butler (1997) was not recognizable, although [C]pa-mb is very prominent, it lacks an adequate antagonist with a sharp crest. Hence, during the shearing stroke, [C]PA-mb/[c]pr-me pinched-off (blunt-sheared) the food rather than cut it. Noteworthy is the second puncture-crushing component at the end of the cycle in which CPX, pa of the distal molar, and me of the mesial molar was involved. Butler (1997) described this puncture-crushing component as an early stage in the development of opposition, in which the buccal flanks of CPX occluded lingually of pa and me, and resulted in a rudimentary crushing action. This oppositional occluding function otherwise occurred for the first time among Jurassic “allotherians” and docodontans (Butler, 1997). This mode of occlusion could not be confirmed by the OFA. In the reconstructions, the upper molar moved buccally past the lower molars, but the resulting compressional-shearing had to lead to some sort of crushing action. It is conceivable, that CPX of another molar position showed this opposition because the CPX of other woutersiid specimens (e.g., SNP 719, Sigogneau-Russell and Hahn, 1995) is more detached from the paracone than the CPX of SNP 720. Concurrently to the

puncture-crushing, blunt- and compressional-shearing, and extensive plane-shearing took place, in which almost the complete buccal area of the lower molars, and their upper antagonists, were involved. Due to the obtuse triangulation of the main cusps, high freedom in the occlusal movement was possible, which benefitted the plane-shearing. The embrasure shearing is rudimentary but recognizable. During the shearing stroke, pr*mr*cpd and cpe*pa*pr embraced the lingual part of the upper molar. It must be noted that a particular region of wear, which was documented in the literature, could not be reached with the *Woutersia butleri* chewing cycle reconstructions. The wear extends from the mesial side of the stylocone onto CPE and meets [C]PA-mb half the way (Sigogneau-Russell, 1983; Sigogneau-Russell and Hahn, 1995; Butler, 1997) (Fig. 20). The region could not be reached, because only isolated molars from different specimens were available for the reconstructions. For this reason, the accuracy of fit is not as precise as with associated molars, but it must be the bucco-distal area of the protoconid that occluded with ST*CPE. However, the herein presented masticatory cycles are a good first approximation, which shows the principle comminuting process of Woutersiidae.

After the crushing-puncturing-stroke of *Kuehneotherium praecursoris* and with the beginning of the shearing stroke, the fractured food was mainly comminuted by the tips of the cusps and their notched crest antagonists (Fang-Notch-Tool). The puncture-shearing was performed temporally offset at four different loci (see Chapter 5.2.2). With further closing, an embrasure shearing function was implemented, in which each cusp was successively led by its opposite flanks. The embrasure shearing has been detected at the following positions:

- protoconid in-between ST-dl and PA-ml
- metacone in-between pa-db and pr-mb
- paracone in-between me-db and cpd-mb
- paraconid in-between PA-dl and ME-ml

Crompton (1971) recognized the same occlusal pattern. Godefroit and Sigogneau-Russell (1999) also described the same embrasure shearing for the paraconid, but are of the opinion, that the protoconid occluded between the stylocone and metacone of the succeeding molar. In addition, they described an occlusion of the paracone onto cpd, instead in-between the metaconid and cpd. Another opinion was presented by Mills (1984). Although he recognized the same occlusal pattern for the protoconid and paracone as Crompton (1971), Mills described an occlusion of the paraconid against the metacone rather than an embrasure shearing of those cusps. Gill (2004b) proposed a similar occlusal pattern, which was described by Mills (1984). She recognized the same embrasure shearing pattern presented here but proposed another mincing process. Gill (2004b) considered, that the main comminuting function in *Kuehneotherium* was in-between ellipsoid spaces, formed by sharp, concave (notched) blades, that moved past each other and trapped and cut food.

This suggestion is not consistent with the OFA analysis. During the chewing movement, no ellipsoidal spaces were formed, but at two locations ([C]PA-m/[c]pr~me and [C]ME~MTS/[c]pr-m) a straight crest moved past a notched crest and shear-cut food particles (Straight-Notch-Tool). However, the dominant comminuting process was the above-mentioned puncture-shearing with a following embrasure shearing (plane-shearing process), as well as a minor shear-cutting, and not the proposed shear-cutting in-between ellipsoid spaces. It is possible, that the different occlusal interpretations are related to local species variations of *Kuehneotherium* (Godefroit and Sigogneau-Russell, 1999). Another reason for the different interpretations of the occlusion could be associated with the molar position or with the considerable freedom in the occlusal movement.

Crompton (1971), as well as Mills (1984), suggested that an extensive remodeling of the *Kuehneotherium* crown by wear is needed to establish an effective occlusion. Gill (2004b) on the contrary, considers that the *Kuehneotherium* molars are well adapted for an effective occlusion at eruption. She supports her point of view with another interpretation of the molar orientation, and on shearing blade details. The OFA analysis confirms the assumption, the molars are well adapted for an effective occlusion at eruption. The almost unworn molars that were used for the OFA analysis fit flawless into each other, even though they are from different specimens.

The shearing stroke in Zhangheotheriidae was dominated by blunt-shearing and plane-shearing processes. The blunt-shearing process was executed in two stages. In the first stage, the blunt-shearing happened between the indentation of the upper and lower main cusps (Notch-Notch-Tool). The blunt-shearing of the second stage is comparable to the blunt-shearing at the end of the Woutersiidae shearing stroke. Both taxa accumulated food particles below the cingulum, which resulted in a compressional-shearing (crushing process). An embrasure shearing occurred between upper and lower molars, and not between cusps as in Kuehneotheriidae. Due to a more acute triangulation of the molar main cusps, the embrasure shearing was more intense than in Woutersiidae. Not only the lingual flank but also the mesial and distal areas of the upper molar were embraced by the mesio-lingual and disto-lingual sides of the lower molars. As a result of the embrasure shearing, a plane-shearing occurred during the entire chewing cycle. The collision areas of the plane-shearing are patchy and restricted to the mesial and distal molar surfaces. Striations on the *Maotherium sinense* premolars and molars with different inclinations indicate, that there was a certain freedom in the occlusal movement. However, due to the acute triangulation of the main cusps, the freedom of occlusal movement was more restricted in zhangheotheriids as in woutersiids. The *M. sinense* collision areas resulting from the OFA analysis are similar to the wear facets described for *Anebodon luoi*, another, early diverging, Zhangheotheriidae (Bi et al., 2016, supplementary information). Hence, the chewing cycle

of both Zhangheotheriidae, and therefore presumably of all Zhangheotheriidae, resembles each other, due to a similar molar morphology.

Bi et al. (2016) proposed that only after considerable wear of zhangheotheriid molars a tight occlusal fit is given, and only then the stylocone and metastyle would participate in the comminuting process. The OFA analysis is showing another scenario. The molars had not to be remodeled by wear to efficiently comminute prey. The purpose of the morphology of the molars was not to shear-cut prey, and therefore sharp crests and a tight occlusion was not necessary. The molars' task was to puncture, crush and blunt-shear (pinch-off) the food particles. Even if ST*CPB'*PA/pr*me*cpd and PA*ME*MTS/cpe*pa*pr have been vastly worn-off, the stylocone and metastyle are too far buccally to get in full contact with the lower molar flanks. Therefore, both the stylocone and metastyle did not participate in a shearing process.

The comminuting process of Spalacotheriidae, on the contrary, was dominated by a shear-cutting process. After an initial puncturing to fix the prey, it was shear-cut in-between sharp mesial and distal crests ([C]pas~/[c]pr~me, [C]pa~MTS/[c]pa~pr). However, the dentition worked similar to pinking shears (Fig. 71). Only a minor amount of really small food particles was then crushed between the flanks of the cusps (plane-shearing). This can be assumed due to the acute triangulation. The acute triangulation allowed only a little freedom of the occlusal movement and a vast embrasure shearing. These observations are mostly consistent with the assumptions of Cifelli and Madsen (1986). They mentioned, that a plane-shearing for Spalacotheriidae has been overemphasized and that the puncture-crushing and shear-cutting were the important comminuting processes. They support their assumption with the occurrence of a heavy worn crest with a concurrent absence of polished mesial and distal wear facets. They also noted, that the cingulids apparently served as a crushing surface or as a “stop mechanism”. The OFA analysis shows that the compressional-shearing process, in which the paracone and the cingulids were involved, had not only the primary function of a “stop mechanism”, but also that of guiding the lower dentition. However, some food particles were crushed in this region. This can be concluded due to some abrasive wear within the v-shaped cingulid crests, and the flattening of the cingulids in occlusal plane in more advanced wear stages (Cifelli and Madsen, 1986). Cifelli and Madsen (1999) assumed a significant roll and lateral translation for spalacotheriids. This assumption is based on an unusual condition of the pterygoid crest and the lateral reflection of the postero-ventral margin of the dentary, which are presumably functionally related to the roll and lateral translation. Another hint is the obliquely oriented striae on the molar’s mesial and distal flanks (Cifelli and Madsen, 1999). The reconstructed shearing stroke supports the high value of lateral translation, but unambiguous evidence for a roll could not be provided. Hence, both chewing cycles are possible, but it is to mention, that a roll would have made the shear-cutting process more efficient.

5.4 *Spalacolestes cretulablatta* and *Dryolestes leiriensis* in comparison (with remarks on zalambdodont and dilambdodont tooth morphologies)

Within “symmetrodontans” the shearing stroke of spalacotheriids resembles that of the dryolestidan *Dryolestes leiriensis* the most. The comminuting process of *D. leiriensis* is dominated by a shear-cutting function, in which the mesial and distal molar crests are involved ([C]ME~MTS/[c]me-pr, [C]PA-ME/[c]pa~pr). The acute-angled triangulation of the main cusps allowed a deep embrasure shearing, and therefore little freedom in occlusal movement. For this reason, the plane-shearing between those flanks had to be of minor importance for food comminution, because there was only little space between the flanks, in which food items could get crushed. Schultz and Martin (2011) recognized for *D. leiriensis*, that the inclination of the striations near the protoconid apex is steeper than the striations above the hypoflexid. The latter striations are parallel to the hypoflexid surface. The same pattern was also recognized for the upper molars. The inclination of the striae near the paracone apex is steeper than near the parastylar region. The inclination difference between the striations near the protoconid (paracone) apex and hypoflexid (parastyle) region is around 10°. This indicates, that the hypoflexid deflected the paracone and the direction of the movement was changed by around 10°. During the paracone/hypoflexid contact a compressional-shearing occurred, in which food particles were crushed. A similar process can be seen in the OFA analysis of *Spalacolestes cretulablatta*, but with some differences. A change in the directional movement could not be recognized. The striations at the protoconid (paracone) apex and at the base of the crown(s) are almost parallel. The paracone antagonists of spalacotheriids are cingulids instead of the hypoflexid. However, the result was the same, a compressional-shearing occurred as well as a guidance of the lower jaw movement.

The last occurrence of “symmetrodontans” in the fossil record is in the Late Cretaceous, so it can be assumed that “symmetrodontans” got extinct before the Mesozoic-Cenozoic boundary. Almost at the same time the metatherians and eutherians underwent an explosive radiation (Luo, 2007), but within modern (tribosphenic) mammals a convergent development, similar to the acute-angled molar structure, took place. The convergently evolved structural molar topologies are called zalambdodont and dilambdodont. Most extant mammals with a zalambdodont or dilambdodont dentition are insectivores or omnivores (with a high content of invertebrates) (Hillson, 2005). Zalambdodont molars are found in extant eutherians like Solenodontidae (Fig. 69), Tenrecidae, Chrysochloridae, and the extant metatherian *Notoryctes*. Additionally, there are various extinct Eutheria (e.g. *Oligoryctes*, *Koniaryctes*, *Parapternodus*, *Apternodus*) and Metatherians (e.g. *Necrolestes, Yalkaparidon*) (Asher and Sánchez-Villagra, 2005). Dilambdodont molars are present in

extant placental mammals like Soricidae, Talpidae, Scandentia, and Vespertilionidae, and in extinct taxa like nyctitheriids, chalicotheres, brontotheres, and Pantolambdidae (Butler, 1996; Lopatin, 2006). Zalambdodont molars generally have a large central molar cusp from which two ridges branch off mesio- and disto-buccally, therefore the molars have a v-shaped appearance in occlusal view (Fig. 69). Dilambdodont mammal molars have a w-shaped appearance in occlusal view, in which from each of two central cusps two ridges branch off towards mesio- and disto-buccally. Another similarity between zalambdodont and dilambdodont molars is a reduced talonid area (Asher and Sánchez-Villagra, 2005). Therefore, the main task of those molars is to shear-cut food, similar to acute-angled “symmetrodontans”.

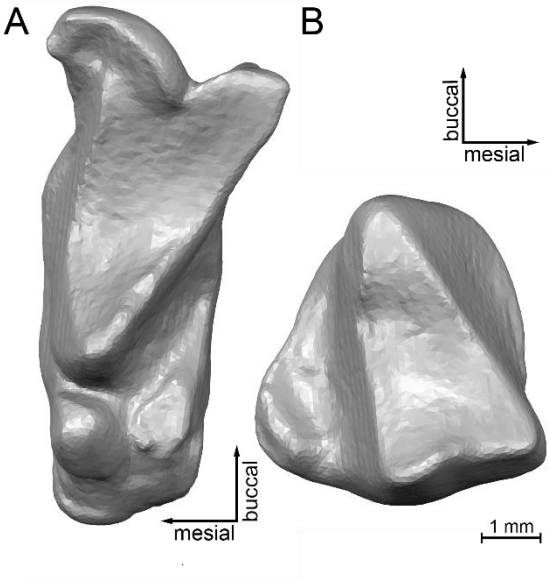

Fig. 69: Zalambdodont dentition of *Solenodon paradoxus* (ZFMK 658, occlusal view). A: Left M3 B: Left m3. (3D-model provided by Andreas Lang)

5.5 The efficiency of “symmetrodontan” mastication with indications of dietary preferences

Mammals need a large amount of energy to maintain the homoeothermic endothermic metabolic system. For this reason, it was necessary to evolve an efficient masticatory system to break down food into small pieces. The smaller the food particles reach the digestive system, the better is their absorption and nutrient assimilation potential and thus the yield of energy (Lumsden and Osborn, 1977; Prinz and Lucas, 1997; Prinz et al., 2003; Clarke and Pörtner, 2010). Additionally, food comminution should be connected with minimal use of energy. Therefore, the adaptation of the tooth morphology to the preferred diet allows mammals to meet their energy requirements with a minimal effort of energy. This principle explains the highly diverse molar morphology within the Mammalia (Lucas and Peters, 2000). In connection with these considerations, it is of interest to determine the efficiency of the “symmetrodontans” comminuting process among one another and in relation to their evolutionary predecessors (“triconodontans”) and successors ((Pre-) tribosphenidans). This chapter shows some tendencies and considerations, despite the fact that for fossil taxa a direct quantification of the efficiency of the comminuting process on the basis of the tooth morphology and occlusal relationship is difficult to determine and to compare. The efficiency of the masticatory complex can be described as the ability to

comminute the food into an optimal particle size, with a minimum of time and energy expenditure (Schultz, 2012). However, methods, which qualify this approach cannot be used for fossil taxa, because living test subjects would be needed for verification. Those methods evaluate the entire masticatory complex, which includes the dentition, jawbones, muscles, tongue, cheeks, saliva, palate, and sensory operations, but for most fossil taxa only hard tissue (dentition and jawbones) is available.

Another method to determine the molar efficiency is to quantify the shearing crests and surfaces. In the literature, the area of available occlusal contacts is generally given as a measure for chewing efficiency (e.g. Moore and Sanson, 1995; Proff, 2010). In this context, a high occlusal contact is equated with a high chewing efficiency. This is an appropriate measurement for dentitions that are used for grinding and crushing (e.g. humans). In the case of dentitions with a primary shear-cut function (e.g. insectivores), the opposite is applicable. A shear-cutting dentition is more efficient the smaller the contact areas are, including a point-cutting action, like a cigar cutter or scissors. In order to increase the point-cutting process notched or concave crests with relief are beneficial (see below). The advantage of point-cutting is a decrease in friction (Evans, 2003), which is therefore associated with lower energy consumption and higher efficiency. Another aspect is the nature of the preferred food to which the dentition is adapted. A carnivore dentition is highly efficient for cutting flesh, but poorly suited for grinding plant material.

Evans and Sanson (2005) differentiated the prey of insectivores into intractable (e.g. Coleoptera, Orthoptera, Hemiptera) and tractable invertebrates (e.g. Oligochaeta, Lepidoptera, Araneae, and larvae). The categorization is mainly based on the cuticle thickness, wherein intractable describes the structural strength, stiffness, and toughness, which increases with the thickness of the cuticle. Furthermore, Evans and Sanson (2005) argued, that larger invertebrates are more likely to be intractable than smaller ones. Therefore, scale becomes an important feature of the biomechanical properties of the diet. Additionally, they concluded that the biomechanical properties of tractable and intractable invertebrates' internal organs are relatively similar. The internal organs of both types are generally ductile and relatively tough. The complex structural nature of the cuticle in connection with ductile and tough internal organs requires multiple initiations of fracture to divide an invertebrate completely. At first, cusps are needed to initiate crack propagation, and then crests to force the propagations of the crack through an entire invertebrate (Evans, 2005). A theoretical, efficient functional insectivorous tooth complex, which meets these requirements, is the protoconoid (Fig. 70). The protoconoid, with its specific arrangement of points, blades and a surrounding tooth surface, was introduced by Evans and Sanson (2003). The following fundamental functional parameters are realized in this theoretical tooth complex:

- Evans and Sanson (1998) demonstrated in an experimental study with metal punches that a high tip, cusp, and edge sharpness is advantageous for intractable as well as for tractable food. The lower the angle of a cusp tip (tip sharpness), the volume of a cusp at an increasing distance of the cusp (cusp sharpness), and the edge of a crest (edge sharpness), the less force and energy is needed to penetrate and drive through the prey.

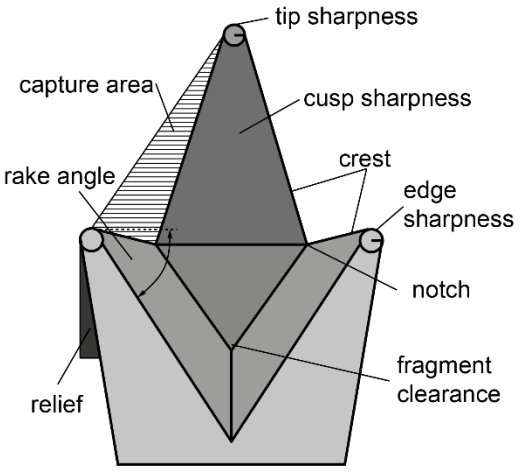

Fig. 70: The “protoconoid”, a theoretical ideal insectivorous molar and its functional parameters. (Modified from Evans, 2005)

- A trigonal pyramidal shape of the cusp, which is analog to a needle of a surgeon that is piercing skin, is beneficial for penetrating tractable items (Freeman, 1979).
- Notched crests reduce the energy costs and capture food particles during the comminution (Anderson, 2009); the same applies to concave curved crests.
- Positive rake angles form a fragment clearance structure and allow food particles to flow away from the crests (Evans and Sanson, 2003). In this way, the working area remains clean.
- An open trigonid is advantageous for fragment clearance, to ensure an undisturbed occlusion.
- A relief behind the crests reduces the friction of the occluding crest (Evans and Sanson, 2003) as well as their associated flanks, and thus the energy consumption when chewing. Another advantage of relief is the reduction of wedging the crests away by food fragments (Lumsden and Osborn, 1977).
- A triangulation of the molar main cusps inflicts more damage with one bite than a cusp in line pattern (Conith et al., 2016) (Fig. 71). In addition, an acute triangulation has a higher probability to hit a food item.

The evolutionary implementation of the protoconoid can be recognized in spalacotheriids and dryolestidans as well as in the zalambdodont tooth morphology of extant insectivorous mammals. The convergent development of the protoconoid in mammals confirms that it was and is an efficient tooth complex for comminuting invertebrates and that there is a functional relationship between tooth morphology and diet (e.g. Strait, 1993; Freeman, 2000; Dumont, 1995; Evans and Sanson, 2005).

Gill et al. (2014) concluded that *Morganucodon watsoni* (“Triconodonta”) presumably was capable of eating a more intractable prey than *Kuehneotherium watsoni*. Both taxa coexisted during the Late Triassic to Early Jurassic, whereby *M. watsoni* exemplifies a linear and *K. praecursoris* a triangular arrangement of the molar main cusps (Fig. 72). The conclusion is based on classical mechanics and finite element analysis of the mandible as well as on a quantitative textural analysis of the microwear. The analyses of the mandible showed, that *M. watsoni* produced larger bite forces with a more robust mandible than *K. praecursoris*. The results of the textural microwear analysis concluded that *M. watsoni* has a rougher microwear than *K. praecursoris*, which implies the consumption of more intractable prey. However, these results do not exclude, that *K. praecursoris* preyed intractable invertebrates, but indicate that the kuehneotheriids were somewhat limited due to their rather slender lower jaw.

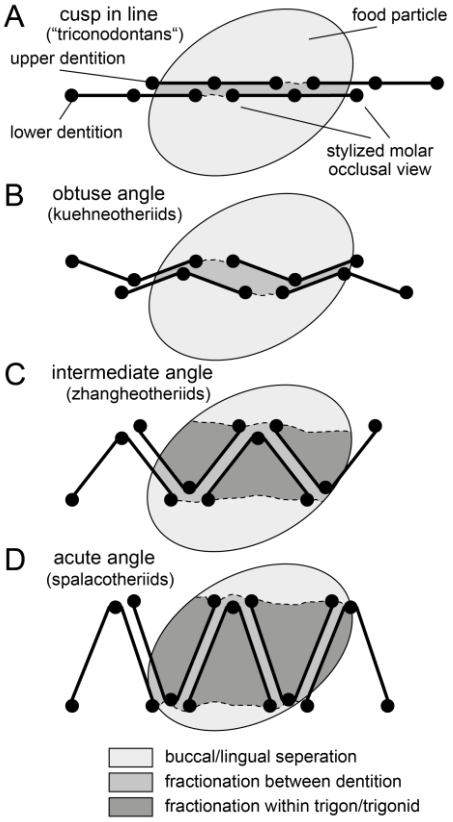

Fig. 71: Simplified illustration of the molar occlusion of the "triconodontans" and "symmetrodontans" in connection with the damage caused to food particles. The comminution rate increases with a higher triangulation. A: The cusp in line molar pattern only separated food particles into two parts, with an neglectable comminution in-between the upper and lower dentition. B: The obtuse molar pattern also separated a food particle into two parts, with a minor comminution in-between the upper and lower dentition. C: In the zhangheotheriid molar pattern a comminution in-between the molar cusps occurred next to the separation and comminution pattern of A and B. D: In the acute angle pattern the comminution in-between the molar cusps was higher as in C.

Evans (2005) argued, that a greater intractability of the diet means increased structural strength. To overcome the structural strength increased bite forces are needed but increased bite forces increase the risk of tooth fracture and wear. To counteract the increased risk of fracture and wear, greater robustness of the tooth is needed, which in turn reduces the functionality of the tooth and consequently the efficiency.

Conith et al. (2016) compared the efficiency of idealized molar tooth rows of *M. watsoni* and *K. praecursoris*. The tooth rows occluded into an insect substitute and various measurements were performed. The results of the experimental research are, that *K. praecursoris* seems to have been more efficient in reducing tractable prey and that there is no difference between these two taxa in their ability to initiate fracture in tractable prey; on the other hand, *M. watsoni* was apparently more efficient in fracture, as well as to initiate fracture, in intractable prey. Moreover, Conith et al. (2016) concluded, that *K. praecursoris* caused substantially more damage to food particles than *M. watsoni*. These conclusions can be drawn from Conith et al. (2016) experimental setup with scaled idealized molars, but Evans and Sanson (1998) argued that tooth function is scale dependent. Even teeth of the same shape but with a different size will require different forces to penetrate the same size of a food item, due to their different cusps, and tip sharpness. They proved this perception in their metal punch experiments (see above). If *M. watsoni* and *K. praecursoris* molars (Fig. 72) are compared under these aspects and without scaling, then the following conclusion can be drawn. *K. praecursoris* molars may have been more efficient, in the comminution of tractable and to a certain extent intractable prey, as *M. watsoni* molars. This postulation is supported by the following considerations:

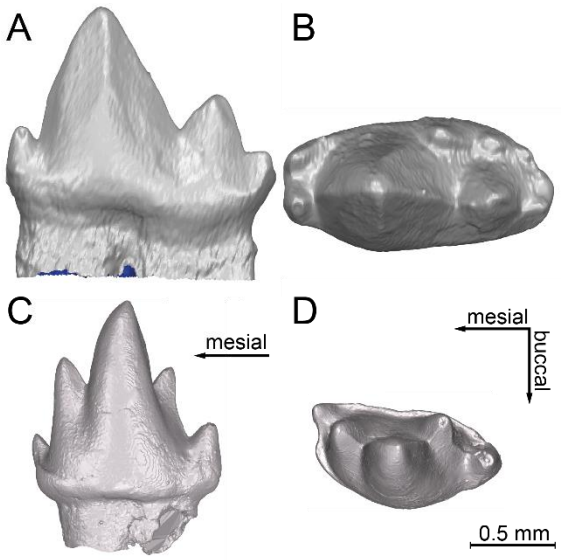

Fig. 72: *Morganucodon watsoni* (A, B, lower left m2, UMZC Eo.cr.1) and *Kuehneotherium praecursoris* (C, D, lower left m3, PV M 19143) in size comparison.
(A and B modified from Jäger et al., 2019)

- *K. praecursoris* molars have a higher tip- and cusp sharpness. A higher tip and cusp sharpness reduces the required force and energy to fracture intractable and tractable prey (Evans and Sanson, 1998). For this reason, *K. praecursoris* does not need such high bite forces as *M. watsoni* to comminute the same type of prey.
- The morphology of the protoconid (cusp a after Crompton and Jenkins, 1968) of *M. watsoni* is square pyramidal, whereas the protoconid of *K. praecursoris* is trigonal pyramidal to half conical. The trigonal shape is advantageous for piercing tractable prey (Freeman, 1979), and thus also for piercing inner organs of tractable and intractable prey. This reduces the needed bite force of *K. praecursoris*.
- The triangulation of the molar main cusps of *K. praecursoris* causes more damage to food items (Fig. 71) than the cusp in-line configuration of *M. watsoni* molars (Conith et al., 2016).
- The mandibles of *M. watsoni* and *K. praecursoris* are comparable in size, but *K. praecursoris* does have a higher molar count due to its smaller molars (Gill et al.,

2014, Fig. 1). Therefore, *K. praecursoris* could have inflicted more damage with one bite (Fig. 71).

Under these considerations, it can be postulated, that, within the overlapping prey range, *K. praecursoris* was more efficient in comminuting prey than *M. watsoni*. However, according to Gill et al. (2014), *K. praecursoris* was more restricted in eating intractable prey than *M. watsoni*.

If the arguments of Evans (2005) about the requirement of molars, which are adopted for intractable food, are followed, then Woutersiidae must be categorized as insectivorous taxon with an expanded adaptation towards intractable invertebrates (low crest and cusp sharpness, slightly elevated cusps, bulbous strong molar base, and strong occlusal wear). Due to the molar adaptation for intractable prey, the efficiency of the Woutersiidae had to be low, presumably even lower than that of *M. watsoni*. The main task of these molars was to crack the exoskeleton by puncture-crushing.

An intermediate state towards the “symmetrodontan” protoconoid molar structure was realized in *Maotherium sinense*. The more acute triangulation of the molar main cusps of the zhangheotheriids resulted in wider molars. Hence, the accessory cusps of the protoconid and paracone are more lingual and buccal respectively, than the accessory cusps of *K. praecursoris*. This leads to the assumption, that *M. sinense* inflicted more damage during one bite, and that the chance of hitting a food particle must have been higher than in *K. praecursoris* (Fig. 71). Furthermore, the mode of occlusion changed due to the more acute triangulation. The embrasure shearing between the cusps of *K. praecursoris* was superseded in *M. sinense* by an embrasure shearing of the molars. As a result, the prey was mainly blunt-sheared by a Notch-Notch-Tool and Straight-Notch-Tool, instead of puncture-sheared as in *K. praecursoris*. With these tools, the notched crest functional parameter of the protoconoid has been realized in *M. sinense*. The notched crests, the embrasure shearing of the cusps, and the triangulation of the main cusps suggest that, during one chewing cycle, food particles were not only divided into two parts, as in “triconodontans” and kuehneotheriids, but were comminuted into several pieces (Fig. 71). That the prey was only blunt-sheared instead of shear-cut, is due to the low crest sharpness of the *M. sinense* molar cusps. Next to the lower crest sharpness, Zhangheotheriidae also has a lower tip and cusp sharpness, which is related to the higher angle of a cusp tip, and higher volume of a cusp at an increasing distance of the cusp, and the larger size compared to *K. praecursoris* molars (Fig. 74). Although *M. sinense* has larger molars, the mandibles of *M. sinense* and *K. praecursoris* have the same dimensions. (compare Gill et al., 2014, Fig. 1, with, Plogschties and Martin, 2019, Fig. 5). This leads to the assumption, that *M. sinense* might have had an expanded dietary spectrum towards prey with a higher intractability, but at the expense of a lesser efficiency of the dentition. This is supported by the argumentation of Evans (2005) regarding the necessary adaptations of the molars to

higher intractable prey. A possible explanation for an adaptation towards higher intractable prey might be the Jehol Entomofauna. Zhang et al. (2010) subdivided the Jehol Entomofauna into three phases. The middle phase includes the record of the insect fossils of the lower-middle Yixian Formation (underlying the Jingangshan Bed, 122.5-130 Ma), which includes the horizons in which the zhangheotheriid fossils were found. During this phase, the Jehol Entomofauna was dominated by coleopterans with a total composition of around 40%, and within the coleopterans, the highly intractable Scarabaeoidea were represented with around 30%.

Another difference between *K. praecursoris* and *M. sinense* is the morphology of the paraconid and metaconid. In *M. sinense*, these two cusps are mesio-lingual/disto-buccal (paraconid) and mesio-buccal/disto-lingual (metaconid) compressed, and therefore change the orientation of the relief and rake surfaces. These changes lead to more pointed occlusal contact zones of the lower molars and their upper antagonists, and causes a lesser total collision area during chewing as for *K. praecursoris* (c.f. Diagrams chapter 4.3 and Fig. 73). A lesser total collision area causes lesser resistance during occlusion, which is associated with a lower force expenditure, and therefore lower energy consumption. Hence, the pointed contact zones increased the efficiency of chewing. Additionally, the buccal crests are pointing away from the protoconid crest, instead of pointing to the protoconid crests, as in *K. praecursoris*, and the lingual crests are pointing to each other. Therefore, cracks, which propagate towards lingual would have met each other, whereas cracks, which are propagating towards buccal, would have met the paracone during closing the mandible. Hence, the comminution rate of the prey during one chewing cycle was more enhanced than that of *K. praecursoris* (Fig. 71).

The most advanced “symmetrodontan” molar pattern is that of the spalacotheriids. Within the “symmetrodontans”, the spalacotheriid molar morphology matches the functional parameters of the protoconoid the most (c.f. Fig. 70). As in zhangheotheriids, the spalacotheriid mode of occlusion is an embrasure shearing between cusps. The more acute triangulation in connection with the higher width/length ratio results in more precise occlusion and higher comminution rate during one chewing cycle, as in zhangheotheriids (Fig. 71). Due to the relief below [c]pr~me and [c]pa~pr as well as above [C]PAS~PA and [C]PA~MTS, the continuity and concavity of these crests, and the lateral movement, only a point cutting occurred between these crests. A point cutting decreases the friction between the crests (Evans, 2003), and therefore decreases the energy consumption. It is to mention, that this is contrary to the results of the total collision area detection during one shearing stroke (Fig. 47), which shows the highest value of the total collision area within the analyzed taxa. The reason for that is, that the OFA reconstructions of this study were done with the same value of collision distance (0.08). Due to the fact, that the large surfaces of pr*me/PAS*PA as well as pa*pr/PA*MTS passing each other below that value, the OFA

interpreted the passing as a collision. The OFA collision distance gradient mode is showing another picture (Fig. 73). The intensity, with which the occlusal surfaces pass each other decreases with the acuteness of the molar triangulation of the respective taxa.

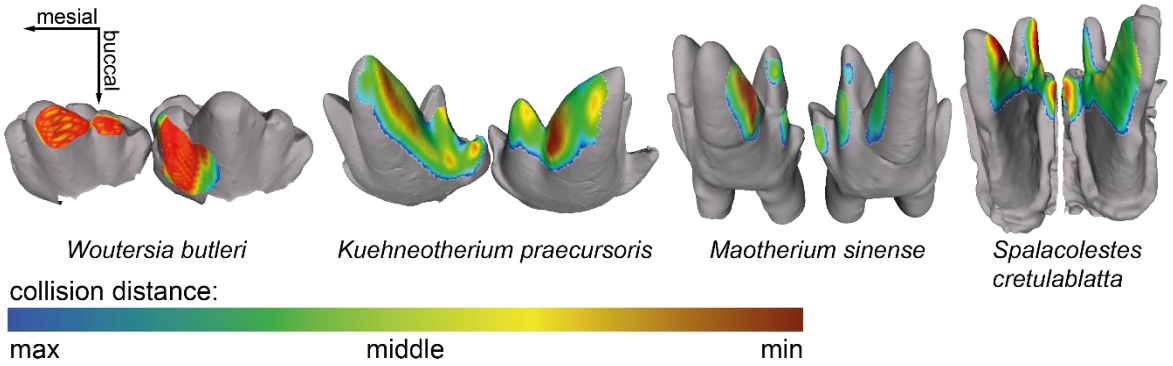

Fig. 73: A distance gradient illustration of the studied “symmetrodontans” resulting from the OFA. The collision distance increases in relation to the increase of the molar cusps triangulation (not scaled).

It is remarkable, that the molars of Spalacotheriidae is varying enormously in size, whereat *Spalacotherium henkeli* (IP FUB TH 11, m1) represents one of the largest specimen, which is around 2 mm in length, *Spalacolestes cretulablatta* (OMNH 027421, m4) is one of the smallest specimens with a length of around 0.8 mm (Fig. 74). In contrast, the molars of kuehneotheriids and zhangheotheriids are of almost equal size (between 1 and 1.5 mm).

It must be assumed, that the “symmetrodontans” were terrestrial opportunistic, generalistic insectivorous mammals with a possible molar adaptation, either to extend the food provision towards more intractable prey (zhangheotheriids), or tractable prey (kuehneotheriids). However, due to the fact that larger invertebrates are more intractable than smaller ones (Evans and Sanson, 2005), prey preference might be more related to size, at least within spalacotheriids. Churchfield and Sheftel (1994) studied the prey preferences of Soricidae and concluded that body dimensions matter, large taxa took more large prey than small taxa, and small taxa took more small prey than large taxa. This was also concluded in a previous research of Dickman (1988), in which he studied the body size, prey size, and community structure of three two-species communities of insectivorous mammals.

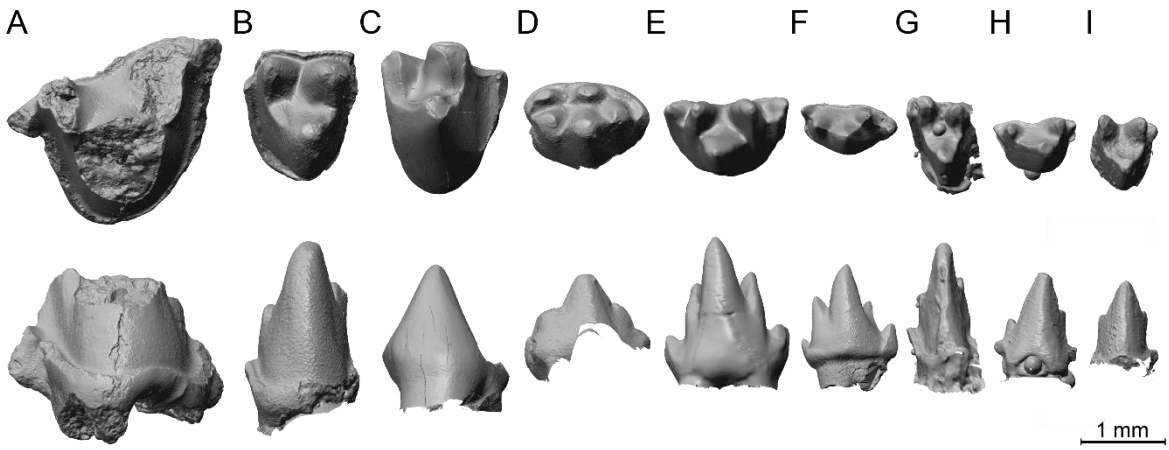

Fig. 74: A *Dryolestes* molar and various “symmetrodontan” molars in comparison (occlusal and buccal views).
A: *Spalacotherium henkeli* (IP FUB TH 11, m1), B: *Spalacolestes inconcinnus* (OMNH VP 033897, m3) C: *Dryolestes leiriensis* (Gui Mam 1155, mx), D: *Woutersia butleri* (SNP 517 W, mx), E: *Maotherium sinense* (YFGB 1724, m3) F: *Kuehneotherium praecursoris* (NHM PV M 19143, m3) G: *Spalacolestes cretulablatta* (OMNH VP 027421, m4), H: *Spalacotherium evansae* (DORCM GS 1075, mx) I: *Spalacotheridium noblei* (OMNH VP 025828, m4).

5.6 The efficiency of dryolestidan and tribosphenic molars

A more efficient insectivore dentition, which follows the symmetrodontan tooth pattern, was realized in the Dryolestida. The higher efficiency was achieved by the neomorphic paracone/hypoflexid functional complex, which provided a Cusp-Channel-Tool, additional to the protoconoid tools. The advantage of this additional tool was a further (compressional) shearing of food particles between PA-m-/hfd-bd subsequent to the shear-cutting of [C]ME~MTS/[c]me~pr and [C]PA~ME/[c]pa~pr (Schultz and Martin, 2014). The additional shearing of food particles led to a finer comminution as in spalacotheriids, and therefore to a higher digestibility (see below).

In the course of evolution towards the tribosphenidans, the hypoflexid lost its important role as a shearing structure, due to the development of the talonid basin. In tribosphenic molars, the hypoflexid is located buccally between the trigonid and the neomorphic talonid that is enclosed by cusp d (hypoconid), hypoconulid, and entoconid. With the development of the talonid and its antagonist, the protocone (mortar and pestle), the chewing cycle was extended to a second phase, in which the protocone sheared, ground, and crushed food particles. Schultz and Martin (2014) suggested that grinding and crushing invertebrate particles allowed a finer comminuting and more efficient extraction of nutritious soft tissue from the almost indigestible exoskeleton. This led to a higher gain of energy via the digestive system. Moore and Sanson (1995) demonstrated that efficient digestion of an insect’s viscera requires to be directly exposed to the digestive enzymes, and therefore comminuting the prey into smaller pieces is advantageous. Furthermore, the tribosphenic molar was the stepping stone towards an omnivorous to herbivorous diet, which was able to utilize energy-rich plant material. This expansion of the food resources was most likely one of the reasons for the evolutionary success of mammals.

6 Conclusion

“Symmetrodontans” were terrestrial opportunistic, generalistic insectivores, due to their high needs of nutrients (energy) to maintain the homoeothermic endothermic metabolic system. To get the nutrients, “symmetrodontans” were probably not choosy. They took every opportunity to consume everything that crawled in front of their nose and was in their range of handling. The most important limitation in prey selection was the intractability of the prey. Another factor in prey selection was presumably the prey’s agility, but this topic was not considered in this study.

The grade of intractability refers to the thickness of the cuticle, whereby larger prey is inherently more intractable. Therefore, the prey selection is mainly oriented towards which prey can be comminuted with as little energy expense as possible, but with the highest energy yield; extant insectivorous mammals prefer the largest possible prey they can handle. The comminution of the prey, in turn, is determined by the efficiency of the masticatory system. To determine the efficiency of the “symmetrodontans” only the dentition and bones of the masticatory system are documented in the fossil record. Nevertheless, some conclusions can be drawn about the efficiency of the food comminution on the basis of the teeth and bones.

The fossil record shows that the morphology of the “symmetrodontan” molars steadily evolved towards a more acute triangulation of the three main cusps and sharp shearing crests. These molars are comparable to a theoretical ideal insectivore molar, the protoconoid (Evans and Sanson, 2003). Due to a higher triangulation, these molars have a higher width/length ratio. With a higher width/length ratio the acute-angled “symmetrodontans” inflicted more damage than the obtuse-angled ones (c.f. Fig. 71).

Traditionally the “symmetrodontans” are classified into the obtuse-angled “symmetrodontans” (Kuehneotheriidae, Tinodontidae, and Woutersiidae) and acute-angled “symmetrodontans” (Zhangheotheriidae, Spalacotheriidae). However, due to a higher overall acuteness of the spalacotheriid molars and lacking shear-cutting crests in zhangheotheriids, the Zhangheotheriidae should be addressed as intermediate-angled “symmetrodontans”.

The latest research assumes that the “symmetrodontans” rolled the mandible. Clear evidence could not be obtained from this study, but there is some evidence, which supports this assumption. The OFA chewing cycle reconstruction showed that for *Kuehneotherium praecursoris* and *Woutersia butleri* some regions of wear could only be reached by a roll of the mandible.

The movement of the one-phased chewing cycle of the lower jaw of “symmetrodontans” was mainly transversely upward with a slight mesial or distal shift. An important feature of the “symmetrodontan” comminuting process was the embrasure shearing, in which two

molars embraced one molar. All studied “symmetrodontans” performed this kind of embrasure shearing, except for *K. praecursoris*. The embrasure shearing of *K. praecursoris* was proceeded within the cusp level.

The comminuting process of the early diverging Woutersiidae was simple and rudimentary. The main task of the dentition was to puncture and crush prey. The low tip, as well as cusp and crest sharpness, suggest that Woutersiidae were able to prey on more intractable invertebrates, but with a low efficiency of comminuting. Important tools for fine comminution of food components are lacking, and woutersiids do not possess molar structures to shear-cut tractable particles efficiently.

The kuehneotheriid molars and lower jaw indicate a preference towards a more tractable diet due to its more slender mandible and a high tip and cusp sharpness. The main task of these molars was to puncture-shear its prey. A minor shear-cutting was also performed. The obtuse triangulation of the main cusps inflicted more damage than the cusp-in-line pattern of “triconodontans”.

Zhangheotheriidae mainly comminuted food particles via blunt-shearing. The low tip, as well as cusp and crest sharpness, suggest a diet selection towards a prey with a higher intractability. This may be in correlation with the high abundance of coleopteran taxa in the fossil record of the same deposits in which the zhangheotheriids were found. The adaptation to higher intractable prey was at the expense of the efficiency, but for the benefit of the sustainability of the molars. Due to the more acute-angle of the main cusp, a food fragment was not only divided into a buccal and lingual segment, as in kuehneotheriids and “triconodontans”, but was comminuted additionally in-between the cusps. Therefore the comminution rate was higher during one chewing cycle in Zhangheotheriidae, than in Kuehneotheriidae, which aided the efficiency. The triangular habitus of the paracone and protoconid, like the tip of a surgeon needle, was also beneficial for the efficiency.

The “symmetrodontan” molars, which resemble that of the protoconoid the most are those of the spalacotheriids. The spalacotheriid molars first pierced, and then shear-cut food particles highly efficient. Due to the highest width/length ratio within the “symmetrodontans”, spalacotheriids inflected the most damage during one chewing cycle.

In the course of evolution towards the tribosphenic molar, the “symmetrodontan” triangular pattern has been retained. In Dryolestidans, an additional shearing complex evolved, in which the paracone slid against the neomorphic hypoflexid. Food particles that were shear-cut by the mesial and distal crests skid down into the interdental space of the lower cusps, and were additionally sheared and crushed in-between PA-m-a/hfd-bd. This is the reason why the dryolestiid dentition is more efficient than an acute-angled “symmetrodontan” dentition. The dryolestiid molar structure was then evolutionarily surpassed by the tribosphenic molar. The tribosphenic tooth pattern, with the talonid/protocone complex (mortar and pestle), was the starting point for the diversity of all

subsequent mammalian molar evolution. The talonid/protocone complex had the function not only to shear but to crush, grind and squeeze food particles. This advanced function, extended the dietary spectrum, towards plant-based diet, which partly helped the mammals to survive the Cretaceous–Paleogene mass extinction.

Interestingly, due to a specialization of several extant mammals towards insectivory, these taxa reduced the tribosphenic molar structure in the course of evolution. These insectivorous mammals, with a zalambdodont or dilambdodont molar pattern, redeveloped the main features of the shear-cutting function, which includes pointed main cups and shearing-crests. This indicates that the structural pattern of the protoconoid was and is highly efficient for consuming invertebrates.

7 References

Anders, U. 2011. Funktionsmorphologische Veränderungen und Funktionalitätserhaltung in bunodonten, selenodonten und secodonten Gebissen. Doctoral thesis, Rheinische Friedrich-Wilhelms-Universität, Bonn.

Anders, U., and W. von Koenigswald, et al. 2011. Generalized individual dental age stages for fossil and extant placental mammals. *Paläontologische Zeitschrift* 85: 341. doi: 10.1007/s12542-011-0101-5.

Anderson, D.J., and B. Matthews (eds.). 1976. *Mastication.* Bristol: John Wright and Sons.

Anderson, P.S.L. 2009. The effects of trapping and blade angle of notched dentitions on fracture of biological tissues. *The Journal of experimental biology* 212: 3627–3632. doi: 10.1242/jeb.033712.

Anderson, P.S.L., and M. La Barbera. 2008. Functional consequences of tooth design: Effects of blade shape on energetics of cutting. *The Journal of experimental biology* 211: 3619–3626. doi: 10.1242/jeb.020586.

Asher, R.J., and M.R. Sánchez-Villagra. 2005. Locking Yourself Out: Diversity Among Dentally Zalambdodont Therian Mammals. *Journal of Mammalian Evolution* 12: 265–282. doi: 10.1007/s10914-005-5725-3.

Averianov, A.O. 2002. Early Cretaceous "symmetrodont" mammal *Gobiotheriodon* from Mongolia and the classification of "Symmetrodonta". *Acta Palaeontologica Polonica* 47: 705–716.

Averianov, A.O., and A.V. Lopatin. 2006. *Itatodon tatarinovi* (Tegotheriidae, Mammalia), a docodont from the Middle Jurassic of Western Siberia and phylogenetic analysis of Docodonta. *Paleontological Journal* 40: 668–677. doi: 10.1134/S0031030106060098.

Averianov, A.O., and T. Martin, et al. 2013. A new phylogeny for basal Trechnotheria and Cladotheria and affinities of South American endemic Late Cretaceous mammals. *Naturwissenschaften* 100: 311–326. doi: 10.1007/s00114-013-1028-3.

Barbour, M.E., and G.D. Rees. 2006. The role of erosion, abrasion and attrition in tooth wear. *Journal of Clinical Dentistry* 17: 88–93.

Bels, V.L., M. Chardon, and P. Vandewalle (eds.). 1994. *Biomechanics of Feeding in Vertebrates*. Advances in Comparative and Environmental Physiology, 0938-2763, vol. 18. Berlin, Heidelberg: Springer.

Berthaume, M.A. 2016. Food mechanical properties and dietary ecology. *American Journal of Physical Anthropology* 159: S79–S104. doi: 10.1002/ajpa.22903.

Bhullar, B.-A.S., and A.R. Manafzadeh, et al. 2019. Rolling of the jaw is essential for mammalian chewing and tribosphenic molar function. *Nature.* doi: 10.1038/s41586-019-0940-x.

Bi, S., and Y.-Q. Wang, et al. 2014. Three new Jurassic euharamiyidan species reinforce early divergence of mammals. *Nature* 514: 579–584. doi: 10.1038/nature13718.

Bi, S., and X. Zheng, et al. 2016. A new symmetrodont mammal (Trechnotheria: Zhangheotheriidae) from the Early Cretaceous of China and trechnotherian character evolution. *Scientific Reports* 6: 1–9. doi: 10.1038/srep26668.

Bonaparte, J.F. 1990. New Late Cretaceous mammals from the Los Alamitos Formation, northern Patagonia. *National Geographic Research* 6: 63–83.

Butler, P.M. 1939. The teeth of the Jurassic mammals. *Proceedings of the Zoological Society of London* B109: 329–356. doi: 10.1111/j.1096-3642.1939.tb00719.x.

Butler, P.M. 1972. Some functional aspects of molar evolution. *Evolution* 26: 475–483.

Butler, P.M. 1978. Molar cusp nomenclature and homology. In *Development, function and evolution of teeth*, ed. P. M. Butler and Kenneth Alan Joysey, 439–453. London, New York: Academic Press.

Butler, P.M. 1996. Dilambdodont molars: A functional interpretation of their evolution. *Palaeovertebrata* 25: 205–213.

Butler, P.M. 1997. An alternative hypothesis on the origin of docodont molar teeth. *Journal of Vertebrate Paleontology* 17: 435–439. doi: 10.1080/02724634.1997.10010988.

Butler, P.M., and K.A. Joysey (eds.). 1978. *Development, function and evolution of teeth.* London, New York: Academic Press.

Chimento, N.R., and F.L. Agnolin, et al. 2012. The Patagonian fossil mammal *Necrolestes*: a Neogene survivor of Dryolestoidea. *Revista del Museo Argentino de Ciencias Naturales, Nueva Serie* 14: 261–306.

Chivers, D.J., B.A. Wood, and A. Bilsborough (eds.). 1984. *Food acquisition and processing in Primates.* Boston, MA: Springer US.

Chun, K., and H. Choi, et al. 2014. Comparison of mechanical property and role between enamel and dentin in the human teeth. *Journal of dental biomechanics* 5: 1-7. doi: 10.1177/1758736014520809.

Churchfield, S., and B.I. Sheftel. 1994. Food niche overlap and ecological separation in a multi-species community of shrews in the Siberian taiga. *Journal of Zoology* 234: 105–124. doi: 10.1111/j.1469-7998.1994.tb06059.x.

Cifelli, R.L. 1990. Cretaceous mammals of southern Utah. III. Therian mammals from the Turonian (early Late Cretaceous). *Journal of Vertebrate Paleontology* 10: 332–345. doi: 10.1080/02724634.1990.10011818.

Cifelli, R.L., and B.M. Davis, et al. 2014. Earliest Cretaceous mammals from the western United States. *Acta Palaeontologica Polonica* 59: 31–52. doi: 10.4202/app.2012.0089.

Cifelli, R.L., and S.K. Madsen. 1986. An Upper Cretaceous symmetrodont (Mammalia) from Southern Utah. *Journal of Vertebrate Paleontology* 6: 258–263. doi: 10.1080/02724634.1986.10011620.

Cifelli, R.L., and S.K. Madsen. 1999. Spalacotheriid Symmetrodonts (Mammalia) from the Medial Cretaceous (Upper Albian or lower Cenomanian) Mussentuchit Local Fauna, Cedar Mountain Formation, Utah, USA. *Geodiversitas* 21: 167–214.

Clarke, A., and H.-O. Pörtner. 2010. Temperature, metabolic power and the evolution of endothermy. *Biological reviews of the Cambridge Philosophical Society* 85: 703–727. doi: 10.1111/j.1469-185X.2010.00122.x.

Clemens, W.A., and P.M. Lees. 1971. A review of English Early Cretaceous mammals. In *Early mammals*, ed. D. M. Kermack and K. A. Kermack, 117–130. London: Academic Press.

Conith, A.J., and M.J. Imburgia, et al. 2016. The functional significance of morphological changes in the dentitions of early mammals. *Journal of the Royal Society, Interface* 13. doi: 10.1098/rsif.2016.0713.

Cope, E.D. 1883. On the trituberculate type of molar tooth in the Mammalia. *Proceedings of the American Philosophical Society* 21: 324–326.

Costa, R.L., and W.S. Greaves. 1981. Experimentally produced tooth wear and the direction of jaw motion. *Journal of Paleontology* 55: 635–638.

Croft, D.A., D.F. Su, and S.W. Simpson (eds.). 2018. *Methods in paleoecology*. Vertebrate paleobiology and paleoanthropology series. Cham, Switzerland: Springer.

Crompton, R.H., and Savage, R. J. G., et al. 1998. The mechanics of food reduction in *Tarsius bancus*: Hard-Object Feeder, Soft-Object Feeder or both? *Folia Primatologica* 69: 41–59. doi: 10.1159/000052698.

Crompton, A.W. 1971. The origin of the tribosphenic molar. In *Early mammals*, ed. D. M. Kermack and K. A. Kermack, 65–87. London: Academic Press.

Crompton, A.W. 1995. Masticatory function in nonmammalian cynodonts and early mammals. In *Functional morphology in vertebrate paleontology*, ed. Jeff Thomason, 55–75. Cambridge, New York: Cambridge University Press.

Crompton, A.W., and K.M. Hiiemäe. 1969. Functional occlusion in tribosphenic molars. *Nature* 222: 678–679. doi: 10.1038/222678b0.

Crompton, A.W., and K.M. Hiiemäe. 1970. Molar occlusion and mandibular movements during occlusion in the American opossum, *Didelphis marsupialis* L. *Zoological Journal of the Linnean Society* 49: 21–47. doi: 10.1111/j.1096-3642.1970.tb00728.x.

Crompton, A.W., and W.L. Hylander. 1986. Changes in mandibular function following the acquisition of a dentary-squamosal joint. In *The Ecology and biology of mammal-like reptiles*, ed. Nicholas Hotton, III, Paul D. Maclean, Jan J. Roth and E. Carol Roth, 263–282. Washington, D.C., London: Smithsonian Institution Press.

Crompton, A.W., and F.A. Jenkins. 1967. American Jurassic symmetrodonts and Rhaetic "Pantotheres". *Science* 155: 1006–1009. doi: 10.1126/science.155.3765.1006.

Crompton, A.W., and F.A. Jenkins. 1968. Molar occlusion in Late Triassic mammals. *Biological Reviews* 43: 427–458. doi: 10.1111/j.1469-185X.1968.tb00966.x.

Crompton, A.W., and F.A. Jenkins. 1973. Mammals from reptiles: a review of mammalian origins. *The Annual Review of Earth and Planetary Sciences* 1: 131–155.

Crompton, A.W., and A. Sita-Lumsden. 1970. Functional significance of the therian molar pattern. *Nature* 227: 197–199. doi: 10.1038/227197a0.

Crompton, A.W., and C.B. Woods, et al. 1994. Differential wear of enamel: A mechanism for maintaining sharp cutting edges. In *Biomechanics of Feeding in Vertebrates*, vol. 18, ed. V. L. Bels, M. Chardon and P. Vandewalle, 321–346. Advances in Comparative and Environmental Physiology, 0938-2763, vol. 18. Berlin, Heidelberg: Springer.

Cuenca-Bescós, G., and J.I. Canudo, et al. 2014. Spalacotheriid 'symmetrodonts' from the Early Cretaceous of Spain. *Journal of Vertebrate Paleontology* 34: 1427–1436. doi: 10.1080/02724634.2014.866574.

Datta, P.M. 1981. The first Jurassic mammal from India*. *Zoological Journal of the Linnean Society* 73: 307–312. doi: 10.1111/j.1096-3642.1981.tb01598.x.

Davies, S., and R.M.J. Gray. 2001. Occlusion: What is occlusion? *British Dental Journal* 191: 235–245. doi: 10.1038/sj.bdj.4801151.

Davis, B.M. 2011. Evolution of the tribosphenic molar pattern in early mammals, with comments on the "dual-origin" hypothesis. *Journal of Mammalian Evolution* 18: 227–244. doi: 10.1007/s10914-011-9168-8.

Debuysschere, M. 2017. The Kuehneotheriidae (Mammaliaformes) from Saint-Nicolas-de-Port (Upper Triassic, France): A systematic review. *Journal of Mammalian Evolution* 24: 127–146. doi: 10.1007/s10914-016-9335-z.

Dickman, C.R. 1988. Body size, prey size, and community structure in insectivorous mammals. *Ecology* 69: 569–580. doi: 10.2307/1941006.

Dumont, E.R. 1995. Enamel thickness and dietary adaptation among extant primates and Chiropterans. *Journal of Mammalogy* 76: 1127–1136. doi: 10.2307/1382604.

Eccles, J.D. 1982. Tooth surface loss from abrasion, attrition and erosion. *Dental Update* 9: 373–381.

Engels, S. 2011. Funktionelle und morphologische Transformationen der Molaren bei frühen Hippomorpha im Hinblick auf den Mastikationsprozess. Doctoral thesis, Rheinischen Friedrich-Wilhelms-Universität, Bonn.

Ensom, P.C., and D. Sigogneau-Russell. 1998. New dryolestoid mammals from the basal Cretaceous Purbeck Limestone Group of southern England. *Palaeontology* 41: 35–55.

Ensom, P.C., and D. Sigogneau-Russell. 2000. New symmetrodonts (Mammalia, Theria) from the Purbeck Limestone Group, Lower Cretaceous, southern England. *Cretaceous Research* 21: 767–779. doi: 10.1006/cres.2000.0227.

Evans, A.R. 2003. Functional dental morphology of insectivorous Microchiropterans: Spatial modelling and functional analysis of tooth form and the influence of tooth wear and dietary properties. Doctoral thesis, Monash University, Melbourne, Australia.

Evans, A.R. 2005. Correspondence between tooth shape and dietary biomechanical properties in insectivorous microchiropterans. *Evolutionary Ecology Research* 7: 453–478.

Evans, A.R., and S. Pineda-Munoz. 2018. Inferring Mammal Dietary Ecology from Dental Morphology. In *Methods in paleoecology*, ed. Darin A. Croft, Denise F. Su and Scott W. Simpson, 37–51. Vertebrate paleobiology and paleoanthropology series. Cham, Switzerland: Springer.

Evans, A.R., and G.D. Sanson. 1998. The effect of tooth shape on the breakdown of insects. *Journal of Zoology* 246: 391–400. doi: 10.1111/j.1469-7998.1998.tb00171.x.

Evans, A.R., and G.D. Sanson. 2003. The tooth of perfection: Functional and spatial constraints on mammalian tooth shape. *Biological Journal of the Linnean Society* 78: 173–191. doi: 10.1046/j.1095-8312.2003.00146.x.

Evans, A.R., and G.D. Sanson. 2005. Biomechanical properties of insects in relation to insectivory: cuticule thickness as an indicator of insect 'hardness' and 'intractability'. *Australian Journal of Zoology* 53: 9–19. doi: 10.1071/ZO04018.

Evans, A.R., and G.D. Sanson. 2006. Spatial and functional modeling of carnivore and insectivore molariform teeth. *Journal of Morphology* 267: 649–662. doi: 10.1002/jmor.10285.

Flynn, J.J., and J.M. Parrish, et al. 1999. A Middle Jurassic mammal from Madagascar. *Nature* 401: 57–60. doi: 10.1038/43420.

Fox, R.C. 1976. Additions to the mammalian local fauna from the Upper Milk River Formation (Upper Cretaceous), Alberta. *Canadian Journal of Earth Sciences* 13: 1105–1118. doi: 10.1139/e76-113.

Freeman, P.W. 1979. Specialized insectivory: Beetle-eating and moth-eating Molossid bats. *Journal of mammalogy* 60: 467–479. doi: 10.2307/1380088.

Freeman, P.W. 2000. Macroevolution in Microchiroptera: Recoupling morphology and ecology with phylogeny. *Evolutionary Ecology Research* 2: 317–335.

Gao, C.-L., and G.P. Wilson, et al. 2010. A new mammal skull from the Lower Cretaceous of China with implications for the evolution of obtuse-angled molars and 'amphilestid' eutriconodonts. *Proceedings. Biological sciences / The Royal Society* 277: 237–246. doi: 10.1098/rspb.2009.1014.

Gelfo, J.N., and R. Pascual. 2001. *Peligrotherium tropicalis* (Mammalia, Dryolestida) from the early Paleocene of Patagonia, a survival from a Mesozoic Gondwanan radiation. *Geodiversitas* 23: 369–379.

Gill, P.G. 2004a. A new symmetrodont from the Early Cretaceous of England. *Journal of Vertebrate Paleontology* 24: 748–752. doi: 10.1671/0272-4634(2004)024[0748:ANSFTE]2.0.CO;2.

Gill, P.G. 2004b. *Kuehneotherium* from the Mesozoic fissure fillings of South Wales. Doctoral thesis, University of Bristol, Bristol.

Gill, P.G., and M.A. Purnell, et al. 2014. Dietary specializations and diversity in feeding ecology of the earliest stem mammals. *Nature* 512: 303–305. doi: 10.1038/nature13622.

Godefroit, P., and D. Sigogneau-Russell. 1999. Kuehneotheriids from Saint-Nicholas-de-Port (Late Triassic of France). *Geologica Belgica* 2: 181–196.

Greaves, W.S. 1973. The inference of jaw motion from tooth wear facets. *Journal of Paleontology* 47: 1000–1001.

Gregory, W.K. 1922. *The origin and evolution of the human dentition.* Baltimore: Williams and Wilkins.

Gregory, W.K. 1934. A half century of tritubercuIy the Cope-Osborn theory of dental evolution with a revised summary of molar evolution from fish to man. *Proceedings of the American Philosophical Society* 73: 169–317.

Grippo, J.O., and M. Simring, et al. 2004. Attrition, abrasion, corrosion and abfraction revisited. *The Journal of the American Dental Association* 135: 1109–1118. doi: 10.14219/jada.archive.2004.0369.

Grossnickle, D.M. 2017. The evolutionary origin of jaw yaw in mammals. *Scientific Reports* 7: 45094. doi: 10.1038/srep45094.

Han, G., and J. Meng. 2016. A new spalacolestine mammal from the Early Cretaceous Jehol Biota and implications for the morphology, phylogeny, and palaeobiology of Laurasian ‘symmetrodontans’. *Zoological Journal of the Linnean Society* 178: 343–380. doi: 10.1111/zoj.12416.

Hiiemäe, K.M. 1976. Masticatory movements in primitive mammals. In *Mastication*, ed. D. J. Anderson and B. Matthews, 105–118. Bristol: John Wright and Sons.

Hillson, S. 2005. *Teeth*. Cambridge manuals in archaeology. New York: Cambridge University Press.

Hotton, N., III, P.D. Maclean, J.J. Roth, and E.C. Roth (eds.). 1986. *The Ecology and biology of mammal-like reptiles.* Washington, D.C., London: Smithsonian Institution Press.

Hu, Y.-M., and Z.-X. Luo, et al. 1997. A new symmetrodont mammal from China and its implications for mammalian evolution. *Nature* 390: 137–142. doi: 10.1038/36505.

Hu, Y.-M., and J. Meng, et al. 2005. Large Mesozoic mammals fed on young dinosaurs. *Nature* 433: 149–152. doi: 10.1038/nature03102.

Hummel, J., and E. Findeisen, et al. 2011. Another one bites the dust: faecal silica levels in large herbivores correlate with high-crowned teeth. *Proceedings. Biological sciences / The Royal Society* 278: 1742–1747. doi: 10.1098/rspb.2010.1939.

Huttenlocker, A.K., and D.M. Grossnickle, et al. 2018. Late-surviving stem mammal links the lowermost Cretaceous of North America and Gondwana. *Nature* 558: 108–112. doi: 10.1038/s41586-018-0126-y.

Ji, Q., and Z.-X. Luo, et al. 2009. Evolutionary development of the middle ear in Mesozoic therian mammals. *Science* 326: 278–281. doi: 10.1126/science.1178501.

Kay, R.F. 1975. The functional adaptations of primate molar teeth. *American Journal of Physical Anthropology* 43: 195–216. doi: 10.1002/ajpa.1330430207.

Kay, R.F., and K.M. Hiiemäe. 1974. Jaw movement and tooth use in recent and fossil primates. *American Journal of Physical Anthropology* 40: 227–256. doi: 10.1002/ajpa.1330400210.

Kermack, K.A. 1954a. PV M 19143. http://data.nhm.ac.uk/object/f2cd5a5d-4b00-4795-bde8-2011862ae746.

Kermack, K.A. 1954b. PV M 19771. http://data.nhm.ac.uk/object/8979bb7d-c496-4bba-bb26-64d34e52eac9.

Kermack, D.M., and K.A. Kermack, et al. 1968. The Welsh pantothere *Kuehneotherium praecursoris*. *Journal of the Linnean Society of London, Zoology* 47: 407–423. doi: 10.1111/j.1096-3642.1968.tb00519.x.

Kermack, D.M., and K.A. Kermack (eds.). 1971. *Early mammals.* London: Academic Press.

Kielan-Jaworowska, Z., R.L. Cifelli, and Z.-X. Luo. 2004. *Mammals from the age of dinosaurs. Origins, evolution, and structure.* New York: Columbia University Press.

Koenigswald, W. von, and U. Anders, et al. 2013. Jaw movement in fossil mammals: Analysis, description and visualization. *Paläontologische Zeitschrift* 87: 141–159. doi: 10.1007/s12542-012-0142-4.

Krause, D.W., and S. Hoffmann, et al. 2014. First cranial remains of a gondwanatherian mammal reveal remarkable mosaicism. *Nature* 515: 512–517. doi: 10.1038/nature13922.

Kretzoi, M. 1960. Zur Benennung des ältesten Symmetrodonten. *Vertebrata Hungarica* 2: 307–309.

Kühne, W.G. 1949. On a triconodont tooth of a new pattern from a fissure-filling in South Glamorgan. *Proceedings of the Zoological Society of London* 119: 345–350. doi: 10.1111/j.1096-3642.1949.tb00883.x.

Kullmer, O., and S. Benazzi, et al. 2009. Technical note: Occlusal fingerprint analysis: Quantification of tooth wear pattern. *American Journal of Physical Anthropology* 139: 600–605. doi: 10.1002/ajpa.21086.

Li, G., and Z.-X. Luo. 2006. A Cretaceous symmetrodont therian with some monotreme-like postcranial features. *Nature* 439: 195–200. doi: 10.1038/nature04168.

Lieberman, D.E., and A.W. Crompton. 2000. Why fuse the mandibular symphysis?: A comparative analysis. *American Journal of Physical Anthropology* 112: 517–540. doi: 10.1002/1096-8644(200008)112:4<517:AID-AJPA7>3.0.CO;2-4.

Lillegraven, J.A., and M.C. McKenna. 1986. Fossil mammals from the ‘‘Mesaverde’’ formation (Late Cretaceous, Judithian) of the Bighorn and Wind River basins, Wyoming, with definitions of Late Cretaceous North American land mammal ‘‘ages’’. *American Museum Novitates* 2840: 1–68.

Litonjua, L.A., and S. Andreana, et al. 2003. Tooth wear: attrition, erosion, and abrasion. *Quintessence International* 34: 435–446.

Lopatin, A.V. 2006. Early Paleogene insectivore mammals of Asia and establishment of the major groups of Insectivora. *Paleontological Journal* 40: S205-S405. doi: 10.1134/S0031030106090012.

Lopatin, A.V., and A.O. Averianov. 2006. Revision of a pretribosphenic mammal *Arguimus* from the Early Cretaceous of Mongolia. *Acta Palaeontologica Polonica* 51: 339–349.

Lucas, P.W. 1979. The dental-dietary adaptations of mammals. *Neues Jahrbuch für Geologie und Paläontologie - Monatshefte* 8: 486–512.

Lucas, P.W. 2004. *Dental functional morphology. How teeth work.* Cambridge [etc.]: Cambridge University Press.

Lucas, P.W., and D.A. Luke. 1984. Chewing It over: Basic principles of food breakdown. In *Food acquisition and processing in Primates*, ed. David J. Chivers, Bernard A. Wood and Alan Bilsborough, 283–301. Boston, MA: Springer US. doi: 10.1007/978-1-4757-5244-1_12.

Lucas, P.W., and C.R. Peters. 2000. Function of postcanine tooth crown shape in mammals. In *Development, function and evolution of teeth*, ed. Mark Franklyn Teaford, Moya Meredith Smith and Ferguson, Mark W. J, 282–289. New York: Cambridge University Press.

Luckett, W.P., and F.S. Szalay (eds.). 1976. *Phylogeny of the Primates. A multidisciplinary approach.* Boston: Springer.

Lumsden, A.G.S., and J.W. Osborn. 1977. The evolution of chewing: a dentist's view of palaentology. *Journal of Dentistry* 5: 269–287.

Luo, Z.-X. 2007. Transformation and diversification in early mammal evolution. *Nature* 450: 1011–1019. doi: 10.1038/nature06277.

Luo, Z.-X., and R.L. Cifelli, et al. 2001. Dual origin of tribosphenic mammals. *Nature* 409: 53–57. doi: 10.1038/35051023.

Luo, Z.-X., and S.M. Gatesy, et al. 2015. Mandibular and dental characteristics of Late Triassic mammaliaform *Haramiyavia* and their ramifications for basal mammal

evolution. *Proceedings of the National Academy of Sciences of the United States of America* 112: E7101-9. doi: 10.1073/pnas.1519387112.

Luo, Z.-X., and Q. Ji. 2005. New study on dental and skeletal features of the Cretaceous “Symmetrodontan” mammal *Zhangheotherium*. *Journal of Mammalian Evolution* 12: 337–357. doi: 10.1007/s10914-005-6958-x.

Luo, Z.-X., and Z. Kielan-Jaworowska, et al. 2002. In quest for a phylogeny of Mesozoic mammals. *Acta Palaeontologica Polonica* 47: 1–78.

Luo, Z.-X., and T. Martin. 2007. Analysis of molar structure and phylogeny of Docodont genera. *Bulletin of Carnegie Museum of Natural History* 39: 27–47. doi: 10.2992/0145-9058(2007)39[27:AOMSAP]2.0.CO;2.

Luo, Z.-X., and C.-X. Yuan, et al. 2011. A Jurassic eutherian mammal and divergence of marsupials and placentals. *Nature* 476: 442–445. doi: 10.1038/nature10291.

Marsh, O.C. 1878. Fossil mammal from the Jurassic of the Rocky Mountains. *American Journal of Science* s3-15: 459. doi: 10.2475/ajs.s3-15.90.459.

Marsh, O.C. 1879. Additional remains of Jurassic mammals. *American Journal of Science (ser.3)* 18: 215–216. doi: 10.2475/ajs.s3-18.105.215.

Marsh, O.C. 1887. I.—American Jurassic Mammals. *Geological Magazine* 4: 241. doi: 10.1017/S0016756800193653.

Martin, T. 1999. Dryolestidae (Dryolestoidea, Mammalia) aus dem Oberen Jura von Portugal. *Abhandlungen der senckenbergischen naturforschenden Gesellschaft* 550: 1–119.

Martin, T. 2002. New stem-lineage representatives of Zatheria (Mammalia) from the Late Jurassic of Portugal. *Journal of Vertebrate Paleontology* 22: 332–348.

Martin, T., and A.O. Averianov. 2010. Mammals from the Middle Jurassic Balabansai Formation of the Fergana Depression, Kyrgyzstan. *Journal of Vertebrate Paleontology* 30: 855–871. doi: 10.1080/02724631003758045.

Maschenko, E.N., and A.V. Lopatin, et al. 2002. A new Early Cretaceous mammal from Western Siberia. *Doklady Biological Sciences* 386: 475–477. doi: 10.1023/A:1020791007455.

McKenna, M.C. 1976. Toward a phylogenetic classification of the Mammalia. In *Phylogeny of the Primates: A multidisciplinary approach*, ed. W. P. Luckett and Frederick S. Szalay, 21–46. Boston: Springer.

Meredith, N., and M. Sherriff, et al. 1996. Measurement of the microhardness and Young's modulus of human enamel and dentine using an indentation technique. *Archives of Oral Biology* 41: 539–545.

Mills, J.R.E. 1955. Ideal dental occlusion in the primates. *Dental Practitioner* 6: 47–61.

Mills, J.R.E. 1964. The dentitions of *Peramus* and *Amphitherium*. *Proceedings of the Linnean Society of London* 175: 117–133. doi: 10.1111/j.1095-8312.1964.tb00925.x.

Mills, J.R.E. 1984. The molar dentition of a Welsh pantothere. *Zoological Journal of the Linnean Society* 82: 189–205. doi: 10.1111/j.1096-3642.1984.tb00542.x.

Moore, S.J., and G.D. Sanson. 1995. A comparison of the molar efficiency of two insect-eating mammals. *Journal of Zoology* 235: 175–192. doi: 10.1111/j.1469-7998.1995.tb05136.x.

Nessov, L.A. 1997. Cretaceous nonmarine vertebrates of northern Eurasia.: Paper completed after the author's death by Golovneva, L. B. and Averianov, A .O. (eds). *University of Saint Petersburg, Institute of the Earth's Crust, Saint Petersburg*: 1–218.

Niethhammer, J., H. Schliemann, and D. Starck (eds.). 1989. *Handbuch der Zoologie.* Berlin, New York: Walter de Gruyter.

Oron, U., and A.W. Crompton. 1985. A cineradiographic and electromyographic study of mastication in *Tenrec ecaudatus*. *Journal of morphology* 185: 155–182. doi: 10.1002/jmor.1051850203.

Osborn, H.F. 1888. The evolution of mammalian molars to and from the tritubercular type. *The American Naturalist* 22: 1067–1079.

Osborn, H.F. 1897. Trituberculy: A review dedicated to the late professor Cope. *The American Naturalist* 31: 993–1016. doi: 10.1086/276747.

Owen, R. 1854. On some fossil reptilian and mammalian remains from the Purbecks. *Quarterly Journal of the Geological Society* 10: 420–433. doi: 10.1144/gsl.jgs.1854.010.01-02.48.

Pan, Y., and J. Sha, et al. 2013. The Jehol Biota: Definition and distribution of exceptionally preserved relicts of a continental Early Cretaceous ecosystem. *Cretaceous Research* 44: 30–38. doi: 10.1016/j.cretres.2013.03.007.

Pascual, R., and F.J. Goin, et al. 2002. New data on the Paleocene monotreme *Monotrematum sudamericanum*, and the convergent evolution of triangulate molars. *Acta Palaeontologica Polonica* 47: 487–492.

Patterson, B. 1955. A symmetrodont from the early cretaceous of North Texas. *Fieldiana: Zoology* 37: 689–693.

Patterson, B. 1956. Early Cretaceous mammals and the evolution of mammalian molar teeth. *Fieldiana: Geology* 13: 1–105.

Plogschties, T., and T. Martin. 2019. New information on the maxilla, dentary, and dentition of *Maotherium sinense*, with comments on the zhangheotheriid dental formulae. *Paläontologische Zeitschrift* 100: 311. doi: 10.1007/s12542-019-00460-3.

Prinz, J.F., and P.W. Lucas. 1997. An optimization model for mastication and swallowing in mammals. *Proceedings of the Royal Society B: Biological Sciences* 264: 1715–1721. doi: 10.1098/rspb.1997.0238.

Prinz, J.F., and Silwood, C. J. L., et al. 2003. Simulated digestion status of intact and exoskeletally-punctured insects and insect larvae: A spectroscopic investigation. *Folia Primatologica* 74: 126–140. doi: 10.1159/000070646.

Proff, P. 2010. Malocclusion, mastication and the gastrointestinal system: A review. *Journal of orofacial orthopedics* 71: 96–107. doi: 10.1007/s00056-010-0909-8.

Rensberger, J.M. 1973. An occlusion model for mastication and dental wear in herbivorous mammals. *Journal of Paleontology* 47: 515–528.

Rougier, G.W., and S. Isaji, et al. 2007a. An Early Cretaceous mammal from the Kuwajima Formation (Tetori Group), Japan, and a reassessment of triconodont phylogeny. *Annals of Carnegie Museum* 76: 73–115. doi: 10.2992/0097-4463(2007)76[73:aecmft]2.0.co;2.

Rougier, G.W., and Q. Ji, et al. 2003. A new symmetrodont mammal with fur impressions from the Mesozoic of China. *Acta Geologica Sinica - English Edition* 77: 7–14. doi: 10.1111/j.1755-6724.2003.tb00104.x.

Rougier, G.W., and A.G. Martinelli, et al. 2007b. New Jurassic mammals from Patagonia, Argentina: A reappraisal of australosphenidan morphology and interrelationships. *American Museum Novitates* 3566: 1–54. doi: 10.1206/0003-0082(2007)507[1:NJMFPA]2.0.CO;2.

Rougier, G.W., and M.J. Novacek, et al. 2001. Gobiconodonts from the Early Cretaceous of Oshih (Ashile), Mongolia. *American Museum Novitates* 3348: 1–32.

Rougier, G.W., and J.R. Wible, et al. 1996. Basicranial anatomy of *Priacodon fruitaensis* (Triconodontidae, Mammalia) from the Late Jurassic of mammaliaform interrelationships. *American Museum Novitates* 3183: 1–38.

Rowe, T. 1988. Definition, diagnosis, and origin of Mammalia. *Journal of Vertebrate Paleontology* 8: 241–264.

Sanson, G.D., and S.A. Kerr, et al. 2007. Do silica phytoliths really wear mammalian teeth? *Journal of Archaeological Science* 34: 526–531. doi: 10.1016/j.jas.2006.06.009.

Schultz, J.A. 2012. Funktionelle Morphologie und Abnutzungsmuster prätribosphenischer Molaren am Beispiel der Dryolestida (Mammalia, Cladotheria). Doctoral thesis, Rheinische Friedrich-Wilhelms-Universität, Bonn.

Schultz, J.A., and B.-A.S. Bhullar, et al. 2017a. Re-examination of the Jurassic Mammaliaform *Docodon victor* by computed tomography and occlusal functional analysis. *Journal of Mammalian Evolution* 33: 1408. doi: 10.1007/s10914-017-9418-5.

Schultz, J.A., and T. Martin. 2011. Wear pattern and functional morphology of dryolestoid molars (Mammalia, Cladotheria). *Paläontologische Zeitschrift* 85: 269–285. doi: 10.1007/s12542-010-0091-8.

Schultz, J.A., and T. Martin. 2014. Function of pretribosphenic and tribosphenic mammalian molars inferred from 3D animation. *Naturwissenschaften* 101: 771–781. doi: 10.1007/s00114-014-1214-y.

Schultz, J.A., and U. Menz, et al. 2017b. Modular Wear Facet Nomenclature for mammalian post-canine dentitions. *Historical Biology* 39: 1–12. doi: 10.1080/08912963.2017.1302442.

Schwermann, A.H. 2015. Über die Funktionsweise prätribosphenischer und tribosphenischer Gebisse. Doctoral thesis, Rheinische Friedrich-Wilhelms-Universität, Bonn.

Sheriff, S.D. 1998. stereonet.xls. http://hs.umt.edu/geosciences/faculty/sheriff/equipment-techniques-and-cheats/stereonet.xls.

Sigogneau-Russell, D. 1983. A new therian mammal from the Rhaetic locality of Saint-Nicolas-de-Port (France). *Zoological Journal of the Linnean Society* 78: 175–186.

Sigogneau-Russell, D. 1991. Nouveaux Mammifères theriens du Crétacé inférieur du Maroc. *Comptes rendus de l'Académie des sciences. Série 2, Mécanique, Physique, Chimie, Sciences de l'univers, Sciences de la Terre* 313: 279–285.

Sigogneau-Russell, D., and P.C. Ensom. 1998. *Thereuodon* (Theria, Symmetrodonta) from the Lower Cretaceous of North Africa and Europe, and a brief review of symmetrodonts. *Cretaceous Research* 19: 445–470. doi: 10.1006/cres.1998.0115.

Sigogneau-Russell, D., and R. Hahn. 1995. Reassessment of the Late Triassic symmetrodont mammal *Woutersia*. *Acta Palaeontologica Polonica* 40: 245–260.

Simpson, G.G. 1925. Mesozoic Mammalia, II; *Tinodon* and its allies. *American Journal of Science* s5-10: 451–470. doi: 10.2475/ajs.s5-10.59.451.

Simpson, G.G. 1929. *American Mesozoic Mammalia.* New Haven: Yale university press. doi: 10.5962/bhl.title.5717.

Simpson, G.G. 1933. Paleobiology of Jurassic mammals. *Palaeobiologica* 5: 127–158.

Simpson, G.G. 1936. Studies of the earliest mammalian dentitions. *Dental cosmos* 78: 791-800 & 940-953.

Slaughter, B.H. 1965. A therian from the Lower Cretaceous (Albian) of Texas. *Postilla* 93: 1–18.

Smith, J.B., and P. Dodson. 2003. A proposal for a standard terminology of anatomical notation and orientation in fossil vertebrate dentitions. *Journal of Vertebrate Paleontology* 23: 1–12.

Strait, S.G. 1993. Molar morphology and food texture among small-bodied insectivorous mammals. *Journal of mammalogy* 74: 391–402. doi: 10.2307/1382395.

Sweetman, S.C. 2008. A spalacolestine spalacotheriid (mammalia, trechnotheria) from the Early Cretaceous (Barremian) of Southern England and its bearing on spalacotheriid evolution. *Palaeontology* 51: 1367–1385. doi: 10.1111/j.1475-4983.2008.00816.x.

Szalay, F.S. 1969. Mixodectidae, Microsyopiday, and the insectivore-primate transition. *Bulletin of the American Museum of Natrual History* 40: 197–324.

Teaford, M.F., M.M. Smith, and Ferguson, Mark W. J (eds.). 2000. *Development, function and evolution of teeth.* New York: Cambridge University Press.

Thenius, E. 1989. Zähne und Gebiß der Säugetiere. In *Handbuch der Zoologie*, Band 8, Teilband 56, ed. J. Niethhammer, H. Schliemann and D. Starck. Berlin, New York: Walter de Gruyter.

Thiery, G., and F. Guy, et al. 2017. Investigating the dental toolkit of primates based on food mechanical properties: Feeding action does matter. *American journal of primatology* 79: 1–15. doi: 10.1002/ajp.22640.

Thomason, J. (ed.). 1995. *Functional morphology in vertebrate paleontology.* Cambridge, New York: Cambridge University Press.

Trofimov, B.A. 1980. A new generic name *Gobiotheriodon* for a symmetrodont mammal. *Acta Palaeontologica Polonica* 42: 496.

Tsubamoto, T., and G.W. Rougier, et al. 2004. New Early Cretaceous spalacotheriid "symmetrodont" mammal from Japan. *Acta Palaeontologica Polonica* 49: 329–346.

Ulhaas, L. 2006. Vergleichende computergestützte funktionsmorphologische Analyse an Molaren cercopithecoider Primaten. Doctoral thesis, Johannes Gutenberg-Universität, Mainz.

Ungar, P.S. 2010. *Mammal teeth. Origin, evolution, and diversity.* Baltimore: Johns Hopkins University press.

Ungar, P.S. 2015. Mammalian dental function and wear: A review. *Biosurface and Biotribology* 1: 25–41. doi: 10.1016/j.bsbt.2014.12.001.

van Valen, L. 1966. Deltatheridia, a new order of mammals. *Bulletin of the American Museum of Natural History* 132: 1–126.

Walker, A., and H.N. Hoeck, et al. 1978. Microwear of mammalian teeth as an indicator of diet. *Science* 201: 908–910.

Woodburne, M.O., and T.H. Rich, et al. 2003. The evolution of tribospheny and the antiquity of mammalian clades. *Molecular biology and evolution* 28: 360–385. doi: 10.1016/S1055-7903(03)00113-1.

Yabe, H., and T. Shikama. 1938. A new Jurassic Mammalia from South Manchuria. *Proceedings of the Imperial Academy (of Japan)* 14: 353–357.

Zhang, H., and B. Wang, et al. 2010. Evolution of insect diversity in the Jehol Biota. *Science China Earth Sciences* 53: 1908–1917. doi: 10.1007/s11430-010-4098-5.

8 Acknowledgment

I am extremely grateful to my supervisor Thomas Martin, for supporting me during the past years. Your valuable advice and guidance were the bedrock to finish this research.

I would like to express my gratitude to my second reviewer Martin Sander for his helpful contributions, as well as Nikolaus Froitzheim and Thomas Bredow for being part of the dissertation committee. Martin, I deeply appreciate your help and your feedback.

I'm profoundly indebted to the Studienstiftung des deutschen Volkes for the generous scholarship, which not only funded my research but also my field work in the USA.

I am extremely thankful to Janet Whitmore and Dave Gillette (Museum of Northern Arizona) Richard Cifelli, Kyle Davies, Joshua Cohen (Sam Noble Museum, Oklahoma), Frédéric Lacombat (Yizhou Fossil & Geology Park), and Carrie Levitt Bussian (Natural History Museum of Utah) to let me study their specimens. Rich, I am particularly grateful for providing me with 3D-models of various specimens, the generous support, and your kindness. Carrie, a special thanks to you for making it possible to loan some specimens from your collection. Janet and Dave, I really appreciate your openness and your overwhelming support in Arizona.

Pamela Gill (University of Bristol), I want also to thank you for the efforts in trying to provide me with SEM-Pictures and 3D-models.

I gratefully acknowledge being a member of the excellent mammal's research lab within the institute of geosciences. Julia Schultz, I am deeply indebted to you for your support, discussion, and encouragement. Kai Jäger and Thomas Engler, a special thanks to you, for being my office mates and colleagues. Not only your discussions and support improved this research, but also your humor, which helped me in desperate times. Andreas Lang, thank you for providing me with 3D-models of zalambdodont molars. Olaf Dülfer, I would like to express my deepest gratitude to you, your extraordinary skill as a preparator, and your help, which cannot be overestimated. I sincerely thank Leonie Schwermann for proofreading my dissertation.

From the bottom of my heart, I am extremely grateful to my beloved family Sashima, Jonathan, and Nonahami Läbe, without their universal, ongoing support, my dissertation would never be completed. Sashima, mother of our children, these past several years have not been an easy ride, both academically and personally. I truly thank you for sticking by my side, especially in hard times. Jonathan and Nonahami, my son and daughter, your distractions and happiness always cheered me up and helped me to keep my head on my shoulders.

To Seela and Siegfried Läbe, I am also deeply grateful to you for backing me (us) up by taking care of your Grandchildren so often.

I also would like to thank Marie-Therese Stein and my father Ernst Günter Plogschties, for never letting me down. The same goes for you Annette, Beate, Sabine and Susanne Plogschties, my mother and sisters, a sincere thank you to you all of you.
And last but not least, I want to thank all my friends (too many to list here but you know who you are!) for providing support and friendship that I needed.

9 Appendix

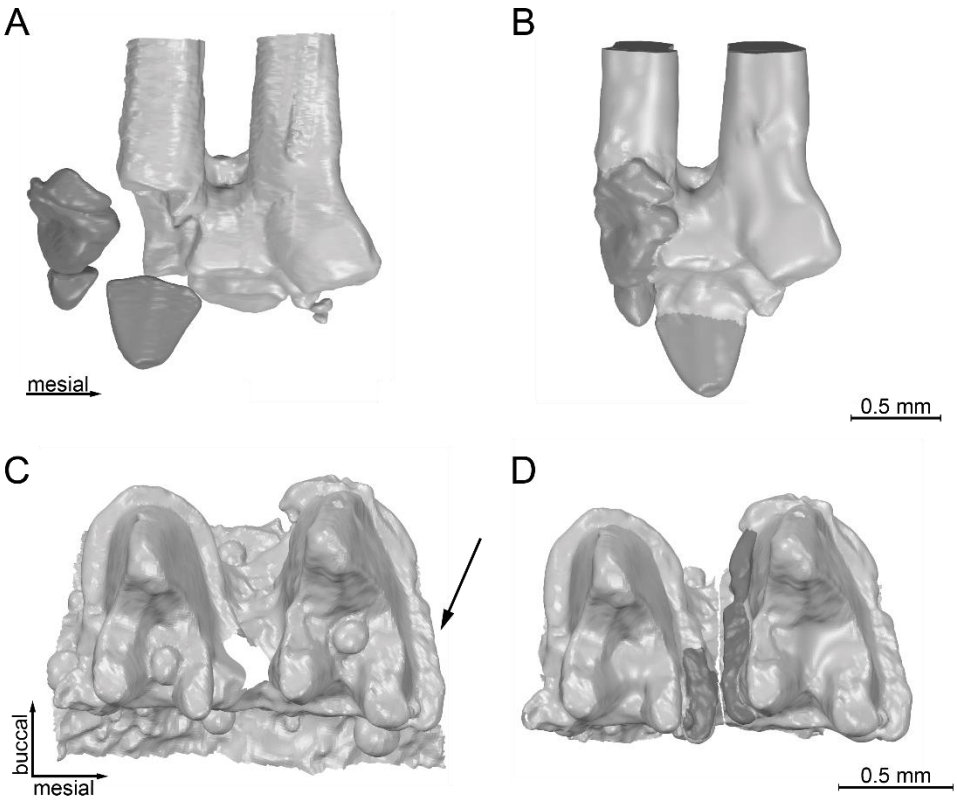

Fig. S1: 3D-model post processing. Changes are marked in darker grey. Some fragments of M2 of specimen YFGP 1724 (*Maotherium sinense*) had to be rearranged (A, B). A: Initial position of the M2 fragments. B: 3D-model after the fragments rearrangement. The distal cingulid of m4, as well as the mesial cingulid of m5 of specimen OMNH VP 027421 (Spalacolestes cretulablatta) is incomplete (C). For completion the mesial cingulid of m4 was modified and modeled into the damaged spots (D).

Tab. S1: List of the studied specimen. All specimen are stored in Bonn. O= Original, C= Cast.

Taxon	Inventory number	Description	Studied	CT-Scan from	SEM study	Stored as
Kuehneotheriidae	HLV 1R	Mx	O	–	–	O
Kuehneotheriidae	RAS 786	mx	O	–	X	O
Kuehneotheriidae	RAS 796	Mx	O	–	–	O
Kuehneotheriidae	RAS 813	px	O	–	–	O
Kuehneotheriidae	RAS 847	Px or px	O	–	–	O
Kuehneotheriidae	RAS 850	px	O	–	–	O
Kuehneotherium praecursoris	NHM PV M 19143	m3	–	O		
Kuehneotherium praecursoris	NHM PV M 19168 ? / C 857	M	C	–	X	C
Kuehneotherium praecursoris	NHM PV M 19771	M4	–	O		
Kuehneotherium stanislavi,	SNP 75 L	Mx	C	–		C
Maotherium sinense	YFGP 1724	maxilla fragment with M2-M3;	O	O	X	C
		mandible fragment with 3p, m1-m5				
Peralestes longirostris (*Spalacotherium tricuspidens*)	NHM PV OR 47740	maxilla fragment with 1P and M1-M6	C	C	–	C
Spalacolestes cretulablatta	OMNH VP 026688	M4	O	C	X	C
Spalacolestes cretulablatta	OMNH VP 026693	M4	O	C	X	C
Spalacolestes cretulablatta	OMNH VP 027421	mandible fragment with m4-m5	O	C		C
Spalacolestes cretulablatta	OMNH VP 029600	mandible fragment with m4-m7	O	C		C
Spalacolestes cretulablatta	OMNH VP 029611	M2	O		X	C
Spalacolestes cretulablatta	OMNH VP 030611	M4	O	C	X	C
Spalacolestes cretulablatta	OMNH VP 030627	m4	O	C	X	C
Spalacolestes cretulablatta	OMNH VP 033043	m5	O	C		C
Spalacolestes cretulablatta	OMNH VP 033060	M3	O	C		C
Spalacolestes cretulablatta	OMNH VP 033231	M4	O	–	X	C
Spalacolestes inconcinnus	MNA V 6247, OMNH VP 69062	Px?	O	–	–	C
Spalacolestes inconcinnus	OMNH VP 033027	dp3?	O	–	–	C
Spalacolestes inconcinnus	OMNH VP 033034	M2	O	C	–	C

Tab. S1: List of the studied specimen. All specimen are stored in Bonn. O= Original, C= Cast, continued.

Taxon	Inventory number	Description	Studied	CT-Scan from	SEM study	Stored as
Spalacolestes inconcinnus	OMNH VP 033897	m3	O	C	X	C
Spalacolestes inconcinnus	OMNH VP 033911	maxilla fragment with M4	O	C	–	C
Spalacotheridium mckennai?	MNA V 6046, OMNH VP 025524	m3?	O	C	–	C
Spalacotheridium noblei	30627	m4	O	C	X	C
Spalacotheridium noblei	OMNH VP 026692	M4	O	C	X	C
Spalacotheridium noblei	OMNH VP 027261	m3	O	–	–	C
Spalacotheridium noblei	OMNH VP 027461	M6	O	C	–	C
Spalacotheridium noblei	OMNH VP 030623	m2	O	C	–	C
Spalacotheridium noblei	OMNH VP 033041	m3	O	–	X	C
Spalacotheridium noblei	OMNH VP 033053	m5	O	–	–	C
Spalacotheridium noblei	OMNH VP 033061	M2	O	C	–	C
Spalacotheridium noblei	OMNH VP 033895	M3	O	–	–	C
Spalacotheridium noblei	OMNH VP 033900	m3	O	C	X	C
Spalacotheriidae	MNA V 6305, OMNH VP 025531	maxilla fragment with Px	O	–		C
Spalacotheriidae	OMNH VP 030610	Mx	O	–	–	C
Spalacotheriidae	OMNH VP 032953	Mx	O	–	–	C
Spalacotheriidae	OMNH VP 071070	mx	O	C	–	C
Spalacotheriidae	OMNH VP 071071	mx	O	C	–	C
Spalacotheriidae	OMNH VP 071072	Mx	O	C	–	C
Spalacotheriidae	OMNH VP 071073	Mx	O	C	–	C
Spalacotherium evansae	DORCM GS 0380	mx	C	–	–	C
Spalacotherium evansae	DORCM GS 0684	Mx	C	C	–	C
Spalacotherium evansae	DORCM GS 1075	mx	C	C	–	C
Spalacotherium evansae?	DROCM GS 0689	Mx	C	C	–	C

Tab. S1: List of the studied specimen. All specimen are stored in Bonn. O= Original, C= Cast, continued.

Taxon	Inventory number	Description	Studied	CT-Scan from	SEM study	Stored as
“Symmetrodonta” indet.	UMNH VP 17294	mx	O	O	–	C
Symmetrodontoides canadensis	OMNH VP 066370	m1	O	C	–	C
Symmetrodontoides canadensis	OMNH VP 066371	m4	O	C	–	C
Symmetrodontoides canadensis	OMNH VP 066372	m6 or m7	O	C	–	C
Symmetrodontoides canadensis	OMNH VP 066373	posterior px	O	–	–	C
Symmetrodontoides canadensis	OMNH VP 066374	px	O	–	–	C
Symmetrodontoides foxi	MNA V 4522; OMNH VP 023800	m7	O	C	X	C
Symmetrodontoides foxi	MNA V 4653, OMNH VP 023814	Mx	O	C	X	C
Symmetrodontoides foxi	MNA V 6461	m7	O	–	X	C
Symmetrodontoides foxi	OMNH VP 020135	m4	O	–	–	C
Symmetrodontoides oligodontos	MNA V 6047; OMNH VP 025525	mx?	O	C	–	C
Symmetrodontoides oligodontos	MNA V 6048; OMNH VP 025526	M1 or M2	O	C	–	C
Symmetrodontoides oligodontos	MNA V 6755; OMNH VP 025538	mx	O	C	–	C
Symmetrodontoides oligodontos	OMNH VP 029040	M2	O	C	–	C
Thereuodon taraktes	DORCM GS 419	deciduous teeth	C	C	–	C
Thereuodon taraktes	DORCM GS 665	deciduous teeth	C	C	–	C
Thereuodon taraktes	DORCM GS 679	deciduous teeth	C	C	–	C
Tinodon bellus	YPM VP 011843	mandible fragment with m1-4	C	C	–	C
Tinodon bellus	YPM VP 013644.A, OMNH VP 056826	mandible fragment with 3p, m1-m4	C	C	–	C
Tinodon lepidus	AMNH 101145	mandible with 1p	C	–	–	C
Tinodon lepidus	USNM 2131; OMNH VP 056835	mandible fragment with c, 3p, m1-3	C	C		C

Tab. S1: List of the studied specimen. All specimen are stored in Bonn. O= Original, C= Cast, continued.

Taxon	Inventory number	Description	Studied	CT-Scan from	SEM study	Stored as
Tinodon lepidus	YPM VP 011845	mandible fragment with m1, m3	C	C	–	C
Tinodon lepidus?	YPM VP 013645	mandible with fragment mx	C	–	–	C
Tinodon micron?	DORCM GS 1110 (GS 550)	px or Px	C	–	–	C
Woutersia butleri	SNP 082 W	Px	C	C	–	C
Woutersia butleri	SNP 088 W	Mx	C	C	X	C
Woutersia butleri	SNP 517 W	mx	C	C		C
Woutersia butleri	SNP 720	Mx	C	C		C
Woutersia mirabilis	SNP 052 W	Mx	C	C	X	C
Woutersia mirabilis	SNP 426 W	px?	C	C		C
Woutersia mirabilis	SNP RAS 706	mx	C	C		C
Woutersia mirabilis	SNP RAS 884	Mx	C	C		C
Woutersia mirabilis	SNP RAS 975	mx	C	C	X	C
Woutersia mirabilis?	SNP 719	Mx	C	C	X	C
Woutersia mirabilis?	SNP 9FW	mx	C	C	–	C

Tab. S2: Color-coding of the OFA collision areas.

Woutersia wor-cycle	lower	pr-d	pr-bd-a	pr-db	me-db	me-d-a				pr-bm			
	upper	PA-m		[CG]_ml	CPX-ml/ PA-ml					ME-ld			
Woutersia wr-cycle	lower	pr-db(2)	pr-bd-a	pr-db(1)	me-db	me-d-a				pr-bm			
	upper	PA-ml(2)		[CG]_ml	PA-ml(1)					ME-ld			
Kuehneotherium wor-cycle	lower	pr-d			me-db			cpd-b	pr-bm	pr-mb(2)	pr-mb(1)		
	upper	PA-m			PA-ml			PA-l	MTS-dl	ME-dl	ST-dl		
Kuehneotherium wr-cycle	lower	pr-d			me-db			cpd-b	pr-bm(1)	pr-bm(2)	pr-b		
	upper	PA-m			PA-ml			PA-l	MTS-dl	ME-ld	ST-l		
Maotherium wor-cycle	lower	pr-db		pr-d	me-bd		me-d			pr-mb		pr-m	
	upper	CP B' ml		[CG]PA_CPB'-m	[CG]PA_CPB'-d		PA-m			ME-dl		[CG]PA_ME-d	
Maotherium wr-cycle	lower	pr-db		pr-db(1)	me-bd		me-d	cpd-bd		pr-mb		pr-m	
	upper	CPB'-ml		[CG]PA_CPB'-m	[CG]PA_CPB'-d		PA-m	PA-lm		ME-dl		[CG]PA_ME-d	
Spalacotherium wor-cycle	lower	pr-b			me-d				pr-bm				
	upper	PAS-m			PA-m(1)				MTS-ld				
Spalacotherium wr-cycle	lower	pr-bd			me-d				pr-bm				
	upper	PAS-lm			PA-m(1)				MTS-ld				
Dryolestes wor-cycle	lower				me-d								
	upper				PA-m								

color-coding												
	R	190	187	6	224	115	188	227	0	163	167	1
	G	22	44	135	165	31	207	223	128	25	75	102
	B	34	57	55	203	101	12	8	128	91	150	51

Tab. S2: Color-coding of the OFA collision areas, continued.

Woutersia wor-cycle	lower		pa-bm-a	pa-b			pa-mb							
	upper			PA*ME			CPX-d							
Woutersia wr-cycle	lower		pa-mb-a	pa-bm		pa-mb(1)	pa-mb(2)							
	upper			PA*ME			CPX-dl							
Kuehneotherium wor-cycle	lower	pa-d					pa-m							
	upper	ME-m					PA-d							
Kuehneotherium wr-cycle	lower	pa-bd					pa-mb			[cg]cpf-mb				
	upper	ME-lm					PA-dl			PA-dl				
Maotherium wor-cycle	lower				pa-b		pa-m	cpe-mb						
	upper				[CG]PA_ME-m		PA-d	PA-dl						
Maotherium wr-cycle	lower				pa-bm		pa-m	cpe-mb						
	upper				[CG]PA_ME-m		PA-d	PA-dl						
Spalacotherium wor-cycle	lower						pa-m		pa*pr	[cg]pr_me	[cg]pa_pr-l	[cg]pa_pr-b	pr*me	
	upper						PA-d (1)		PA*MTS	PA-m(2)	PA-d(2)		PAS*PA	
Spalacotherium wr-cycle	lower						pa-m		pa*pr	[cg]pr_me	[cg]pa_pr-l	[cg]pa_pr-b	pr*me	
	upper						PA-d(1)		PA*MTS	PA-m(2)	PA-d(2)		PAS*PA	
Dryolestes wor-cycle	lower						pa-m		pr*pa	hfd-bd			pr*me	
	upper						PA-d		PA*ME*MTS	PA-m-a			PA*ST	

color-coding													
	R	242	203	252	59	157	42	177	214	49	55	102	132
	G	145	123	194	187	200	75	127	125	153	186	129	49
	B	4	17	14	237	34	155	73	39	102	207	192	137

Tab S3: OFA setup, which was used in this study

OFA setting setup		
Collision:		
	Handler:	octree kdtree threaded pool list global
	Set distance:	0.08
Trajectory:		
	Approximation:	yes, using e^-x = 5
	Deflection:	yes, using angles allowed smaller than: 72, and use smallest angle if above defined angle
	Activate skipping of path points:	no
	Activate break free:	yes, using given degree steps for break free: 5, and maximum degree for break free: 350
	Show every x result triangles:	2
	Proper motion:	check only against own group, and allow moving back
OFA option setup		
Global:		
	Presets	
Project:		
	System:	metric system
	Compression rate:	9 = high compression
Scene:		
	Transformation and their corresponding speed rating:	mouse wheel speed: middle; mouse left + right: low; mouse right: low; mouse middle button: low
	Background color:	presets
	Selected points:	1
	Stereo option:	stereo mode: none; disparity: 0.60
	Level of detail:	level per mill: 1000
Collison:		
	Collision groups:	calculate predecessor; use face adjaceny
	Realtime collision test:	activate realtime collision; % of points to use: 50
Trajectory:		
	Automated collision reports:	deactivated
	System beep on trajectory finish:	enabled
Grab:		
	Video:	max. tempfile-size (MB): 50; fps: 25; bitrate: 1200; use memory buffer: yes
Indentation:		
	Presets	
Export:		
	Decimal delimiter:	set the decimal delimiter: ,
Collisionpath:		
	Timestep	0.01

9.1 Supplementary DVD/Online contents

File	Description
Dryolestes_wor.ofaproject	OFA project of *Dryolestes leiriensis* without roll
Kuehneotherium_wor.ofaproject	OFA project of *Kuehneotherium praecursoris* without roll
Kuehneotherium_wr.ofaproject	OFA project of *Kuehneotherium praecursoris* with roll
Maotherium_wor.ofaproject	OFA project of *Maotherium sinense* without roll
Maotherium_wr.ofaproject	OFA project of *Maotherium sinense* with roll
Spalacotherium_wor.ofaproject	OFA project of *Spalacotherium cretulablatta* without roll
Spalacotherium_wr.ofaproject	OFA project of *Spalacotherium cretulablatta* with roll
Woutersia_wor.ofaproject	OFA project of *Woutersia butleri* without roll
Woutersia_wr.ofaproject	OFA project of *Woutersia butleri* with roll